2015

ENGINEERING APPROACHES FOR SUPPRESSING DELETERIOUS HOST RESPONSES TO MEDICAL IMPLANTS

Connor McCarthy
Michigan Technological University, cwmccart@mtu.edu

ENGINEERING APPROACHES FOR SUPPRESSING DELETERIOUS HOST RESPONSES TO MEDICAL IMPLANTS

By

Connor W. McCarthy

A DISSERTATION

Submitted in partial fulfillment of the requirements for the degree of

DOCTOR OF PHILOSOPHY

In Biomedical Engineering

MICHIGAN TECHNOLOGICAL UNIVERSITY

2015

This dissertation has been approved in partial fulfillment of the requirements for the Degree of DOCTOR OF PHILOSOPHY in Biomedical Engineering.

Department of Biomedical Engineering

Dissertation Co-Advisor:	*Dr. Megan C. Frost*
Dissertation Co-Advisor:	*Dr. Jeremy Goldman*
Committee Member:	*Dr. Rupak Rajachar*
Committee Member:	*Dr. Bruce P. Lee*
Committee Member:	*Dr. Jaroslaw Drelich*
Department Chair:	*Dr. Sean J. Kirkpatrick*

Table of Contents

List of Figures

List of Tables

List of Abbreviations

AISI..... American Iron and Steel Institute
ATP. .....Adenosine triphosphate
Bcl-2.....B-cell lymphoma 2
bFGF .....Basic fibroblast growth factor
BH_4..... Tetrahydrobiopterin
BMS ..... Bare metal stent
CABG .....Coronary artery bypass graft
CaM .....Calmodulin
CAD ..... Coronary artery disease
CcO .....Cytochrome c oxidase
cGMP ..... guanosine 3',5'-cyclic monophosphate
CO_2.....Carbon dioxide
DAPI .....4',6-diamidino-2-phenylindole
DBSA..... Dodecylbenzenesulfonic acid
DMEM .....Dulbecco's Modified Eagles Medium
DNA..... Deoxyribonucleic acid
DTNB.....5,5'-dithiobis-(2-nitrobenzoic acid) (Ellman's reagent)
ECM..... Extracellular matrix
EDRF ..... Endothelium derived relaxing factor
eNOS.....Endothelial NOS, NOS 3
ePTFE. .....Expanded polytetrafluoroethylene
$FADH_2$ .....Flavin adenine dinucleotide-hydroquinone form
FESEM..... Field emission scanning electron microscope
FGF. .....Fibroblast growth factor
FMN..... Flavin mononucleotide
FTIR.....Fourier transform infrared spectroscopy
GAGs. .....Glycosaminoglycans
GSH .....Glutathione
GSNO.....S-nitrosoglutathione
GTP..... guanosine-5'-phosphate
H&E .....Hematoxylin & eosin
Hb..... Hemoglobin
HFIP..... Hexafluoro-2-propanol
HPLC .....High performance (pressure) liquid chromatography
IACUC ..... Internal care and use committee
ICAM-1.....Intracellular adhesion molecule-1
ICP-OES .....Inductively coupld plasma – optical emission spectrometry

IFN-ϒ.....Interferon gamma
IL-1 .....Interleukin-1
IMA..... Internal mammary artery
iNOS ..... Inducible NOS, NOS 2
LC-MS .....Liquid chromatography – mass spectrometry
LED.....Light emitting diode
LPS.....Lipopolysaccharide
metHb.....Methemoglobin
N_2O_3 .....Dinitrogen trioxide
NADPH.....Nicotinamide-adenine-dinucleotide phosphate
NAP ..... N-acetyl-D-penicillamine
NED ..... N-(1-napthyl)-ethylenediamine
NF-κB ..... Nuclear factor kappa B
NIH .....National Institutes of Health
nNOS .....Neuronal NOS, NOS 1
NO.....Nitric oxide, (NO•), (˙N=O)
NO^+ ..... Nitrosonium cation
NO^- .....Nitroxyl anion
NO_2* .....Excited state nitrogen dioxide
NO_3 ..... Nitrate
NO_3^- ..... Nitrate anion
NONOates.....N-diazeniumdiolates
NOS ..... Nitric oxide synthase
NOXs .....Non-phagocytic oxidases
O_2^- ..... Superoxide anion
$ONOO^-$/ONOOH .....Peroxynitrite
$ONOOCO_2^-$.....Nitrosoperoxocarbonate anion
PBS .....Phosphate buffered saline
PCL .....Polycaprolactone
PCU.....Polycarbonate urethane
PDGF ..... Platelet-derived growth factor
PEU..... Polyether urethane
PGA .....Poly(glycolic acid)
PLLA .....Poly(L-lactic acid)
PMT ..... Photomultiplier tube
PPB .....Parts per billion
PPM .....Parts per million
ROS.....Reactive oxygen species

RS˙ ..... Thiyl radical
RSNO ..... S-nitrosothiol, thionitrite
RSSR ..... Disulfide
sGC ..... soluble Guanylate Cyclase
-SH ..... Sulfhydryl
SOD ..... Superoxide dismutase
SNAP ..... S-nitroso-N-acetyl-D-penicillamine
SNOC ..... S-nitrosocysteine
SNOHb ..... S-nitrosohemoglobin
TEVG ..... Tissue engineered vascular graft
TGF-β ..... Transforming growth factor-β
TNF-α ..... Tumor necrosis factor-α
UV ..... Ultraviolet
UV/Vis ..... Ultraviolet visible light spectroscopy
vECs ..... Vascular endothelial cells
VEGF ..... Vascular endothelial growth factor
vSMCs ..... Vascular smooth muscle cells
VVG ..... Verhoeff's - Van Gieson

Preface

Chapter 4, “Fabrication and Short-Term *In Vivo* Performance of a Natural Elastic Lamina - Polymeric Hybrid Vascular Graft”, has been previously published in *ACS Applied Materials & Interfaces* 7(30), (2015) 16202-16212. Connor McCarthy was the first author and Dr. Jeremy Goldman was the corresponding author in this publication. Connor McCarthy was responsible for collecting the majority of the data, analyzing the data, and writing the paper. Pat Bowen assisted in the collection of mechanical data. Danielle Ahrens, David Joda, and Tyler Curtis were responsible for the collection of some sections of data. Connor McCarthy, Pat Bowen, Dr. Megan Frost, and Dr. Jeremy Goldman were responsible for proofreading and editing the final document.

Chapter 5, “Synthesis and Characterization of the Novel Nitric Oxide (NO) Donating Compound, S-nitroso-N-acetyl-D-penicillamine Derivatized Cyclam (SNAP-Cyclam)”, is planned for publication in *ACS Applied Materials & Interfaces*. Connor McCarthy was the first author while Dr. Jeremy Goldman and Dr. Megan Frost were the corresponding authors. Connor McCarthy and Dr. Megan Frost were responsible for conducting the experimental work. Connor McCarthy was responsible for analyzing the data and writing the paper. All authors were responsible for proofreading and editing the article prior to publication.

Chapter 6, “Transition Metal Mediated Release of Nitric Oxide (NO) from S-nitroso-N-acetyl-D-penicillamine (SNAP): Potential Applications for Endogenous Release of NO on the Surface of Stents via Corrosion Products”, is planned for publication in *ACS Applied Materials & Interfaces*. Connor McCarthy was the first author while Dr. Jeremy Goldman and Dr. Megan Frost were the corresponding authors. Connor McCarthy was responsible for conducting the experimental work, analyzing the data, and writing the paper. Roger J. Guillory II was responsible for the collection of Figure 6.7. All authors were responsible for proofreading and editing the article prior to publication.

Acknowledgments

I would like to acknowledge my co-advisors, Dr. Megan Frost and Dr. Jeremy Goldman, for their support and guidance during my graduate career. I would also like to thank my committee members; Dr. Rupak Rajachar, Dr. Bruce Lee, and Dr. Jaroslaw Drelich, for their time and continued involvement in my research. I am grateful to the National Institutes of Health, the National Science Foundation, and the Biomedical Engineering department for the financial support received over the past five years.

Abstract

Small diameter (< 6 mm) vascular grafts suffer from serious deleterious effects not encountered with their larger diameter relatives, leading to premature graft failure through restenosis. Platelet activation, inflammation, and smooth muscle cell proliferation are leading contributors to thrombosis and neointimal hyperplasia, both contributors to the progression of restenosis. It may be possible to suppress negative biological responses to vascular implants through the modification of surface properties and incorporation of drug release into blood contacting materials. In this work, bioengineering approaches are presented to improve the biocompatibility of small diameter vascular grafts.

We demonstrate a novel engineering approach for incorporating natural, decollagenized elastin matrices into PEU 1074A reinforced vascular grafts through spray-coating and electrospinning processes in a manner that retains elastin's excellent blood contacting properties. A vascular construct with excellent mechanical and surgical handling properties demonstrating the suppression of neointimal hyperplasia is presented after 21 days *in vivo*.

Nitric oxide (NO) has been investigated over the past several decades due to its platelet, inflammation, and smooth muscle cell suppressing effects; and if appropriately delivered, could positively mediate the contributors to restenosis. Here, we characterize a novel macrocyclic NO donor developed by linking S-nitroso-N-acetyl-D-penicillamine (SNAP) directly to 1,4,8,11-tetraazacyclotetradecane (cyclam). Here, we present characterization data for SNAP-Cyclam and demonstrate stable, long term NO release at physiologically relevant levels for more than 90 days when incorporated into poly(L-lactic acid) films.

Transition metals, such as copper and iron, are known to initiate NO production from S-nitrosothiols. It is reported in this work that additional transition metal ions; Co^{2+}, Ni^{2+}, and Zn^{2+}, which have not been reported to generate NO from RSNOs have the capacity to generate NO from the S-nitrosothiol, S-nitroso-N-acetyl-D-penicillamine. *In vivo* data alludes to the possibility that Zn^{2+} may be able to generate NO from endogenous donors and provide beneficial effects.

These three novel developments form the basis for the potential construction of clinically relevant small diameter vascular grafts capable of suppressing the deleterious effects, namely thrombosis and neointimal hyperplasia, commonly encountered in current small diameter vascular grafts.

Chapter 1: Introduction to Nitric Oxide

1.1. Background of Nitric Oxide

Nitric oxide's (NO) physiological presence was first theorized in the 16th and 17th centuries, but it wasn't until the 1970's that Ferid Murad began investigating vasodilators and their effect on guanylate cyclase activity[1]. Around 1986, NO and endothelium derived relaxing factor (EDRF) were theorized simultaneously as the same molecule by Ignarro et al. and Furchgott et. al[1-2]. In 1987, NO was positively identified as EDRF by Ignarro et. al[1-6]. All three scientists were awarded the Nobel Prizes in 1998 for their discovery of the NO/EDRF association.

NO is a free radical ($^{\bullet}N{=}O$), lipophilic gas under standard atmospheric conditions with a bond length of 1.15 Å[7-8]. In its ground state, NO contains a single electron in its 2p-π antibonding orbital. A loss of this electron results in the formation of a nitrosonium cation (NO^+), while an additional electron added to the antibonding orbital elicits a nitroxyl anion (NO^-)[3, 7, 9-10]. The presence of an unpaired electron gives NO the ability to react with oxygen (O_2), superoxide (O_2^-), and transition metals[3, 7]. Coupled with the reactive nature of thiols, the formation of S-nitrosothiols (RSNOs) from NO is highly favored in biological systems[7].

As a free radical, NO was perceived as a physiologically toxic substance prior to its link to EDRF. This was in part due to the typical weak intermolecular forces of other signaling molecules, which were not believed to be applicable to NO. However, NO mediated by guanosine 3',5'-cyclic monophosphate (cGMP) binds to the iron containing heme group of soluble guanylate cyclase (sGC) in a metal-nitrosyl complex coupling with several factors including cGMP-dependent protein kinase-G[5, 11]. In the absence of cGMP, NO can act in low concentrations through interactions with complexes containing transition metals. Reactions between NO and the thiyl radical (RS•) readily produce S-nitrosothiols (Equation 1)[12]. This mechanism of formation may be responsible for the formation of protein based S-nitrosothiols in the presence of NO[12]. In addition, NO can mediate cell signaling through the formation of S-nitrosothiols by the S-nitrosylation of cysteine residues, shown to regulate the activity of proteins involved in cellular regulation[5, 13].

$$RS\cdot + \cdot NO \longrightarrow RSNO \qquad (1)$$

Since its discovery, the understanding of NO's functions within the body have expanded significantly to include roles in almost every major system. NO maintains several diverse

functions throughout the body, including intercellular signaling[14-15], immune response and platelet aggregation[16-19], wound repair[5, 19-20], nervous system function[21], respiration[5, 22], and vascular regulation[19, 23-28]. In low concentrations, NO functions as a signal transducer within the physiological environment[5]. Importantly, metabolites of NO including nitrites, nitrates, and S-nitrosothiols are mediators of its cytotoxic or cytoprotective effects, and have been shown to regulate cellular apoptosis and necrosis, protein and deoxyribonucleic acid (DNA) damage, and inhibition of mitochondrial respiration[5, 29]. Due to the extensive involvement of NO in physiological functions, deficiencies in its synthesis and delivery have been linked to many diseases[30-31].

1.2. Physiological Production of Nitric Oxide

Endogenous NO is produced enzymatically through several classes of homodimers known as nitric oxide synthases (NOS)[3, 11, 13, 32-35]. To accomplish this, the amino acid L-arginine is catalyzed through sequential, five electron oxidation into L-citrulline and NO in a calmodulin (CaM) dependent response to physiological stimuli with the involvement of nicotinamide-adenine-dinucleotide phosphate (NADPH) and molecular oxygen (Figure 1.1)[3, 13, 33, 35-36]. Three isoforms of NOS have been indentified: nNOS (NOS 1; neuronal), iNOS (NOS 2; inducible), and eNOS (NOS 3; endothelial)[3, 6, 13, 34, 36-40]. Table 1.1 lists their corresponding properties.

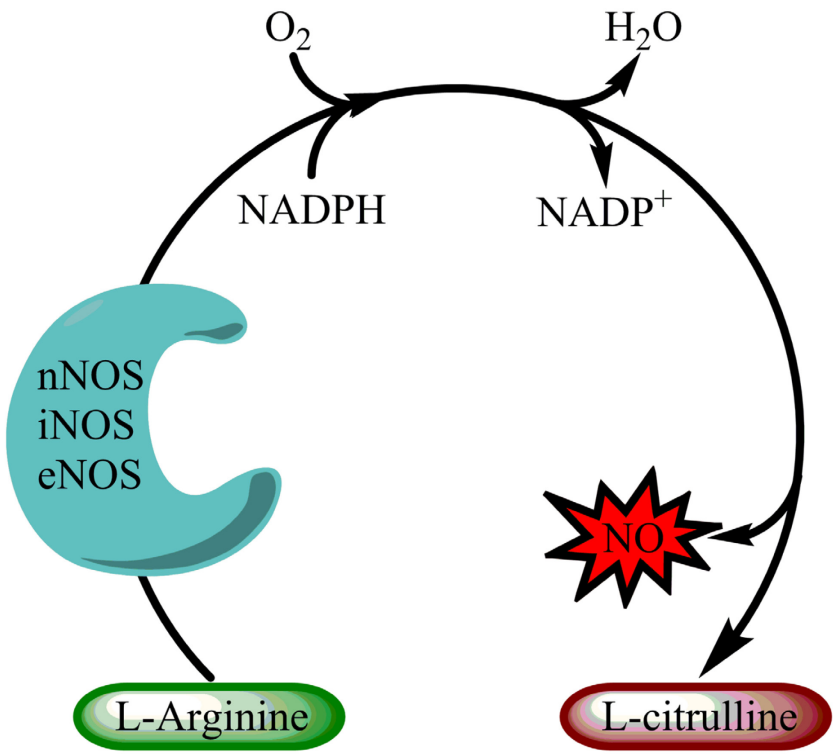

Figure 1.1. Physiological production of nitric oxide from L-arginine. Figure 1.1 shows the production of nitric oxide and L-citrulline from L-arginine. Production occurs via nitric oxide synthases (NOSs).

Table 1.1. Summary of nitric oxide synthase enzyme properties. Table 1.1 summarizes the nitric oxide synthase isoforms and their relevant properties.

	nNOS	iNOS	eNOS
Gene	NOS 1	NOS 2	NOS 3
Mass	130 kDa	150–160 kDa	135 kDa
Type	Constitutive	Inducible	Constitutive
Regulation	Ca^{2+} Dependent	• Transcriptional Regulation • Ca^{2+} Independent	• Ca^{2+} Dependent • Phosphorylation
Location	• Nervous Tissue • Skeletal Muscle	• Immune System • Cardiovascular System	Endothelium
Function	• Neurotransmission • Potentiation	• Inflammation • Host Defense	• Platelet Inhibition • Inhibition of SMC Proliferation • Regulation of Vascular Tone
NO Production	Low, transient levels	High, limited duration	Low, transient levels

The three isoforms maintain an amino acid sequence similarity of 55%[34]. The factors influencing the generation of NO from NOSs are shown in Figure 1.2.

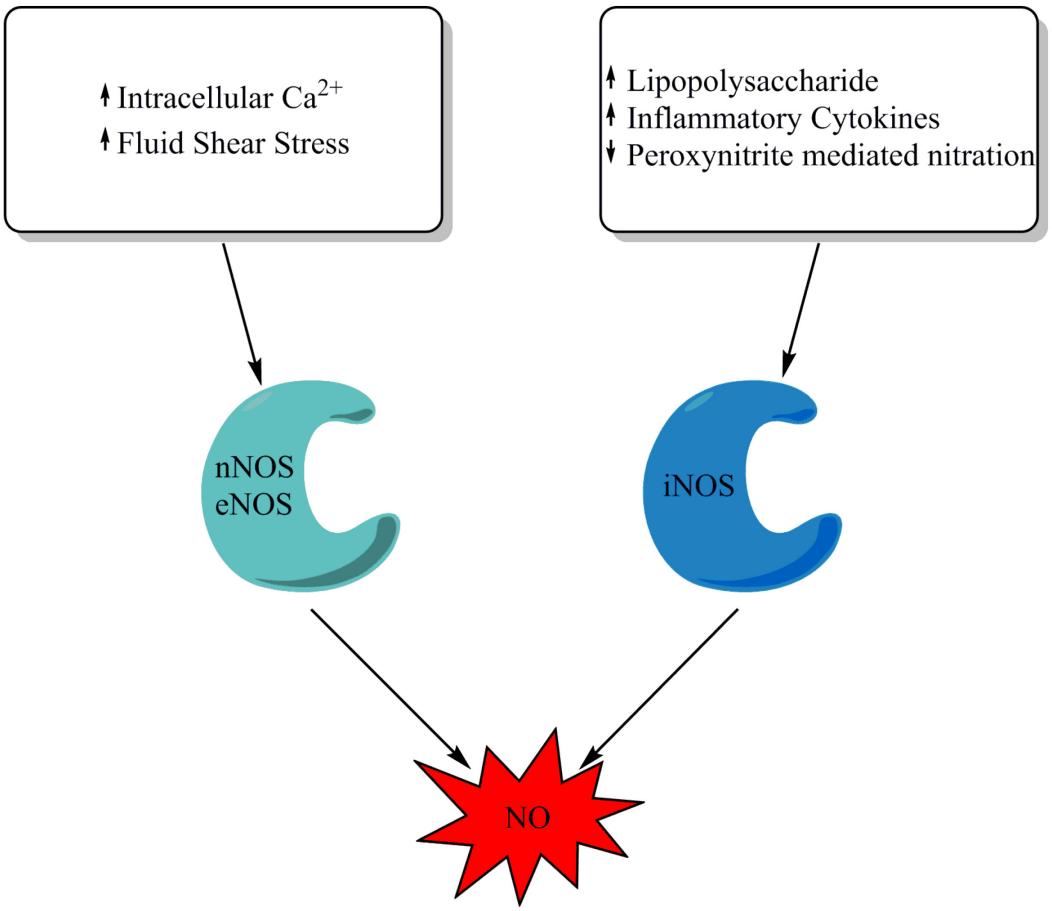

Figure 1.2. Factors affecting physiological nitric oxide production. Figure 1.2 shows the factors influencing the production of NO from the NOS isoforms.

nNOS is responsible for the production of NO in macrophages during inflammation and phagocytosis, resulting in the macrophages cytotoxic properties[11, 33]. nNOS is expressed within certain neurons in the brain and has recently been implicated in regulating functions such as learning and memory. In the central nervous system, nNOS mediates long-term potentiation and inhibition of synaptic signals[33]. The most well-known activator of nNOS is lipopolysaccharide (LPS), produced by gram negative bacteria, specifically *Escherichia Coli*, during sepsis[34]. nNOS is also activated by the presence of L-arginine and one or more inflammatory cytokines including tumor necrosis factor-α (TNF-α), interferon gamma (IFN-ϒ), and interleukin-1 (IL-1)[13, 34]. Additionally, the activity of iNOS can be down regulated through peroxynitrite-mediated nitration, decreasing its catalytic activity[13].

iNOS, first characterized in macrophages and termed inducible NOS, is not usually present within cells. Though it is generally associated with macrophages, any cell is capable of expressing iNOS given that the requisite inducing agent is present[33, 41]. Unlike eNOS and nNOS, iNOS is constantly active and does not have a dependency on intracellular Ca^{2+} concentration, as it is permanently bound to CaM due to its high binding affinity even at low intracellular calcium concentrations[5, 11, 13].

eNOS is usually found within the endothelium, but has been detected in other cell types such as cardiomyocytes, platelets, and neurons. eNOS, unlike nNOS, can be upregulated by increased fluid shear stress due to blood flow by phosphorylation of its reductase domains[3, 34, 42].

eNOS and nNOS are referred to as constitutive NOSs, and are generally dormant under normal physiological conditions[34, 37]. eNOS and nNOS are capable of producing nanomolar concentrations of NO over relatively short time periods, whereas iNOS is able to produce micromolar concentrations over longer time periods, on the order of hours to days, which matches their respective physiological functions[5]. Differing from iNOS, eNOS and nNOS synthesize NO in a periodic manner. The production of NO by eNOS and nNOS is regulated by a Ca^{2+} dependent CaM pathway[3, 33-34, 40-41], where activation of CaM is heavily dependent on intracellular calcium levels. Acetylcholine has been found to increase intracellular Ca^{2+} concentrations in endothelial cells[13]. A conformational change in flavin mononucleotide (FMN) post-CaM activation results in NO synthesis by eNOS and nNOS[5].

1.3. Physiological Reactions of Nitric Oxide

In the physiological environment, NO is capable of reacting with transition metals, oxygen, and superoxide, among others. Common products generated from these reactions include metal-nitrosyl compounds, nitrogen oxides, and peroxynitrites, respectively[3, 11, 13]. The three main contributors to the formation of metal-nitrosyl complexes during interactions with NO are copper, iron, and zinc[13]. Enzymatic regulation is possible through interactions of NO with transition metals present in the enzyme or associated proteins[13]. NO acts on sGC in a reaction with its ferrous heme center to convert guanosine-5'-phosphate (GTP) into cGMP, by forming a ferrous-nitrosyl-heme complex[3, 13]. Even low concentrations (< 100 nM) of NO are capable of activating sGC. Activation of sGC can lead to a 400–500 fold increase in the rate of cGMP synthesis[13, 43]. Mitochondrial respiration is inhibited by NO through a reversible reaction with cytochrome c oxidase (CcO), responsible for mitochondrial adenosine triphosphate (ATP) synthesis[44-45]. CcO contains two heme moieties and two Cu^{2+} centers[13].

Due to NO's existence as a free radical gas, its unpaired electron is capable of interacting with other reactive oxygen species (ROS). ROSs, in low concentration, are believed to

play key roles in the physiological environment, including regulation of cell signaling and gene expression[46]. Conversely, high levels of ROSs can contribute to vascular dysfunction, inhibited cellular proliferation and growth, as well as genetic damage[46]. These reactions are briefly discussed below.

NO is able to react with molecular oxygen, and as O_2 is a triplet molecule, it is favored to react with molecules containing unpaired electrons, such as NO. The result of the reaction between NO and O_2 produces NO_2^-, with intermediates of N_2O_3, nitrosonium (NO^+) and NO_2 [3, 11, 13, 47-50]. This reaction scheme is shown in equations 2.1–2.4. The lipid bilayer is a probable site for the reaction between NO and O_2, as both are preferentially drawn to the hydrophobic environment[12]. The conversion of NO and O_2 into N_2O_3 is termed NO autoxidation[13]. These intermediates are believed to be involved in S-nitrosation through the nitrosolation of the nitrosonium intermediate with thiols, secondary amines, and phenolics[13, 51]. This autoxidation is heavily dependent on the concentrations of NO and O_2, which result in high concentrations of N_2O_3 at the reaction site. N_2O_3 has been implicated in the alkylation of DNA through the formation of N-nitrosoamines[52]. The reaction kinetics from NO to NO_2^- is a third order, rate determining reaction[13]. NO can react with oxygenated hemoglobin (Hb) to produce methemoglobin (metHb) (Equation 3) and with deoxygenated Hb to produce S-nitrosohemoglobin (SNOHb)[53].

$$2NO + O_2 \longrightarrow 2NO_2 \quad (2.1)$$

$$NO + NO_2 \rightleftharpoons N_2O_3 \quad (2.2)$$

$$N_2O_3 + H_2O \longrightarrow 2NO_2^- + 2H^+ \quad (2.3)$$

$$2NO_2 + H_2O \longrightarrow NO_2^- + NO_3^- \quad (2.4)$$

$$HbO_2 + NO \longrightarrow metHb + NO_3^- \quad (3)$$

Reactions of NO with other physiological radicals proceed in a nearly diffusion rate-controlled manner. In addition, NO is the least reactive of all the free radicals present in the physiological environment, endowing NO with antioxidant properties[11]. The superoxide anion, O_2^-, interacts with NO to form peroxynitrite ($ONOO^-$) in a rapid, diffusion rate limited reaction[3, 49, 54]. This reaction is shown in Equation 4[11].

$$NO + O_2^- \longrightarrow {}^-OONO \quad (4)$$

Peroxynitrite is a highly reactive molecule, though not a free radical[55], thought to be produced in mitochondria and immune cells[13, 55]. The intermediate of peroxynitrite, ONOOH•, is thought to be capable of nitrating and oxidizing lipids, proteins, and nucleotides, causing irreparable damage to DNA and protein structures[13, 55]. It has been theorized that single strand DNA damage as a result of elevated peroxynitrite formation can be linked to attacks on DNA's sugar-phosphate backbone[52]. Reactions with superoxide in the formation of peroxynitrite may limit the amount of physiological NO available, as this reaction is not reversible[53]. Equimolar ratios of NO and superoxide are favored for the production of peroxynitrite[3]. In addition, overproduction of peroxynitrite has been implicated in cellular apoptosis and necrosis[13].

One of the largest sources of superoxide is located in the inner mitochondrial membrane, as incomplete respiration causes molecular oxygen to be reduced[54]. In the cytosol, several enzymes catalyze the one electron reduction of oxygen to superoxide. Additional mechanisms for the formation of superoxide include oxidative decomposition of molecules, such as flavin adenine dinucleotide-hydroquinone form ($FADH_2$)[54]. An important mechanism of superoxide production in the vasculature is the autoxidation of oxygenated Hb to its reduced metHb form[54]. Since superoxide has a shorter lifetime than NO, peroxynitrite is generated in areas adjacent to superoxide sources[54].

eNOS uncoupling can initiate the production of superoxide from eNOS rather than NO[38, 46]. Several mechanisms can result in a phenomenon known as eNOS uncoupling, including a reduced bioavailability of tetrahydrobiopterin (BH_4). This uncoupling reaction will propagate due to the continued production of superoxide. Superoxide generated during uncoupling reacts with NO to generate peroxynitrite, while NADPH oxidases participate in the cascade as a superoxide producer. In a similar cascade, overexpression of eNOS in the absence of a similar increase of BH_4 can result in eNOS uncoupling due to a disproportionate amount of the enzyme in relation to the cofactor[38].

In physiological environments, peroxynitrite may exist in the anion form or acid form ($ONOO^-$/ONOOH) (Equation 5)[3, 11]. Protonation of the acid form results in the production of the nitrate anion (Equation 6). Peroxynitrite reacts with physiologically present carbon dioxide (CO_2) to form nitrosocarboxoperoxylate ($ONOOCO_2^-$) (Equation 7)[54]. $ONOOCO_2^-$, a stronger nitrosating agent than peroxynitrite, has been shown to generate NO_2• and CO_3^-•, finally producing a nitronium ion (NO_3) (Equation 8)[3, 11, 54-58]. Peroxynitrite is also able to react with free thiols to form disulfides and sulfenic acid (Equation 9). Peroxynitrite formation is more likely under infectious or inflammatory conditions in which high NO and O_2^{-}• concentrations exist, increasing the reactions with CO_2 and production of $ONOOCO_2^-$ [3, 11, 56-57]. Under these conditions, NO_2• and CO_3^-•

are formed in higher relative quantities[3, 11, 56-57]. $CO_3^{-\bullet}$ has been proven to form protein-protein and DNA-DNA crosslinks, and has been implicated in the tissue damage associated with inflammatory and infectious states[11, 59-60].

$$ONOO^- + H^+ \rightleftharpoons ONOOH \quad (5)$$

$$ONOOH \longrightarrow NO_3^- + H^+ \quad (6)$$

$$ONOO^- + CO_2 \longrightarrow ONOOCO_2^- \quad (7)$$

$$ONOOCO_2^- \longrightarrow \cdot NO_2 + CO_3^{\bullet -} \quad (8)$$

$$OONO^- + RSH \longrightarrow RSSR, RSOH \quad (9)$$

The reaction between NO and the superoxide anion is three times as rapid as the activity of superoxide dismutase (SOD)[13, 46]. SOD decomposes superoxide to form molecular oxygen and hydrogen peroxide (Equation 10)[42], depleting superoxide supplies required to form peroxynitrite while performing a vital antioxidant function[13]. Nitrite generation is a potential fate of NO in a reaction with •OH, formed as byproducts of hydroxyl radical formation from H_2O_2 produced from the dismutation of superoxide (Equation 11)[3]. Much like the NOS enzymes, three forms of SOD are physiologically present in humans: SOD 1 (Cu-Zn-SOD) in the cytoplasm, SOD 2 (Mn-SOD) present in mitochondria, and SOD 3 which is extracellular[42, 46]. SODs act to mediate the cytotoxic effects of superoxide[46]. Since the reaction between SOD and NO is the most efficient reaction known in the realm of NO chemistry, the biological half-life of NO is highly dependent on local SOD concentrations[46]. Physiological NO can be generated in sufficient quantities that its reaction with superoxide is able to exceed the capacity of endogenous SOD[55]. A critical function of SOD is to protect NO and NO-mediated signaling pathways[46]. The production of hydrogen peroxide by SOD likely contributes to intracellular signaling, as hydrogen peroxide is relatively stable and easily diffuses through cell membranes[46].

$$2O_2^- + 2H^+ \xrightarrow{SOD} O_2 + H_2O_2 \quad (10)$$

$$NO + \cdot OH \longrightarrow HNO_2 \rightleftharpoons NO_2^- + H^+ \quad (11)$$

1.4. Physiological Transport of Nitric Oxide

Though NO is both nonpolar and uncharged, it is shown to be reasonably soluble in aqueous solutions (1.9 mM at 298K; 1 atm)[61]. In hydrophobic solvents, its solubility increases by a factor of approximately 10 [62]. Transport of NO within physiological

systems has been theorized to occur through simple diffusion across the lipid bilayer[11]. In physiological buffer, the diffusion rate of NO is around 3300 $\mu m^2 \cdot s^{-1}$ [63]. In part, this permits NO to function intracellularly without being reliant on membrane transport proteins, while also being capable of passing into the intracellular space[11]. As a free radical gas, NO has an effective lifespan of less than 1 second in physiological environments due to its short half-life, which limits its activity to a radius of approximately 100 μm from its production source[31, 64-66]. The freedom of movement of NO makes it an extremely potent therapeutic agent as it can diffuse through tissue without external aids, will behave based on the generated concentration gradient, and its short half-life limits its activity within location adjacent to its production source.

1.5. Concentration Effects of Nitric Oxide

Interestingly, the level and duration of NO release has been demonstrated to have widely varying effects within the physiological environment, and NO has been classified as a bimodal agent for this reason[5, 19]. Overproduction of NO has been attributed to increased incidents of cancer[4] and has been found to play a role in neuronal death following a cerebrovascular stroke[67]. High levels of NO have also been linked to depleted energy reserves due to inhibition of mitochondrial respiration and glycolysis, both vital cellular functions[68-69].

Though NO has shown promise as a cytotoxic agent to microbes, viruses, and tumor cells, high concentrations of NO can also negatively affect the surrounding environment and healthy organisms[3, 33]. When NO releasing materials are applied *in vivo*, the overproduction or excessive release of NO can damage neighboring cells and tissues through several mechanisms. Initially, NO can cause direct harm at elevated concentrations to cellular structures. As local concentrations of O_2^- increase, NO concentrations are affected as the equilibrium shifts towards higher $ONOO^-$ concentrations, resulting in the suppression of NO activity[33].

Because it is a free radical, NO is capable of causing damage to healthy cells and tissue, especially during production by iNOS due to the significantly higher output as compared to the constitutive NOS isoforms. As a control for NO, large quantities of O_2^- are generated in conjunction with NO. The two components then form $ONOO^-$/ONOOH, which functions as a cytotoxic mediator to reduce the tissue damage associated with increased NO concentrations[34, 70-71]. Interestingly, cells responsible for the production of significant quantities of NO are not themselves harmed by its toxic effects. In macrophages, the expected cause of this self-protection is due to anti-oxidative systems[72], whereas in endothelial cells, the elevated levels of intracellular calcium are thought to inhibit guanylate cyclase activity[34, 73].

1.6. Endogenous Nitric Oxide Donors

S-nitrosation of components endogenously present within the body can form stable NO donors. NO produced by the constitutive NOS enzymes is stored as a nitrosothiol in albumin, and may become physiologically active as S-nitrosoglutathione or S-nitrosocysteine[34, 74-75]. To date, over 100 such substrates have been identified as being capable of S-nitrosation[76].

Indirect disulfide formation with reduced glutathione (GSH) forms S-nitrosoglutathione (GSNO), a reversible reaction[12, 77]. Direct redox reactions between GSH and NO are slow, and the formation of GSNO would follow the previously mentioned third order reaction between NO and molecular oxygen[12, 78]. GSNO has been thought to be critical for NO's physiological functions[12]. GSNO has been shown to be more stable than S-nitrosocysteine[12]. Studies have shown decreased susceptibility of GSNO to copper ion mediated decomposition than S-nitrosocysteine[12]. An additional mechanism of GSNO decomposition is through a trans-nitrosation reaction, where GSNO can donate its nitroso functional group to other free thiols (Equation 12)[12].

$$\mathrm{RSNO + R'SH \longrightarrow RSH + R'SNO} \qquad (12)$$

It has been theorized that the trans-nitrosation reaction, with a rate constant of 1–300 $M^{-1} \cdot s^{-1}$, is responsible for the biological activity of GSNO through the transfer of the nitroso group to a more labile molecule capable of moving through the cellular membrane. These trans-nitrosation reactions with intracellular components may be responsible for the reduced biological activity of GSNO[12]. S-nitrosation of cysteine is a post-translational, reversible process critical in the regulation of protein function and cell signalling[79-80]. S-nitrosocysteine (SNOC) is less stable than GSNO, and little is known about it in comparison[81].

1.7. Overview of Wound Healing

NO plays critical roles in the wound healing cascade. Wound healing begins immediately following insult or injury to tissues, persisting from several days to several months depending on the severity and location of the damaged tissue. The wound healing timeline (Figure 1.3) is composed of 5 stages: blood coagulation, inflammation, cell proliferation, lesion contraction, and remodeling[19, 82]. These stages do not proceed linearly; rather, instances of each overlap the preceding and following phases in a delicate balance. If interrupted or delayed, the wound healing process can be marginally extended or devolve into a chronic, non-healing state[83].

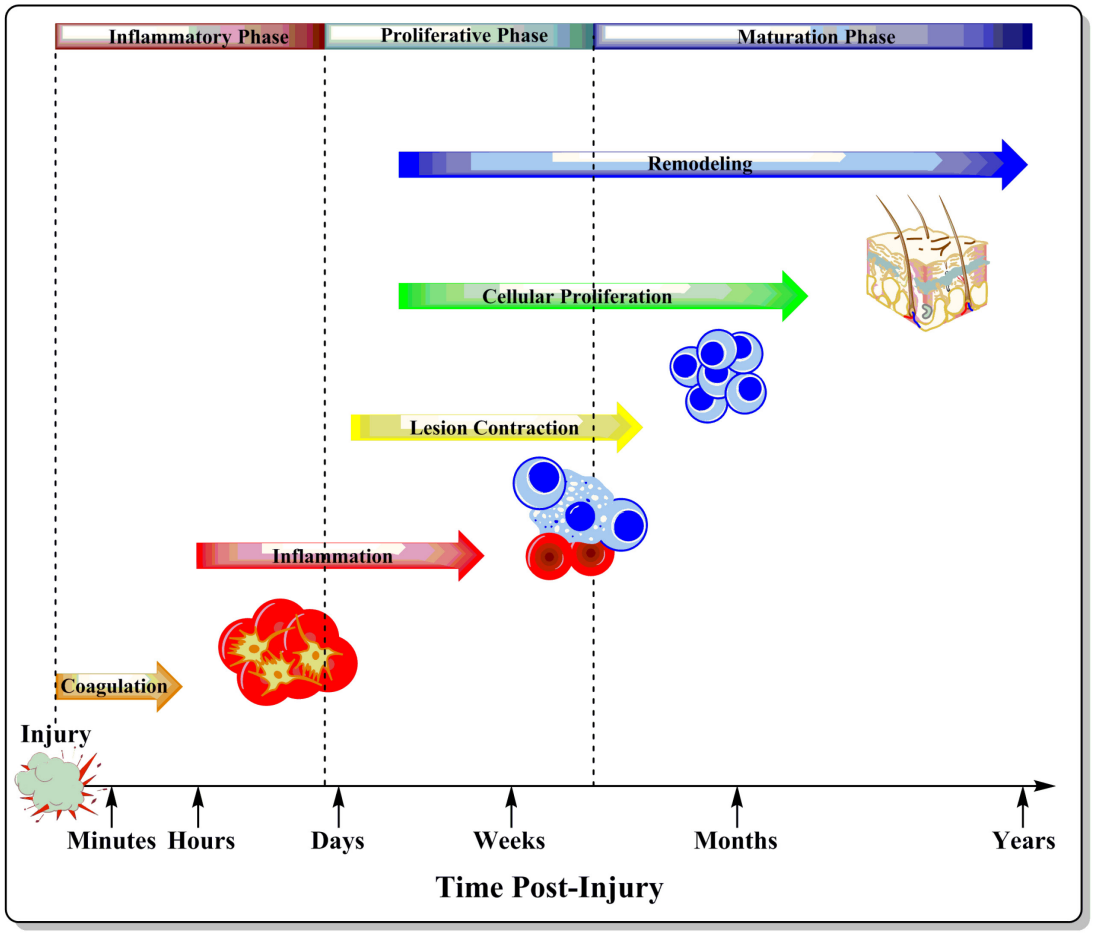

Figure 1.3. Wound healing timeline. This figure shows the relative timeline of the wound healing process and its phases.

Platelet adhesion and fibrin deposition begin the coagulation process in an attempt to stem the loss of blood, eventually forming a blood clot[19, 82]. Importantly, platelets will not adhere to healthy, normal endothelial cells, but will adhere to injured and exposed connective tissues through surface membrane adhesion receptors recognizing the amino acid sequence arginine-glycine-aspartic acid, commonly found in collagen[82]. Platelets will adhere to man-made materials, such as those typically employed in biomedical implants. At this point, the coagulation cascade, described above, is activated. Simultaneous growth factor secretion activates fibroblasts and endothelial cells, and beings macrophage recruitment to the affected area[19, 82].

The inflammation phase begins by recruiting neutrophils, lymphocytes, and macrophages to protect the exposed tissue. Additionally, macrophages begin removing the damaged tissue in preparation for tissue regeneration and scar formation[19]. The vasculature becomes leaky, and alterations the normal flow of blood may occur[84]. Granulation tissue,

defined by the numerous capillaries and red coloration, is indicative of a normal resolution of the inflammatory phase of the wound healing process[19, 82].

The proliferation phase of wound healing generally overlaps the inflammation phase and begins by encouraging angiogenesis at the wound site to develop the architecture required for continued remodeling and repair, often occurring approximately 3 days after the primary insult[83]. Growth factors, such as those released from activated platelets, attract neutrophils and monocytes from the flowing blood[82]. These initial growth factors are then degraded through protease reduction to be replaced by growth factors, such as vascular endothelial growth factor (VEGF) and fibroblast growth factor (FGF), produced by the recruited neutrophils, endothelial cells, macrophages, and fibroblasts. In addition, fibroblast migration and re-epithelialization occurs. This process can last up to several weeks[19, 82].

The lesion contraction phase is a dynamic, loosely condensed set of processes which prepares the wound site for the remodeling phase. Cells, especially fibroblasts, deposit extracellular matrix (ECM) proteins beginning at the wound margin proceeding inward. Transforming growth factor-β (TGF-β) stimulates fibroblasts to produce collagen, fibronectin, and glycosaminoglycans (GAGs), while platelet-derived growth factor (PDGF) encourages the production of fibronectin and hyaluronic acid. ECM deposition forms a provisional matrix allowing cellular migration, protein synthesis, and further support for angiogenesis. Concurrently, neovascularization continues through this stage to support the newly formed tissue. VEGF, released by both macrophages and endothelial cells, plays a critical role in the formation of angiogenic sprouts required to supply nutrients and oxygen to the rapidly forming tissue. Just prior to the remodeling phase, the granulation tissue developed throughout the inflammation and proliferation phases begins to retract and become a more densely packed, compacted structure. The mechanism behind this phenomenon is attributed to the contractile activity of myofibroblasts[19, 82].

The remodeling phase begins with tissue deposition in areas containing abundant collagen. During this phase, cells undergo apoptosis to form a relatively acellular scar, while growth factor migration subsides. Tissue remodeling during this stage results in changes to the collagen synthesis, where the ratios of the types of collagens and their structure and organization differ from normal, healthy tissue. The remodeling phase can last from weeks to several years[19, 82].

1.8. Nitric Oxide's Role in Wound Repair

NO's presence and role in wound repair is demonstrated in every major step, from the mediation of inflammation to recruitment and control over macrophages, angiogenesis, platelet aggregation and clot formation, and finally matrix deposition and eventual tissue remodeling[3, 19, 82, 85]. During inflammation, reactive nitrogen and reactive oxygen species

are released by activated platelets and inflammatory cells, causing localized tissue damage, including damage to surrounding healthy cells[5, 86].

NO plays an important role in angiogenesis, which is a critical step in the wound healing process. Without neovascularization, nutrients, oxygen and waste are unable to be transported from the neo-tissue. Similarly to other physiological roles of NO, the level and duration of exposure is a large contributing factor to the pro-angiogenic or anti-angiogenic response to NO[5]. NO can promote angiogenesis through inhibition of endogenous anti-angiogenic factors and has demonstrated an ability to recruit bone marrow-derived cells and perivascular cells during angiogenesis[5]. VEGF, shear stress, angiopoietins, and metabolic stress are potential factors causing endothelium-derived NO expression by eNOS[5, 87].

1.9. Nitric Oxide's Role in the Immune Response & Inflammation

During early research into immune function, NO was known to be a component in the function of activated macrophages. Since then, a significant number of NO's roles in the immune response have been discovered. These include a broader understanding of its function in infection control, regulation of signaling cascades, transcription factors, leukocyte activity and cytokine production, as well as leukocyte proliferation and apoptosis[13, 37, 88-89]. Transcriptional regulation, such as that demonstrated in the nuclear factor kappa B (NF-κB)/Rel pathway[5, 13, 90-92], by NO of cellular responses to nitrosative and oxidative stress is also a large component in the immune response[13].

NO has been shown to regulate the function of neutrophils, including the degranulation, superoxide generation, and chemotactic movement. It is also known as a regulator of recruitment[13]. Endogenous NO and NO donors have demonstrated regulation of leukocyte rolling and adhesion to injured endothelium, with a potential dependency on cGMP[93-94]. Globally, NO is known to down regulate leukocyte adhesion molecules such as E-selectin[95], P-selectin[96], and intracellular adhesion molecule-1 (ICAM-1)[13, 94].

NO also has roles in the regulation of immune function. As an immune regulator, NO is believed to function by regulating cell proliferation and death through the inhibition of specific genes[34]. As in other functions throughout the body, NO is also believed to possess anti-apoptotic effects. NO has been shown to regulate mast cell function, and when produced with IFN-ϒ, inhibits the immunoglobin based secretions of mast cells, to include histamines[34].

Conversely to these observations, NO has also demonstrated some capacity to inhibit factors and processes normally though to be beneficial in the immune response, including inhibition of cytokines produced by lymphocytes, monocytes, and eosinophils[97-98]. These cytokines include several classes of interleukins, IFN-ϒ, and TNF-α[34, 99].

While an important part of the immune response, significant quantities of the superoxide anion generated in leukocytes can cause damage to healthy endothelium, resulting in vascular permeability and apoptosis[34, 100]. Recent evidence suggests that NO can contribute to the inflammation response through regulation of inflammation mediators through the production of intracellular ROSs. In particular, non-phagocytic oxidases (NOXs) can be constitutively released in several tissue types[34, 101]. ROSs produced by these enzymes have demonstrated control over adhesion molecule regulation as well as chemokine and cytokine expression[102-103]. Stimulation of MAP-kinase activity has been linked to these ROSs, activating transcription factors[34].

NO has several roles in both the acute and chronic inflammatory processes. In the acute stage of inflammation, NO production from eNOS induces vascular smooth muscle cell relaxation, ultimately leading to increased vascular permeability due to leaky endothelial cells. This response is, in part, responsible for the swelling and redness associated with the early stage inflammation response[104]. Septic shock is believed to originate from an overproduction of NO by iNOS in response to the bacterial infection, eliciting an acute, systemic inflammatory response[104]. Production of both peroxynitrite and superoxide are increased during inflammation[13], which has been implicated in further damage to the surrounding medium. In addition, superoxide production may deplete NO reserves in the local environment.

1.10. Nitric Oxide's Role in Cellular Proliferation

As in other aspects of NO's functionality, its effect on cellular proliferation maintains a significant dependency on the level, duration and timing of NO exposure. NO is simultaneously capable of inhibiting cellular migration and inducing senescence, while also promoting cellular proliferation[29, 105-107]. In human umbilical vein and coronary artery endothelial cells, NO has been shown to inhibit their proliferation at concentrations above 100 μM[108]. Vascular smooth muscle cell (vSMC) proliferation is inhibited in a dose dependent manner by NO through cGMP dependent and independent mechanisms[9, 40]. In contrast, NO is also known to cause cellular proliferation in cultures containing nanomolar concentrations of NO[107, 109-110]. Up regulation of VEGF stimulates NO production from eNOS, eliciting endothelial cell proliferation, migration, and organization to form angiogenic sprouts[9, 111-113].

NO also maintains some control over cellular apoptosis through the p53 tumor suppressor gene, B-cell lymphoma 2 (Bcl-2), and mitochondria[114]. High concentrations of extracellular NO induce apoptosis through the aforementioned inhibition of mitochondrial ATP production and direct oxidative and nitrosative damage of cellular membranes[115]. NO can regulate apoptosis through S-nitrosylation of NF-κB and Bcl-2[92, 116]. Alternatively, and of particular interest in anti-tumorigenic therapies, p53 can lead to

cellular apoptosis after oxidative DNA damage by NO[5]. NO can inhibit apoptosis through radical interferences and cGMP[117-118]. These effects have been observed in endothelial cells, vascular smooth muscle cells, and hepatocytes[5, 119].

1.11. Nitric Oxide's Role in the Vascular System

In addition to the previously mentioned effects of NO on the vascular system, laminar shear stress exerted on the endothelial arterial and venous lining maintains a propensity to elicit NO generation via eNOS production[120]. Shear stress increases up regulation of NO output from eNOS by acutely increasing the intracellular Ca^{2+} levels, leading to an increased prevalence of calmodulin binding to eNOS[121]. Though the initiation of shear induced NO generation seems to be due to intracellular Ca^{2+} levels, the production of NO during shear stress far exceeds the ability of Ca^{2+} alone[120, 122]. Intracellular calcium-independent production of NO due to shear stress is a direct result of phosphorylation of sites on eNOS resulting in an electron flow from the reductase to the oxygenase domains[120, 123-124]. The most common of these in human eNOS are Ser1177 and Thr495[42]. After several hours of exposure to laminar shear stress, eNOS production is upregulated, permitting the production of higher NO concentrations[120].

Oscillatory shear stress, on the order of ± 15 dynes$\cdot$cm^{-2}, also stimulates NO generation and eNOS synthesis through a similar pathway as in the laminar shear stress case. Unlike the pathway leading to an increase in NO production under laminar flow conditions, ROSs including superoxide and hydrogen peroxide are produced in the endothelial cells during oscillatory flow conditions and lead to the observed increase in NO through a separate, but related, mechanism as determined in the laminar shear state[42, 120, 125-126].

Under both laminar and oscillatory shear conditions, superoxide and hydrogen peroxide are produced by NADPH oxidase, albeit under different pathways[42, 120, 127]. Concomitantly, superoxide dismutase and glutathione peroxidase is produced to scavenge these components, respectively[120, 128-129].

1.12. Physiological Nitric Oxide Measurement Techniques

NO measurement from biological sources is of the utmost importance in gaining an understanding of its seemingly endless roles within the body. When the task of *in situ* measurement is approached, researchers often encounter severe limitations in both access to the source and interference from other potential contaminants. Because it is a free radical and extremely labile molecule, NO readily reacts with molecular oxygen, ubiquitously present in the environment and physiology[130]. Coupled with its extremely short half-life, this makes the measurement of NO challenging. The relatively miniscule amounts of NO available also make its measurement a daunting task. Several techniques have been developed which allow researchers to determine the total amount of NO produced, however few offer the ability to detect, in real time, the generated NO flux.

Both types of information are required to make solid conclusions about the efficacy of NO as a therapeutic agent[131].

One of the earliest indirect measurement techniques applied to NO was a diazotization assay described by Peter Griess in 1879[132-133]. It is the most commonly used NO analysis technique today due its simplicity, cost, and robustness[131]. In this assay, the stable autoxidation product of NO, nitrite (NO_2^-), is analyzed to estimate the amount of NO produced within a sample, and compared to a $NaNO_2^-$ or $NaNO_3^-$ standard curve[36, 131, 134]. The Griess reagents consist of sulfanilamide, HCl, and N-(1-napthyl)-ethylenediamine (NED)[36, 63, 135]. The reaction produces an azo dye that can be analyzed through an absorption measurement with a spectrophotometer at 458 nm[63]. As NO can be oxidized to nitrate (NO_3^-), the sample must first be treated to reduce NO_3^- to NO_2^- [134]. The Griess reagent assay can effectively detect nitrite in the range of 0.1–40 μmol/L with a sensitivity of approximately 1 μmol/L[63, 131, 134].

The most common downfalls reported with the Griess assay are the low detection limits compared to alternative methods and the necessity of eliminating contributions due to background NO_2^- and NO_3^- [131, 134]. Additionally, Griess reagent detection of NO is unable to be used for real-time analysis of NO production due to the necessary detection methods and chemical reactions[131].

Direct amperometric measurements by electroxidation of NO with platinum, carbon, or polymeric porphyrin electrodes are possible due to the oxidation reaction at the electrode's tip[36, 63, 134-135]. A three electron transfer from NO to the grounded anode generates NO^+ which is further converted to nitrite (NO_2^-) in the presence of OH^- (Equations 13.1–13.3)[36, 63, 134]. The current generated in the oxidation reaction is directly proportional to the concentration of NO. This technique provides favorable results with a linear response over small concentration ranges, with reported nanomolar (10 nmol/L) sensitivity[130, 134]. To date, detection limits as low as 83 pM and dynamic linear ranges of 0.2 nM–4.0 μM have been reported[63, 131, 136]. The high sensitivity and response times make this measurement technique favorable for *in situ* analysis of NO kinetics[36]. Trapping of NO under the probe tip can lead to artificially elevated NO levels. In these cases, microelectrodes with tip sizes ranging from 30–200 μm can be used to minimize this effect[134]. Small probe sizes allow NO measurements to be taken from single cells[63].

$$NO \longrightarrow NO^+ + e^- \quad (13.1)$$

$$NO^+ + OH^- \longrightarrow HNO_2 \quad (13.2)$$

$$HNO_2 + H_2O \longrightarrow NO_3^- + 2e^- + 3H^+ \quad (13.3)$$

An incredibly versatile, direct measurement assay is the chemiluminescent analysis of NO. Developed initially to detect NO in smog[130], this technique has been adopted both in the physiological measurement of NO in research, but also in clinical settings from exhaled breath. In a reaction with ozone, NO generates an excited state radical NO_2 and molecular oxygen[36, 63, 131, 134, 137]. As the radical relaxes and returns back to its ground state, it emits photons whose wavelengths vary between 640–3000 nm with a peak in intensity seen at 1100 nm[3, 135]. The reaction is shown in equations 14.1–14.2. This technique is often coupled with a photomultiplier tube (PMT) to detect gaseous NO above the headspace of a liquid or solid sample, and the generated PMT signal is directly proportional to the NO levels, and is thus linear[36, 63, 131, 135]. The PMT itself is capable of detecting wavelengths between 600–900 nm[63, 130-131, 134, 138]. Though this reduces the detection limit, it is still sufficient for chemiluminescence to be the most sensitive NO detection method currently available[3]. A reduction in the reaction chamber pressure sharply decreases the number of potential molecules that could quench the signal[3].

$$NO + O_3 \longrightarrow NO_2^* + O_2 \quad (14.1)$$

$$NO_2^* \longrightarrow NO_2 + h\nu \quad (14.2)$$

The rate of reaction between NO and O_3 is approximately 10^7 $L \cdot mol^{-1} \cdot s^{-1}$, while the sensitivity of NO_2* detection of light emitted from the reaction is 100 pmol/L[134]. These reaction rates, coupled with PMT based detection, offers real-time NO measurement, allowing significant insight into the reaction kinetics of NO generation[63]. The gaseous NO is transported to the reaction cell under vacuum in combination with an inert sweeping gas (often nitrogen) to prevent reaction with O_2. The specificity of the assay technique is very high, where only NO and one other component may be detected. H_2S will react with ozone in the same manner as NO, however the emission wavelength generated will be of a different wavelength, easily removed from the signal by a red band pass filter[36, 130-131, 134]. In addition, gas phase measurement ensures that nitrites, nitrates, and other common biological components that would otherwise react with O_3 are excluded[130]. The response time of the measurement is dependent on the concentration of NO and the integration time of the PMT. The sensitivity of chemiluminescent detection is commonly reported between 20–50 pmol[130]. The dynamic range of the instrument is exceptionally large, with detectable limits between 0.5 ppb (0.66 pM in 100 mL PBS) to 500 ppm[63, 131].

Often, groups investigating the behavior and applications of NO report its presence in concentrations. This method is useful in the chemical analysis of NO, however it can be misleading when reported in therapeutic applications. Many groups have found that

reporting NO values as a flux delivered over an area to be a better assessment of the true dose received by the target. The discrepancies between the reporting methods and subsequent difficulty in comparing values and doses between groups has become a significant hurdle as NO becomes a more desirable therapeutic agent. Often, key information including the flux, duration and rate of release, and method of delivery are not given in published research. Additionally, the mass, volume, or porosity of the sample is required to normalize the data to other published results. To truly assess the efficacy of NO as a therapeutic agent, this information is required for an accurate comparison[131].

The predicted concentration of NO in physiological environments is estimated between 1 nM and 100 nM, while other methods predict significantly lower values of 100 pM–5 nM[11, 139-142]. On activation of macrophages during illness, injury, or inflammation, these levels will increase by several orders of magnitude. Though many groups utilize concentration based measurements of NO, others have found that a measurement of NO's basal flux is a more accurate method of determining NO dosage in therapeutic applications. The currently accepted estimate for the endogenous NO flux generated from an intact, healthy endothelium is $0.5–4\times10^{-10}$ mols·cm^{-2}·sec^{-1} [143-144].

1.13. Classes of Nitric Oxide Donors

Several classes of NO donors, including S-nitrosothiols, N-diazeniumdiolates, nitrosamines, metal nitrosyl complexes, and nitrates have been developed, however translation to clinical use has been lacking in their continued development[19, 145]. In order to attain clinical relevancy, NO donors must be able to deliver specific, easily definable therapeutic levels of NO. Here, N-diazeniumdiolates and S-nitrosothiols will be explored.

N-diazeniumdiolates (NONOates; X-[$^{-}$N(O)=ON^{-}]) were first synthesized in 1960 by Drago and Pualuk by combining diethylamine and NO[146]. N-diazeniumdiolates are formed through a reaction between two moles of NO and materials containing primary or secondary amines under high pressure, creating a relatively stable donor capable of releasing NO from 2 seconds to 17 days[147-151]. Two moles of NO can be generated from one mole of compound[149-150]. As this results in a negative charge being imparted on the N-diazeniumdiolate, a counteraction (Na^{+}) must be present. A zwitterionic compound can be formed to stabilize the N-diazeniumdiolate by protonating another amine on the same molecule[147, 152].

N-diazeniumdiolates are often used for the spontaneous generation of NO, either in aqueous solutions or as device coatings[148]. The decomposition rate is dependent on the structure of the nucleophile[146]. The decomposition of N-diazeniumdiolates proceeds through first-order kinetics, independent of biological mediators and catalysis by thiols, and thus their decomposition rate is predictable[146]. The spontaneous decomposition of N-

diazeniumdiolates under physiological conditions offers an easy method of delivery with a wide range of applications[149]. N-diazeniumdiolates are often tailored to a specific application through alterations of the pH, amine structure of the precursor, and the temperature[148]. Many groups have successfully incorporated N-diazeniumdiolates into polymers through covalent attachment for use in implantable devices[151, 153-156]. After some clinical use, N-diazeniumdiolate administration for patients with ischemic heart disease was discontinued after some evidence of tolerance to the organic nitrates was observed[157].

S-nitrosothiols have been shown to decompose through several mechanisms: S–N bond homolysis, transition metal ion catalyzed decomposition, photolytic S–N bond cleavage, direct interactions with ascorbate, and hydrolysis[12, 151, 158]. Homolytic decomposition of an RSNO generates NO and an alkyl thiyl radical (RS•) (Equation 15.1), while heterolytic decomposition produces either NO^- or NO^+ and a corresponding RS^+ or RS^- (Equation 15.2)[10, 53, 64, 159]. Generally, both mechanisms are involved in the decomposition of NO. Homolytic decomposition generally occurs through thermal or photolytic pathways and is slow in the absence of these contributors[53].

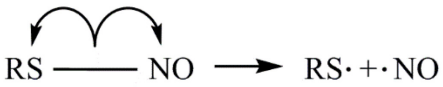

$$RS\text{—}NO \longrightarrow RS\cdot + \cdot NO \quad (15.1)$$

$$RSNO \longrightarrow \begin{matrix} RS^+ + NO^- \\ RS^- + NO^+ \end{matrix} \quad (15.2)$$

Transition metal cleavage requires a transition metal, such as Cu^{2+}, to be reduced to Cu^+. Cu^+ reacts with the nitrosothiol to generate NO forming sulfhydryl (-SH) and regenerating Cu^{2+} (Equations 16.1–16.2)[147]. Photolytic cleavage of an RSNO evolves NO and a disulfide compound formed from the parent thiols[145]. In the formation of S-nitrosothiols, it is generally accepted that a nitrosothiol is not produced via the direct reaction of NO and thiol. Rather, a mechanism incorporating molecular oxygen has been proposed[160].

$$2Cu^{2+} + 2RS^- \longrightarrow 2Cu^+ + RSSR \quad (16.1)$$

$$Cu^+ + RSNO \longrightarrow Cu^{2+} + RS^- + NO \quad (16.2)$$

Release of NO from SNAP by photolytic cleavage is most efficient at wavelengths corresponding to its S-nitroso absorption bands (330–350 nm and 550–600 nm)

(Equation 17)[161]. The molar absorptivity of SNAP is reported as ε_{340}=1075 $M^{-1}\cdot cm^{-1}$ and ε_{590}=12.4 $M^{-1}\cdot cm^{-1}$ [162-163].

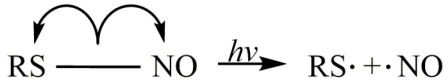

(17)

Generally, tertiary S-nitrosothiols appear green, whereas primary or secondary S-nitrosothiols appear red[159]. UV/Vis spectrophotographic measurements of S-nitrosothiols show absorption peaks between 225–261 ($\pi\rightarrow\pi^*$), 330–350 ($n_0\rightarrow\pi^*$), and 550–600 ($n_N\rightarrow\pi^*$) nm[50, 159]. Tertiary RSNOs shows two distinct absorbance maxima at 340 nm ($\pi\rightarrow\pi^*$) and 590 nm ($n_N\rightarrow\pi^*$) with a broad shoulder extending towards 550 nm, providing a simple method for positive identification of tertiary RSNO formation[53, 163]. When analyzed together, these peaks allow a reaction's progress, successful formation of the RSNO, and eventual decay to be monitored[50, 163-164]. Typically, the least energetic bands are used to monitor the progress of reactions involving S-nitrosothiols.

S-nitrosothiol stability is dependent on the substituent organic structure, as evidenced by the relative instability of primary RSNOs as compared to the long-term stability of tertiary RSNOs[165]. S-nitrosothiols, such as S-nitroso-N-acetyl-D-penicillamine (SNAP), generally exhibit –SNO moieties with an anti-orientation almost exclusively[165]. This RSNO is thought to exhibit extended stability over NO alone; due, in part, to the production of the free radical NO at the point of use[161]. SNAP is a well-known and extensively studied biocompatible NO donor which maintains excellent stability in the physiological environment[19, 53, 64, 78, 163, 166].

Some groups consider S-nitrosothiols to be donors of NO^+ through heterolytic cleavage of the SN bond, allowing easy transfer across the plasma membrane[53, 146]. This form of release is attributable to trans-nitrosation, and would allow additional thiols to pass on the biological activity without the release of free NO, making deleterious side reactions less likely while protecting NO from side reactions with oxygen species[146]. Dimerization of the thiyl radical forms a disulfide (RSSR) (Equation 18)[64, 159].

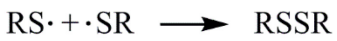

(18)

In an implanted system, overproduction or excessive delivery of NO is circumvented through the implementation of controlled release mechanisms. In the event that these fail, the physiological reactions described above will convert the free NO to less harmful compounds to reduce the potential harmful effects of NO on surrounding tissue. Since the

effects of NO are diffusion and degradation rate limited, the extent of any damage would be localized to within NO's radius of activity of 100 μm[31, 64-66].

1.14. Medical Applications of Nitric Oxide Donors

Due to NO's pervasive nature in the physiological environment and myriad of functions, synthetic delivery of NO via donors can be valuable both in the basic biological understanding of NO, but also as a clinically relevant, therapeutic agent.

As research tools, well characterized and understood NO donors can provide effective methods to replicate and verify theories and models about NO's effect on the physiological environment. Dose dependencies and basal release of NO from cells can be determined[167]. In addition to their potential as research tools, NO donors have found a well-deserved place in medical research and clinical practice. First used medicinally in 1849 in the form of nitroglycerine, NO donors have been in successful clinical use for over 150 years[1]. Over the past several decades, once the connection between EDRF and NO was discovered[168], the breadth of knowledge pertaining to improved delivery and storage mechanisms of NO has led to remarkable gains in the field of drug delivery[30, 147, 169-170], vascular substitutes[8, 19, 153, 171-172], cancer treatments[29, 173-176], respiratory illnesses[177-180], and neural regeneration[181-183]. Additionally, NO is now able to be used in the diagnosis of certain clinical pathologies[184-192].

1.15. References

1. Marsh, N.; Marsh, A. A Short History of Nitroglycerine and Nitric Oxide in Pharmacology and Physiology. *Clinical and Experimental Pharmacology and Physiology* **2000,** *27* (4), 313-319.
2. Moncada, S.; Palmer, R. M.; Higgs, E. A. The Discovery of Nitric Oxide as the Endogenous Nitrovasodilator. *Hypertension* **1988,** *12* (4), 365-372.
3. Feelisch, M.; Stamler, J. S., *Methods in Nitric Oxide Research*. John Wiley & Sons Ltd.: **1996**; p 712.
4. Choudhari, S. K.; Chaudhary, M.; Bagde, S.; Gadbail, A. R.; Joshi, V. Nitric Oxide and Cancer: A Review. *World J Surg Oncol* **2013,** *11* (118), 118.
5. Burke, A. J.; Sullivan, F. J.; Giles, F. J.; Glynn, S. A. The Yin and Yang of Nitric Oxide in Cancer Progression. *Carcinogenesis* **2013,** *34* (3), 503-512.
6. Wallis, J. Nitric Oxide and Blood: A Review. *Transfusion Medicine* **2005,** *15* (1), 1-11.
7. Lamattina, L.; Garcia-Mata, C.; Graziano, M.; Pagnussat, G. Nitric Oxide: The Versatility of an Extensive Signal Molecule. *Annu Rev Plant Biol* **2003,** *54*, 109-136.
8. de Mel, A.; Murad, F.; Seifalian, A. M. Nitric Oxide: A Guardian for Vascular Grafts? *Chem Rev* **2011,** *111* (9), 5742-5767.
9. Walford, G.; Loscalzo, J. Nitric Oxide in Vascular Biology. *Journal of Thrombosis and Haemostasis* **2003,** *1* (10), 2112-2118.
10. Hou, Y.; Janczuk, A.; Wang, P. Current Trends in the Development of Nitric Oxide Donors. *Current pharmaceutical design* **1999,** *5* (6), 417-442.
11. Toledo, J. C., Jr.; Augusto, O. Connecting the Chemical and Biological Properties of Nitric Oxide. *Chem Res Toxicol* **2012,** *25* (5), 975-989.
12. Broniowska, K. A.; Diers, A. R.; Hogg, N. S-Nitrosoglutathione. *Biochim Biophys Acta* **2013,** *1830* (5), 3173-3181.
13. Korhonen, R.; Lahti, A.; Kankaanranta, H.; Moilanen, E. Nitric Oxide Production and Signaling in Inflammation. *Current Drug Targets-Inflammation & Allergy* **2005,** *4* (4), 471-479.
14. Lahdenranta, J.; Hagendoorn, J.; Padera, T. P.; Hoshida, T.; Nelson, G.; Kashiwagi, S.; Jain, R. K.; Fukumura, D. Endothelial Nitric Oxide Synthase Mediates Lymphangiogenesis and Lymphatic Metastasis. *Cancer Res* **2009,** *69* (7), 2801-2808.
15. Moncada, S.; Higgs, E. A. Molecular Mechanisms and Therapeutic Strategies Related to Nitric Oxide. *FASEB J* **1995,** *9* (13), 1319-1330.
16. Riddell, D. R.; Owen, J. S. Nitric Oxide and Platelet Aggregation. **1997,** *57*, 25-48.
17. Campelo, A. E.; Cutini, P. H.; Massheimer, V. L. Testosterone Modulates Platelet Aggregation and Endothelial Cell Growth through Nitric Oxide Pathway. *J Endocrinol* **2012,** *213* (1), 77-87.
18. Radomski, M.; Palmer, R.; Moncada, S. An L-Arginine/Nitric Oxide Pathway Present in Human Platelets Regulates Aggregation. *Proceedings of the National Academy of Sciences* **1990,** *87* (13), 5193-5197.
19. Carpenter, A. W.; Schoenfisch, M. H. Nitric Oxide Release: Part Ii. Therapeutic Applications. *Chem Soc Rev* **2012,** *41* (10), 3742-3752.

20. Shi, H. P.; Efron, D. T.; Most, D.; Tantry, U. S.; Barbul, A. Supplemental Dietary Arginine Enhances Wound Healing in Normal but Not Inducible Nitric Oxide Synthase Knockout Mice. *Surgery* **2000,** *128* (2), 374-378.
21. Garthwaite, J.; Garthwaite, G.; Palmer, R. M. J.; Moncada, S. Nmda Receptor Activation Induces Nitric Oxide Synthesis from Arginine in Rat Brain Slices. *European Journal of Pharmacology: Molecular Pharmacology* **1989,** *172* (4-5), 413-416.
22. Hirst, D. G.; Robson, T. Nitric Oxide Physiology and Pathology. *Methods Mol Biol* **2011,** *704*, 1-13.
23. Bohl, K. S.; West, J. L. Nitric Oxide-Generating Polymers Reduce Platelet Adhesion and Smooth Muscle Cell Proliferation. *Biomaterials* **2000,** *21* (22), 2273-2278.
24. Sarkar, R. Mechanisms of Inhibition of Vascular Smooth Muscle Cell Function by Nitric Oxide. University of Michigan, **1995**.
25. Chen, C.; Hanson, S. R.; Keefer, L. K.; Saavedra, J. E.; Davies, K. M.; Hutsell, T. C.; Hughes, J. D.; Ku, D. N.; Lumsden, A. B. Boundary Layer Infusion of Nitric Oxide Reduces Early Smooth Muscle Cell Proliferation in the Endarterectomized Canine Artery. *J Surg Res* **1997,** *67* (1), 26-32.
26. Bohlen, H. G.; Wang, W.; Gashev, A.; Gasheva, O.; Zawieja, D. Phasic Contractions of Rat Mesenteric Lymphatics Increase Basal and Phasic Nitric Oxide Generation in Vivo. *Am J Physiol Heart Circ Physiol* **2009,** *297* (4), H1319-1328.
27. Hagendoorn, J.; Padera, T. P.; Kashiwagi, S.; Isaka, N.; Noda, F.; Lin, M. I.; Huang, P. L.; Sessa, W. C.; Fukumura, D.; Jain, R. K. Endothelial Nitric Oxide Synthase Regulates Microlymphatic Flow Via Collecting Lymphatics. *Circ Res* **2004,** *95* (2), 204-209.
28. Gkaliagkousi, E.; Ferro, A. Nitric Oxide Signalling in the Regulation of Cardiovascular and Platelet Function. *Front Biosci (Landmark Ed)* **2011,** *16*, 1873-1897.
29. Fukumura, D.; Kashiwagi, S.; Jain, R. K. The Role of Nitric Oxide in Tumour Progression. *Nat Rev Cancer* **2006,** *6* (7), 521-534.
30. Riccio, D. A.; Schoenfisch, M. H. Nitric Oxide Release: Part I. Macromolecular Scaffolds. *Chem Soc Rev* **2012,** *41* (10), 3731-3741.
31. Ignarro, L. J., *Nitric Oxide: Biology and Pathobiology*. Academic Press: San Diego, CA, **2000**; Vol. 2.
32. Bonavida, B.; Khineche, S.; Huerta-Yepez, S.; Garban, H. Therapeutic Potential of Nitric Oxide in Cancer. *Drug Resist Updat* **2006,** *9* (3), 157-173.
33. Forstermann, U.; Sessa, W. C. Nitric Oxide Synthases: Regulation and Function. *Eur Heart J* **2012,** *33* (7), 829-837, 837a-837d.
34. Guzik, T.; Korbut, R.; Adamek-Guzik, T. Nitric Oxide and Superoxide in Inflammation and Immune Regulation. *Journal of physiology and pharmacology* **2003,** *54*, 469-487.
35. Aktan, F. Inos-Mediated Nitric Oxide Production and Its Regulation. *Life Sci* **2004,** *75* (6), 639-653.
36. Ricciardolo, F. Multiple Roles of Nitric Oxide in the Airways. *Thorax* **2003,** *58* (2), 175-182.
37. Bogdan, C. Nitric Oxide and the Immune Response. *Nat Immunol* **2001,** *2* (10), 907-916.

38. Gielis, J. F.; Lin, J. Y.; Wingler, K.; Van Schil, P. E.; Schmidt, H. H.; Moens, A. L. Pathogenetic Role of Enos Uncoupling in Cardiopulmonary Disorders. *Free Radic Biol Med* **2011,** *50* (7), 765-776.
39. Luo, J. D.; Chen, A. F. Nitric Oxide: A Newly Discovered Function on Wound Healing. *Acta Pharmacol Sin* **2005,** *26* (3), 259-264.
40. Moncada, S.; Higgs, E., Nitric Oxide and the Vascular Endothelium. In *The Vascular Endothelium I*, Springer: **2006**; pp 213-254.
41. Forstermann, U., Regulation of Nitric Oxide Synthase Expression and Activity. In *Handbook of Experimental Pharmacology—Nitric Oxide*, Mayer, B., Ed. Springer: Berlin, **2000**; pp 71 - 91.
42. Forstermann, U. Nitric Oxide and Oxidative Stress in Vascular Disease. *Pflugers Arch* **2010,** *459* (6), 923-939.
43. Davis, K. L.; Martin, E.; Turko, I. V.; Murad, F. Novel Effects of Nitric Oxide. *Annu Rev Pharmacol Toxicol* **2001,** *41*, 203-236.
44. Beltran, B.; Quintero, M.; Garcia-Zaragoza, E.; O'Connor, E.; Esplugues, J. V.; Moncada, S. Inhibition of Mitochondrial Respiration by Endogenous Nitric Oxide: A Critical Step in Fas Signaling. *Proc Natl Acad Sci U S A* **2002,** *99* (13), 8892-8897.
45. Hogg, N. The Biochemistry and Physiology of S-Nitrosothiols. *Annual review of pharmacology and toxicology* **2002,** *42* (1), 585-600.
46. Faraci, F. M.; Didion, S. P. Vascular Protection: Superoxide Dismutase Isoforms in the Vessel Wall. *Arterioscler Thromb Vasc Biol* **2004,** *24* (8), 1367-1373.
47. Pogrebnaya, V.; Usov, A.; Baranov, A.; Nesterenko, A.; Bezyazychnyi, P. Oxidation of Nitric-Oxide by Oxygen in Liquid-Phase. *Journal of Applied Chemistry of the USSR* **1975,** *48* (5), 1004-1007.
48. Chen, B.; Keshive, M.; Deen, W. M. Diffusion and Reaction of Nitric Oxide in Suspension Cell Cultures. *Biophysical Journal* **1998,** *75* (2), 745-754.
49. Beckman, J. S.; Koppenol, W. H. Nitric Oxide, Superoxide, and Peroxynitrite: The Good, the Bad, and Ugly. *American Journal of Physiology-Cell Physiology* **1996,** *271* (5), C1424-C1437.
50. Williams, D. L. H. The Chemistry of S-Nitrosothiols. *Accounts of Chemical Research* **1999,** *32* (10), 869-876.
51. Gardner, P. R.; Gardner, A. M.; Hallstrom, C. K. Dioxygen-Dependent Metabolism of Nitric Oxide. *Methods Mol Biol* **2004,** *279*, 133-150.
52. Xu, W.; Liu, L. Z.; Loizidou, M.; Ahmed, M.; Charles, I. G. The Role of Nitric Oxide in Cancer. *Cell Res* **2002,** *12* (5-6), 311-320.
53. Morakinyo, M. K. S-Nitrosothiols: Formation, Decomposition, Reactivity and Possible Physiological Effects. Portland State Univeristy, **2010**.
54. Herold, S.; Fago, A. Reactions of Peroxynitrite with Globin Proteins and Their Possible Physiological Role. *Comp Biochem Physiol A Mol Integr Physiol* **2005,** *142* (2), 124-129.
55. Ronson, R. S.; Nakamura, M.; Vinten-Johansen, J. The Cardiovascular Effects and Implications of Peroxynitrite. *Cardiovascular research* **1999,** *44* (1), 47-59.

56. Augusto, O.; Bonini, M. G.; Amanso, A. M.; Linares, E.; Santos, C. C. X.; De Menezes, S. l. L. Nitrogen Dioxide and Carbonate Radical Anion: Two Emerging Radicals in Biology. *Free Radical Biology and Medicine* **2002,** *32* (9), 841-859.
57. Medinas, D. B.; Cerchiaro, G.; Trindade, D. F.; Augusto, O. The Carbonate Radical and Related Oxidants Derived from Bicarbonate Buffer. *IUBMB Life* **2007,** *59* (4-5), 255-262.
58. Squadrito, G. L.; Pryor, W. A. Mapping the Reaction of Peroxynitrite with Co2: Energetics, Reactive Species, and Biological Implications. *Chemical Research in Toxicology* **2002,** *15* (7), 885-895.
59. Yun, B. H.; Geacintov, N. E.; Shafirovich, V. Generation of Guanine-Thymidine Cross-Links in DNA by Peroxynitrite/Carbon Dioxide. *Chem Res Toxicol* **2011,** *24* (7), 1144-1152.
60. Medinas, D. B.; Gozzo, F. C.; Santos, L. F.; Iglesias, A. H.; Augusto, O. A Ditryptophan Cross-Link Is Responsible for the Covalent Dimerization of Human Superoxide Dismutase 1 During Its Bicarbonate-Dependent Peroxidase Activity. *Free Radic Biol Med* **2010,** *49* (6), 1046-1053.
61. Armor, J. N. Influence of Ph and Ionic Strength Upon Solubility of Nitric Oxide in Aqueous Solution. *Journal of Chemical & Engineering Data* **1974,** *19* (1), 82-84.
62. Shaw, A. W.; Vosper, A. J. Solubility of Nitric Oxide in Aqueous and Nonaqueous Solvents. *Journal of the Chemical Society, Faraday Transactions 1: Physical Chemistry in Condensed Phases* **1977,** *73* (0), 1239.
63. Hunter, R. A.; Storm, W. L.; Coneski, P. N.; Schoenfisch, M. H. Inaccuracies of Nitric Oxide Measurement Methods in Biological Media. *Anal Chem* **2013,** *85* (3), 1957-1963.
64. Al-Sa'doni, H.; Ferro, A. S-Nitrosothiols: A Class of Nitric Oxide-Donor Drugs. *Clin Sci (Lond)* **2000,** *98* (5), 507-520.
65. Vaughn, M. W.; Kuo, L.; Liao, J. C. Effective Diffusion Distance of Nitric Oxide in the Microcirculation. *Am J Physiol* **1998,** *274* (5 Pt 2), H1705-1714.
66. Goldstein, S.; Czapski, G. Kinetics of Nitric Oxide Autoxidation in Aqueous Solution in the Absence and Presence of Various Reductants. The Nature of the Oxidizing Intermediates. *Journal of the American Chemical Society* **1995,** *117* (49), 12078-12084.
67. Lipton, S.; Choi, Y.; Pan, Z.; Lei, S.; Chen, H.; Sucher, N.; Loscalzo, J.; Singel, D.; Stamler, J. A Redox-Based Mechanism for the Neuroprotective and Neurodestructive Effects of Nitric Oxide and Related Nitroso-Compounds. *Nature* **1993,** *364* (6438), 7.
68. Brown, G. C. Nitric Oxide and Mitochondria. *Front Biosci* **2007,** *12* (1024-1033), 452.
69. Brown, G. C.; Borutaite, V. Nitric Oxide Inhibition of Mitochondrial Respiration and Its Role in Cell Death. *Free Radical Biology and Medicine* **2002,** *33* (11), 1440-1450.
70. Channon, K.; Guzik, T. Mechanisms of Superoxide Production in Human Blood. *Journal of Physiology and Pharmacology* **2002,** *53* (4), 515-524.
71. Guzik, T. J.; West, N. E. J.; Pillai, R.; Taggart, D. P.; Channon, K. M. Nitric Oxide Modulates Superoxide Release and Peroxynitrite Formation in Human Blood Vessels. *Hypertension* **2002,** *39* (6), 1088-1094.
72. Coleman, J. W. Nitric Oxide in Immunity and Inflammation. *International Immunopharmacology* **2001,** *1* (8), 1397-1406.

73. Knowles, R. G.; Palacios, M.; Palmer, R.; Moncada, S. Formation of Nitric Oxide from L-Arginine in the Central Nervous System: A Transduction Mechanism for Stimulation of the Soluble Guanylate Cyclase. *Proceedings of the National Academy of Sciences* **1989,** *86* (13), 5159-5162.
74. Marcinkiewicz, J. Nitric Oxide and Antimicrobial Activity of Reactive Oxygen Intermediates. *Immunopharmacology* **1997,** *37* (1), 35-41.
75. Moro, M. A.; Darley-Usmar, V. M.; Goodwin, D. A.; Read, N. G.; Zamora-Pino, R.; Feelisch, M.; Radomski, M. W.; Moncada, S. Paradoxical Fate and Biological Action of Peroxynitrite on Human Platelets. *Proceedings of the National Academy of Sciences* **1994,** *91* (14), 6702-6706.
76. Hess, D. T.; Matsumoto, A.; Kim, S.-O.; Marshall, H. E.; Stamler, J. S. Protein S-Nitrosylation: Purview and Parameters. *Nature Reviews Molecular Cell Biology* **2005,** *6* (2), 150-166.
77. Muntane, J.; la Mata, M. D. Nitric Oxide and Cancer. *World J Hepatol* **2010,** *2* (9), 337-344.
78. Zhao, Y.-L.; Houk, K. Thionitroxides, Rsnho: The Structure of the Sno Moiety in "S-Nitrosohemoglobin", a Possible No Reservoir and Transporter. *Journal of the American Chemical Society* **2006,** *128* (5), 1422-1423.
79. Doulias, P.-T.; Greene, J. L.; Greco, T. M.; Tenopoulou, M.; Seeholzer, S. H.; Dunbrack, R. L.; Ischiropoulos, H. Structural Profiling of Endogenous S-Nitrosocysteine Residues Reveals Unique Features That Accommodate Diverse Mechanisms for Protein S-Nitrosylation. *Proceedings of the National Academy of Sciences* **2010,** *107* (39), 16958-16963.
80. Thomas, D. D.; Jourd'heuil, D. S-Nitrosation: Current Concepts and New Developments. *Antioxid Redox Signal* **2012,** *17* (7), 934-936.
81. Peterson, L. A.; Wagener, T.; Sies, H.; Stahl, W. Decomposition of S-Nitrosocysteine Via S- to N-Transnitrosation. *Chem Res Toxicol* **2007,** *20* (5), 721-723.
82. Dee, K.; Puleo, D.; Bizios, R., *An Introduction to Tissue-Biomaterial Interactions*. John Wiley & Sons, Inc.: Hoboken, NJ, **2002**; p 228.
83. Guo, S.; DiPietro, L. A. Factors Affecting Wound Healing. *Journal of dental research* **2010,** *89* (3), 219-229.
84. Ryan, G. B.; Majno, G. Acute Inflammation. A Review. *The american journal of pathology* **1977,** *86* (1), 183.
85. Rizk, M.; Witte, M. B.; Barbul, A. Nitric Oxide and Wound Healing. *World J Surg* **2004,** *28* (3), 301-306.
86. Ying, L.; Hofseth, L. J. An Emerging Role for Endothelial Nitric Oxide Synthase in Chronic Inflammation and Cancer. *Cancer Res* **2007,** *67* (4), 1407-1410.
87. Sessa, W. C. Enos at a Glance. *Journal of cell science* **2004,** *117* (12), 2427-2429.
88. Rawlingson, A. Nitric Oxide, Inflammation and Acute Burn Injury. *Burns* **2003,** *29* (7), 631-640.
89. Cross, R. K.; Wilson, K. T. Nitric Oxide in Inflammatory Bowel Disease. *Inflammatory Bowel Diseases* **2003,** *9* (3), 179-189.

90. Tak, P. P.; Firestein, G. S. Nf-Kappab: A Key Role in Inflammatory Diseases. *J Clin Invest* **2001,** *107* (1), 7-11.
91. Connelly, L.; Palacios-Callender, M.; Ameixa, C.; Moncada, S.; Hobbs, A. Biphasic Regulation of Nf-Kb Activity Underlies the Pro-and Anti-Inflammatory Actions of Nitric Oxide. *The Journal of Immunology* **2001,** *166* (6), 3873-3881.
92. Marshall, H. E.; Stamler, J. S. Nitrosative Stress-Induced Apoptosis through Inhibition of Nf-Kb. *Journal of Biological Chemistry* **2002,** *277* (37), 34223-34228.
93. Kosonen, O.; Kankaanranta, H.; Malo-Ranta, U.; Moilanen, E. Nitric Oxide-Releasing Compounds Inhibit Neutrophil Adhesion to Endothelial Cells. *European Journal of Pharmacology* **1999,** *382* (2), 111-117.
94. Ou, J.; Carlos, T. M.; Watkins, S. C.; Saavedra, J. E.; Keefer, L. K.; Kim, Y. M.; Harbrecht, B. G.; Billiar, T. R. Differential Effects of Nonselective Nitric Oxide Synthase (Nos) and Selective Inducible Nos Inhibition on Hepatic Necrosis, Apoptosis, Icam-1 Expression, and Neutrophil Accumulation During Endotoxemia. *Nitric Oxide* **1997,** *1* (5), 404-416.
95. Kosonen, O.; Kankaanranta, H.; Uotila, J.; Moilanen, E. Inhibition by Nitric Oxide-Releasing Compounds of E-Selectin Expression in and Neutrophil Adhesion to Human Endothelial Cells. *European journal of pharmacology* **2000,** *394* (1), 149-156.
96. Lefer, D. J.; Jones, S. P.; Girod, W. G.; Baines, A.; Grisham, M. B.; Cockrell, A. S.; Huang, P. L.; Scalia, R. Leukocyte-Endothelial Cell Interactions in Nitric Oxide Synthase-Deficient Mice. *Am J Physiol-Heart C* **1999,** *276* (6), H1943-H1950.
97. Marcinkiewicz, J. Regulation of Cytokine Production by Eicosanoids and Nitric Oxide. *Archivum immunologiae et therapiae experimentalis* **1996,** *45* (2-3), 163-167.
98. Marcinkiewicz, J.; Chain, B. Differential Regulation of Cytokine Production by Nitric Oxide. *Immunology* **1993,** *80* (1), 146.
99. Bogdan, C. Nitric Oxide and the Regulation of Gene Expression. *Trends in Cell Biology* **2001,** *11* (2), 66-75.
100. Tiidus, P. M. Radical Species in Inflammation and Overtraining. *Canadian journal of physiology and pharmacology* **1998,** *76* (5), 533-538.
101. Guzik, T. J.; West, N. E.; Black, E.; McDonald, D.; Ratnatunga, C.; Pillai, R.; Channon, K. M. Vascular Superoxide Production by Nad (P) H Oxidase Association with Endothelial Dysfunction and Clinical Risk Factors. *Circulation research* **2000,** *86* (9), e85-e90.
102. Kimura, T.; Iwase, M.; Kondo, G.; Watanabe, H.; Ohashi, M.; Ito, D.; Nagumo, M. Suppressive Effect of Selective Cyclooxygenase-2 Inhibitor on Cytokine Release in Human Neutrophils. *International immunopharmacology* **2003,** *3* (10), 1519-1528.
103. Brzozowski, T.; Konturek, P. C.; Konturek, S. J.; Kwiecień, S.; Sliwowski, Z.; Pajdo, R.; Duda, A.; Ptak, A.; Hahn, E. G. Implications of Reactive Oxygen Species and Cytokines in Gastroprotection against Stress-Induced Gastric Damage by Nitric Oxide Releasing Aspirin. *International journal of colorectal disease* **2003,** *18* (4), 320-329.
104. Zamora, R.; Vodovotz, Y.; Billiar, T. R. Inducible Nitric Oxide Synthase and Inflammatory Diseases. *Molecular Medicine* **2000,** *6* (5), 347.
105. Sohn, J. J.; Schetter, A. J.; Yfantis, H. G.; Ridnour, L. A.; Horikawa, I.; Khan, M. A.; Robles, A. I.; Hussain, S. P.; Goto, A.; Bowman, E. D.; Hofseth, L. J.; Bartkova, J.; Bartek, J.;

Wogan, G. N.; Wink, D. A.; Harris, C. C. Macrophages, Nitric Oxide and Micrornas Are Associated with DNA Damage Response Pathway and Senescence in Inflammatory Bowel Disease. *PLoS One* **2012,** *7* (9), e44156.
106. Krischel, V.; Bruch-Gerharz, D.; Suschek, C.; Kroncke, K. D.; Ruzicka, T.; Kolb-Bachofen, V. Biphasic Effect of Exogenous Nitric Oxide on Proliferation and Differentiation in Skin Derived Keratinocytes but Not Fibroblasts. *J Invest Dermatol* **1998,** *111* (2), 286-291.
107. Villalobo, A. Nitric Oxide and Cell Proliferation. *FEBS J* **2006,** *273* (11), 2329-2344.
108. Heller, R. Nitric Oxide Inhibits Proliferation of Human Endothelial Cells Via a Mechanism Independent of Cgmp. *Atherosclerosis* **1999,** *144* (1), 49-57.
109. Luczak, K.; Balcerczyk, A.; Soszynski, M.; Bartosz, G. Low Concentration of Oxidant and Nitric Oxide Donors Stimulate Proliferation of Human Endothelial Cells in Vitro. *Cell Biol Int* **2004,** *28* (6), 483-486.
110. Du, M.; Islam, M.; Lin, L.; Ohmura, Y.; Moriyama, Y.; Fujimura, S. Promotion of Proliferation of Murine Balb/C3t3 Fibroblasts Mediated by Nitric Oxide at Lower Concentrations. *IUBMB Life* **1997,** *41* (3), 625-631.
111. Dulak, J.; Józkowicz, A.; Dembinska-Kiec, A.; Guevara, I.; Zdzienicka, A.; Zmudzinska-Grochot, D.; Florek, I.; Wójtowicz, A.; Szuba, A.; Cooke, J. P. Nitric Oxide Induces the Synthesis of Vascular Endothelial Growth Factor by Rat Vascular Smooth Muscle Cells. *Arteriosclerosis, thrombosis, and vascular biology* **2000,** *20* (3), 659-666.
112. Ziche, M.; Parenti, A.; Ledda, F.; Dell'Era, P.; Granger, H. J.; Maggi, C. A.; Presta, M. Nitric Oxide Promotes Proliferation and Plasminogen Activator Production by Coronary Venular Endothelium through Endogenous Bfgf. *Circulation research* **1997,** *80* (6), 845-852.
113. Cooke, J. P. Nitric Oxide and Angiogenesis. *Circulation* **2002,** *105* (18), 2133-2135.
114. Tarr, J.; Eggleton, P.; Winyard, P. Nitric Oxide and the Regulation of Apoptosis in Tumour Cells. *Current pharmaceutical design* **2006,** *12* (34), 4445-4468.
115. Brown, G. C. Nitric Oxide and Mitochondrial Respiration. *Biochimica et Biophysica Acta (BBA)-Bioenergetics* **1999,** *1411* (2), 351-369.
116. Aranda, E.; López-Pedrera, C.; R De La Haba-Rodriguez, J.; Rodriguez-Ariza, A. Nitric Oxide and Cancer: The Emerging Role of S-Nitrosylation. *Current molecular medicine* **2012,** *12* (1), 50-67.
117. Brüne, B. Nitric Oxide: No Apoptosis or Turning It On? *Cell Death & Differentiation* **2003,** *10* (8), 864-869.
118. Kim, J.-E.; Tannenbaum, S. R. S-Nitrosation Regulates the Activation of Endogenous Procaspase-9 in Ht-29 Human Colon Carcinoma Cells. *Journal of Biological Chemistry* **2004,** *279* (11), 9758-9764.
119. Olson, S. Y.; Garbán, H. J. Regulation of Apoptosis-Related Genes by Nitric Oxide in Cancer. *Nitric Oxide* **2008,** *19* (2), 170-176.
120. Harrison, D. G.; Widder, J.; Grumbach, I.; Chen, W.; Weber, M.; Searles, C. Endothelial Mechanotransduction, Nitric Oxide and Vascular Inflammation. *J Intern Med* **2006,** *259* (4), 351-363.

121. Corson, M. A.; James, N. L.; Latta, S. E.; Nerem, R. M.; Berk, B. C.; Harrison, D. G. Phosphorylation of Endothelial Nitric Oxide Synthase in Response to Fluid Shear Stress. *Circulation Research* **1996,** *79* (5), 984-991.
122. Kuchan, M.; Frangos, J. Role of Calcium and Calmodulin in Flow-Induced Nitric Oxide Production in Endothelial Cells. *American Journal of Physiology-Cell Physiology* **1994,** *266* (3), C628-C636.
123. Gallis, B.; Corthals, G. L.; Goodlett, D. R.; Ueba, H.; Kim, F.; Presnell, S. R.; Figeys, D.; Harrison, D. G.; Berk, B. C.; Aebersold, R. Identification of Flow-Dependent Endothelial Nitric-Oxide Synthase Phosphorylation Sites by Mass Spectrometry and Regulation of Phosphorylation and Nitric Oxide Production by the Phosphatidylinositol 3-Kinase Inhibitor Ly294002. *Journal of Biological Chemistry* **1999,** *274* (42), 30101-30108.
124. Dimmeler, S.; Fleming, I.; Fisslthaler, B.; Hermann, C.; Busse, R.; Zeiher, A. M. Activation of Nitric Oxide Synthase in Endothelial Cells by Akt-Dependent Phosphorylation. *Nature* **1999,** *399* (6736), 601-605.
125. Cai, H.; McNally, J. S.; Weber, M.; Harrison, D. G. Oscillatory Shear Stress Upregulation of Endothelial Nitric Oxide Synthase Requires Intracellular Hydrogen Peroxide and Camkii. *Journal of molecular and cellular cardiology* **2004,** *37* (1), 121-125.
126. McNally, J. S.; Davis, M. E.; Giddens, D. P.; Saha, A.; Hwang, J.; Dikalov, S.; Jo, H.; Harrison, D. G. Role of Xanthine Oxidoreductase and Nad (P) H Oxidase in Endothelial Superoxide Production in Response to Oscillatory Shear Stress. *Am J Physiol-Heart C* **2003,** *285* (6), H2290-H2297.
127. Laurindo, F.; de A Pedro, M.; Barbeiro, H. V.; Pileggi, F.; Carvalho, M.; Augusto, O.; da Luz, P. L. Vascular Free Radical Release. Ex Vivo and in Vivo Evidence for a Flow-Dependent Endothelial Mechanism. *Circulation Research* **1994,** *74* (4), 700-709.
128. Inoue, N.; Ramasamy, S.; Fukai, T.; Nerem, R. M.; Harrison, D. G. Shear Stress Modulates Expression of Cu/Zn Superoxide Dismutase in Human Aortic Endothelial Cells. *Circulation research* **1996,** *79* (1), 32-37.
129. Takeshita, S.; Inoue, N.; Ueyama, T.; Kawashima, S.; Yokoyama, M. Shear Stress Enhances Glutathione Peroxidase Expression in Endothelial Cells. *Biochemical and biophysical research communications* **2000,** *273* (1), 66-71.
130. Archer, S. Measurement of Nitric Oxide in Biological Models. *The FASEB journal* **1993,** *7* (2), 349-360.
131. Coneski, P. N.; Schoenfisch, M. H. Nitric Oxide Release: Part Iii. Measurement and Reporting. *Chem Soc Rev* **2012,** *41* (10), 3753-3758.
132. Griess, P. Bemerkungen Zu Der Abhandlung Der Hh. Weselsky Und Benedikt „Ueber Einige Azoverbindungen". *Berichte der deutschen chemischen Gesellschaft* **1879,** *12* (1), 426-428.
133. Sun, J.; Zhang, X.; Broderick, M.; Fein, H. Measurement of Nitric Oxide Production in Biological Systems by Using Griess Reaction Assay. *Sensors* **2003,** *3* (8), 276-284.
134. Tarpey, M. M.; Fridovich, I. Methods of Detection of Vascular Reactive Species Nitric Oxide, Superoxide, Hydrogen Peroxide, and Peroxynitrite. *Circulation research* **2001,** *89* (3), 224-236.

135. Hetrick, E. M.; Schoenfisch, M. H. Analytical Chemistry of Nitric Oxide. *Annual review of analytical chemistry (Palo Alto, Calif.)* **2009,** *2*, 409.
136. Shin, J. H.; Privett, B. J.; Kita, J. M.; Wightman, R. M.; Schoenfisch, M. H. Fluorinated Xerogel-Derived Microelectrodes for Amperometric Nitric Oxide Sensing. *Anal Chem* **2008,** *80* (18), 6850-6859.
137. MacArthur, P. H.; Shiva, S.; Gladwin, M. T. Measurement of Circulating Nitrite and S-Nitrosothiols by Reductive Chemiluminescence. *J Chromatogr B Analyt Technol Biomed Life Sci* **2007,** *851* (1-2), 93-105.
138. Zafiriou, O. C.; McFarland, M. Determination of Trace Levels of Nitric Oxide in Aqueous Solution. *Analytical Chemistry* **1980,** *52* (11), 1662-1667.
139. Nakajima, T.; Sato, M.; Akaza, N.; Umezawa, Y. Cell-Based Fluorescent Indicator to Visualize Brain-Derived Neurotrophic Factor Secreted from Living Neurons. *ACS Chem Biol* **2008,** *3* (6), 352-358.
140. Sato, M.; Nakajima, T.; Goto, M.; Umezawa, Y. Cell-Based Indicator to Visualize Picomolar Dynamics of Nitric Oxide Release from Living Cells. *Anal Chem* **2006,** *78* (24), 8175-8182.
141. Nausch, L. W.; Ledoux, J.; Bonev, A. D.; Nelson, M. T.; Dostmann, W. R. Differential Patterning of Cgmp in Vascular Smooth Muscle Cells Revealed by Single Gfp-Linked Biosensors. *Proc Natl Acad Sci U S A* **2008,** *105* (1), 365-370.
142. Batchelor, A. M.; Bartus, K.; Reynell, C.; Constantinou, S.; Halvey, E. J.; Held, K. F.; Dostmann, W. R.; Vernon, J.; Garthwaite, J. Exquisite Sensitivity to Subsecond, Picomolar Nitric Oxide Transients Conferred on Cells by Guanylyl Cyclase-Coupled Receptors. *Proc Natl Acad Sci U S A* **2010,** *107* (51), 22060-22065.
143. Vaughn, M. W.; Kuo, L.; Liao, J. C. Estimation of Nitric Oxide Production and Reaction Rates in Tissue by Use of a Mathematical Model. *Am J Physiol-Heart C* **1998,** *274* (6), H2163-H2176.
144. Reynolds, M. M.; Frost, M. C.; Meyerhoff, M. E. Nitric Oxide-Releasing Hydrophobic Polymers: Preparation, Characterization, and Potential Biomedical Applications. *Free Radic Biol Med* **2004,** *37* (7), 926-936.
145. Riccio, D. A.; Dobmeier, K. P.; Hetrick, E. M.; Privett, B. J.; Paul, H. S.; Schoenfisch, M. H. Nitric Oxide-Releasing S-Nitrosothiol-Modified Xerogels. *Biomaterials* **2009,** *30* (27), 4494-4502.
146. Miller, M. R.; Megson, I. L. Recent Developments in Nitric Oxide Donor Drugs. *Br J Pharmacol* **2007,** *151* (3), 305-321.
147. Frost, M. C.; Reynolds, M. M.; Meyerhoff, M. E. Polymers Incorporating Nitric Oxide Releasing/Generating Substances for Improved Biocompatibility of Blood-Contacting Medical Devices. *Biomaterials* **2005,** *26* (14), 1685-1693.
148. Rothrock, A. R.; Donkers, R. L.; Schoenfisch, M. H. Synthesis of Nitric Oxide-Releasing Gold Nanoparticles. *J Am Chem Soc* **2005,** *127* (26), 9362-9363.
149. Naghavi, N.; de Mel, A.; Alavijeh, O. S.; Cousins, B. G.; Seifalian, A. M. Nitric Oxide Donors for Cardiovascular Implant Applications. *Small* **2013,** *9* (1), 22-35.

150. Fitzhugh, A. L.; Keefer, L. K. Diazeniumdiolates. *Free Radical Biology and Medicine* **2000,** *28* (10), 1463-1469.
151. Varu, V. N.; Tsihlis, N. D.; Kibbe, M. R. Basic Science Review: Nitric Oxide--Releasing Prosthetic Materials. *Vasc Endovascular Surg* **2009,** *43* (2), 121-131.
152. Hrabie, J. A.; Klose, J. R.; Wink, D. A.; Keefer, L. K. New Nitric Oxide-Releasing Zwitterions Derived from Polyamines. *The Journal of Organic Chemistry* **1993,** *58* (6), 1472-1476.
153. Reynolds, M. M.; Hrabie, J. A.; Oh, B. K.; Politis, J. K.; Citro, M. L.; Keefer, L. K.; Meyerhoff, M. E. Nitric Oxide Releasing Polyurethanes with Covalently Linked Diazeniumdiolated Secondary Amines. *Biomacromolecules* **2006,** *7* (3), 987-994.
154. Keefer, L. K. Biomaterials: Thwarting Thrombus. *Nature materials* **2003,** *2* (6), 357-358.
155. DeRosa, F.; Kibbe, M. R.; Najjar, S. F.; Citro, M. L.; Keefer, L. K.; Hrabie, J. A. Nitric Oxide-Releasing Fabrics and Other Acrylonitrile-Based Diazeniumdiolates. *Journal of the American Chemical Society* **2007,** *129* (13), 3786-3787.
156. Eroy-Reveles, A. A.; Mascharak, P. K. Nitric Oxide-Donating Materials and Their Potential in Pharmacological Applications for Site-Specific Nitric Oxide Delivery. *Future medicinal chemistry* **2009,** *1* (8), 1497-1507.
157. Chipinda, I.; Simoyi, R. H. Formation and Stability of a Nitric Oxide Donor: S-Nitroso-N-Acetylpenicillamine. *J Phys Chem B* **2006,** *110* (10), 5052-5061.
158. Dicks, A. P.; Swift, H. R.; Williams, D. L. H.; Butler, A. R.; Al-Sa'doni, H. H.; Cox, B. G. Identification of Cu+ as the Effective Reagent in Nitric Oxide Formation from S-Nitrosothiols (Rsno). *Journal of the Chemical Society, Perkin Transactions 2* **1996,** (4), 481.
159. Wang, P. G.; Xian, M.; Tang, X.; Wu, X.; Wen, Z.; Cai, T.; Janczuk, A. J. Nitric Oxide Donors: Chemical Activities and Biological Applications. *Chemical Reviews* **2002,** *102* (4), 1091-1134.
160. Martinez-Ruiz, A.; Lamas, S. S-Nitrosylation: A Potential New Paradigm in Signal Transduction. *Cardiovasc Res* **2004,** *62* (1), 43-52.
161. Brisbois, E. J.; Handa, H.; Major, T. C.; Bartlett, R. H.; Meyerhoff, M. E. Long-Term Nitric Oxide Release and Elevated Temperature Stability with S-Nitroso-N-Acetylpenicillamine (Snap)-Doped Elast-Eon E2as Polymer. *Biomaterials* **2013,** *34* (28), 6957-6966.
162. Ichimori, K.; Ishida, H.; Fukahori, M.; Nakazawa, H.; Murakami, E. Practical Nitric Oxide Measurement Employing a Nitric Oxide-Selective Electrode. *Review of scientific instruments* **1994,** *65* (8), 2714-2718.
163. Colletta, A.; Wu, J.; Wo, Y.; Kappler, M.; Chen, H.; Xi, C.; Meyerhoff, M. E. S-Nitroso-N-Acetylpenicillamine (Snap) Impregnated Silicone Foley Catheters: A Potential Biomaterial/Device to Prevent Catheter-Associated Urinary Tract Infections. *ACS Biomaterials Science & Engineering* **2015,** *1* (6), 416-424.
164. Wang, K.; Wen, Z.; Zhang, W.; Xian, M.; Cheng, J.-P.; Wang, P. G. Equilibrium and Kinetics Studies of Transnitrosation between S-Nitrosothiols and Thiols. *Bioorganic & medicinal chemistry letters* **2001,** *11* (3), 433-436.
165. Bartberger, M. D.; Houk, K. N.; Powell, S. C.; Mannion, J. D.; Lo, K. Y.; Stamler, J. S.; Toone, E. J. Theory, Spectroscopy, and Crystallographic Analysis Ofs-

Nitrosothiols: Conformational Distribution Dictates Spectroscopic Behavior. *Journal of the American Chemical Society* **2000,** *122* (24), 5889-5890.
166. Xing, Q.; Vogt, C.; Bailey, A.; Yates, K.; Zhao, F.; Frost, M. C.; He, W. Effects of Local Nitric Oxide Release on Human Mesenchymal Stem Cell Attachment and Proliferation on Gelatin Hydrogel Surface. *Surface Innovations* **2013,** *1* (4), 224-232.
167. Malinski, T.; Taha, Z. Nitric Oxide Release from a Single Cell Measured in Situ by a Porphyrinic-Based Microsensor. *Nature* **1992,** *358* (6388), 676-678.
168. Palmer, R. M.; Ferrige, A. G.; Moncada, S. Nitric Oxide Release Accounts for the Biological Activity of Endothelium-Derived Relaxing Factor. *Nature* **1987,** *327* (6122), 524-526.
169. Nichols, S. P.; Storm, W. L.; Koh, A.; Schoenfisch, M. H. Local Delivery of Nitric Oxide: Targeted Delivery of Therapeutics to Bone and Connective Tissues. *Advanced drug delivery reviews* **2012,** *64* (12), 1177-1188.
170. McKinlay, A.; Eubank, J.; Wuttke, S.; Xiao, B.; Wheatley, P.; Bazin, P.; Lavalley, J.-C.; Daturi, M.; Vimont, A.; De Weireld, G. Nitric Oxide Adsorption and Delivery in Flexible Mil-88 (Fe) Metal–Organic Frameworks. *Chemistry of Materials* **2013,** *25* (9), 1592-1599.
171. Sarkar, S.; Sales, K. M.; Hamilton, G.; Seifalian, A. M. Addressing Thrombogenicity in Vascular Graft Construction. *J Biomed Mater Res B Appl Biomater* **2007,** *82* (1), 100-108.
172. Kushwaha, M.; Anderson, J. M.; Bosworth, C. A.; Andukuri, A.; Minor, W. P.; Lancaster, J. R.; Anderson, P. G.; Brott, B. C.; Jun, H.-W. A Nitric Oxide Releasing, Self Assembled Peptide Amphiphile Matrix That Mimics Native Endothelium for Coating Implantable Cardiovascular Devices. *Biomaterials* **2010,** *31* (7), 1502-1508.
173. Weiming, X.; LIU, L. Z.; Loizidou, M.; AHMED, M.; CHARLES, I. G. The Role of Nitric Oxide in Cancer. *Cell research* **2002,** *12* (5), 311-320.
174. Wink, D.; Vodovotz, Y.; Cook, J.; Krishna, M.; Kim, S.; Coffn, D.; DeGraff, W.; Deluca, A.; Liebmann, J.; Mitchell, J. Reviews-the Role of Nitric Oxide Chemistry in Cancer Treatment. *Biochemistry-New York-English Translation of Biokhimiya* **1998,** *63* (7), 802-809.
175. Mocellin, S.; Bronte, V.; Nitti, D. Nitric Oxide, a Double Edged Sword in Cancer Biology: Searching for Therapeutic Opportunities. *Med Res Rev* **2007,** *27* (3), 317-352.
176. Coulter, J.; McCarthy, H.; Xiang, J.; Roedl, W.; Wagner, E.; Robson, T.; Hirst, D. Nitric Oxide—a Novel Therapeutic for Cancer. *Nitric oxide* **2008,** *19* (2), 192-198.
177. Ballard, R. A.; Truog, W. E.; Cnaan, A.; Martin, R. J.; Ballard, P. L.; Merrill, J. D.; Walsh, M. C.; Durand, D. J.; Mayock, D. E.; Eichenwald, E. C. Inhaled Nitric Oxide in Preterm Infants Undergoing Mechanical Ventilation. *New England Journal of Medicine* **2006,** *355* (4), 343-353.
178. Kinsella, J. P.; Cutter, G. R.; Walsh, W. F.; Gerstmann, D. R.; Bose, C. L.; Hart, C.; Sekar, K. C.; Auten, R. L.; Bhutani, V. K.; Gerdes, J. S. Early Inhaled Nitric Oxide Therapy in Premature Newborns with Respiratory Failure. *New England Journal of Medicine* **2006,** *355* (4), 354-364.
179. Adhikari, N. K.; Dellinger, R. P.; Lundin, S.; Payen, D.; Vallet, B.; Gerlach, H.; Park, K. J.; Mehta, S.; Slutsky, A. S.; Friedrich, J. O. Inhaled Nitric Oxide Does Not Reduce Mortality in Patients with Acute Respiratory Distress Syndrome Regardless of Severity: Systematic Review and Meta-Analysis*. *Critical care medicine* **2014,** *42* (2), 404-412.

180. Mapel, D.; Warshoff, N.; Fogarty, C.; Martinez, F.; Heyrman, R.; Greene, D. The Effect of Pulsed Inhaled Nitric Oxide on Pulmonary Hemodynamics and Systemic Oxygenation in Patients with Pulmonary Hypertension Associated with Copd (Ph-Copd) on Long-Term Oxygen Therapy (Ltot). *Am J Respir Crit Care Med* **2015,** *191*, A3831.
181. Knott, A. B.; Bossy-Wetzel, E. Nitric Oxide in Health and Disease of the Nervous System. *Antioxidants & redox signaling* **2009,** *11* (3), 541-553.
182. Gibbons, H. M.; Dragunow, M. Microglia Induce Neural Cell Death Via a Proximity-Dependent Mechanism Involving Nitric Oxide. *Brain research* **2006,** *1084* (1), 1-15.
183. Moncada, S.; Bolaños, J. P. Nitric Oxide, Cell Bioenergetics and Neurodegeneration. *Journal of neurochemistry* **2006,** *97* (6), 1676-1689.
184. Hamid, Q.; Springall, D. R.; Polak, J.; Riveros-Moreno, V.; Chanez, P.; Bousquet, J.; Godard, P.; Holgate, S.; Howarth, P.; Redington, A. Induction of Nitric Oxide Synthase in Asthma. *The Lancet* **1993,** *342* (8886), 1510-1513.
185. Kharitonov, S.; Yates, D.; Robbins, R.; Barnes, P.; Logan-Sinclair, R.; Shinebourne, E. Increased Nitric Oxide in Exhaled Air of Asthmatic Patients. *The Lancet* **1994,** *343* (8890), 133-135.
186. Smith, A. D.; Cowan, J. O.; Brassett, K. P.; Herbison, G. P.; Taylor, D. R. Use of Exhaled Nitric Oxide Measurements to Guide Treatment in Chronic Asthma. *New England Journal of Medicine* **2005,** *352* (21), 2163-2173.
187. Mitrovic, B.; Ignarro, L.; Montestruque, S.; Smoll, A.; Merrill, J. Nitric Oxide as a Potential Pathological Mechanism in Demyelination: Its Differential Effects on Primary Glial Cellsin Vitro. *Neuroscience* **1994,** *61* (3), 575-585.
188. MacMicking, J.; Xie, Q.-w.; Nathan, C. Nitric Oxide and Macrophage Function. *Annual review of immunology* **1997,** *15* (1), 323-350.
189. Katusic, Z. S.; Austin, S. A. Endothelial Nitric Oxide: Protector of a Healthy Mind. *European heart journal* **2013**, eht544.
190. Carnicer, R.; Crabtree, M. J.; Sivakumaran, V.; Casadei, B.; Kass, D. A. Nitric Oxide Synthases in Heart Failure. *Antioxidants & redox signaling* **2013,** *18* (9), 1078-1099.
191. Steinert, J. R.; Chernova, T.; Forsythe, I. D. Nitric Oxide Signaling in Brain Function, Dysfunction, and Dementia. *The Neuroscientist* **2010,** *16* (4), 435-452.
192. Keum, D. H.; Jung, H. S.; Wang, T.; Shin, M. H.; Kim, Y. E.; Kim, K. H.; Ahn, G.; Hahn, S. K. Cancer Detection: Microneedle Biosensor for Real-Time Electrical Detection of Nitric Oxide for in Situ Cancer Diagnosis During Endomicroscopy (Adv. Healthcare Mater. 8/2015). *Advanced healthcare materials* **2015,** *4* (8), 1152-1152.

Chapter 2: Introduction to Small Diameter Vascular Grafts

2.1 The Arterial Structure

Arteries are composed of a concentric, layered structure which endows them with the ability to respond to physiological and chemical cues to alter their physical structure. The arterial structure can be subdivided into three major, histologically distinct, components: the intima, the media, and the adventitia[1]. Further subdivisions can be made and are shown in Figure 2.1.

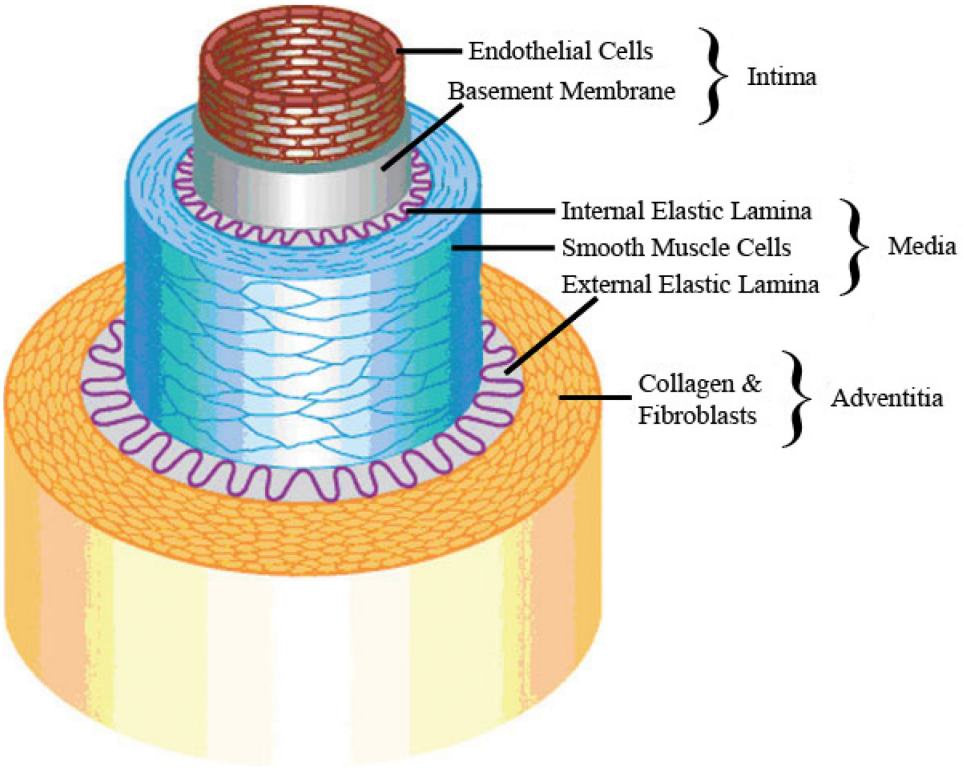

Figure 2.1. The structure of an artery. Figure 2.1 shows the typical organization of the tissue in the arterial wall. Reprinted with permission from John Wiley & Sons[1].

The intima, which forms the lumen of the vessel, is composed of a monolayer of vascular endothelial cells (vEC) connected to a basement membrane composed of collagen IV and laminin[2]. The vEC's functions include regulation of angiogenesis, the creation and maintenance of a selective barrier, and the formation of a non-thrombogenic blood contacting layer[2-3]. While the vEC monolayer presents a non-thrombogenic surface to the blood, the basement membrane presents a highly thrombogenic surface. Thus, when

damage occurs to the endothelium, platelets will adhere to the exposed underlying basement membrane. In a case where more extensive damage has occurred, the highly thrombogenic collagen of the sub-endothelial connective tissue will promote platelet attachment to the exposed surface, instigating a thrombotic response[1]. The fenestrated internal elastic lamina covers the basement membrane[2].

The medial layer, composed largely of collagens I and III, consists of a layer of vSMCs bounded by an internal and external elastic lamina[1-2]. The vSMC layer has a circumferential orientation along the central axis of the vessel. Due to their arrangement, the coordinated contraction or relaxation of vSMCs results in the regulation of vascular tone and diameter through a response to cues from circulating cytokines and endothelial cells[2]. The external elastic lamina separates the medial layer from the collagen containing adventitia[2].

The adventitial layer is mainly composed of connective tissues, including collagen and embedded fibroblasts[1]. These components contribute to the mechanical strength of the artery while promoting integration with the surrounding environment. On the adventitial surface, collagen acts as a substrate for the vasa vasorum[1].

Native arterial mechanical properties have been found to be anisotropic in nature, endowing arterial vessels with high elasticity under low pressure conditions while maintaining low distensibility and increased stiffness at high pressures[4]. The laminar and circumferential arrangement of collagen and elastin fibers confers these properties to arterial vessels[4]. Studies have demonstrated that elastin fibers are active elements under pressure until approximately 120 mmHg, after which the stress is transferred fully to collagen fibrils[4].

2.2. The Current Status of Small Diameter Vascular Grafts

To date, few viable options exist in the treatment of pathologies involving small diameter arteries (< 6 mm), though the saphenous vein, internal mammary artery (IMA), the umbilical cord artery, and radial artery are all viable options[5-7]. The saphenous vein is the current standard for coronary artery bypass grafts (CABGs) (Figure 2.2). However, complications, previous surgeries, and pre-existing pathologies can render that route of treatment inappropriate for approximately 5–33% of the patient population[6-8]. Autologous arteries and veins used as vascular grafts account for approximately 500,000 procedures each year and are the gold standard in vascular interventions[9-10]. Currently, no engineered construct is capable of reliably replacing autologous vascular substitutes.

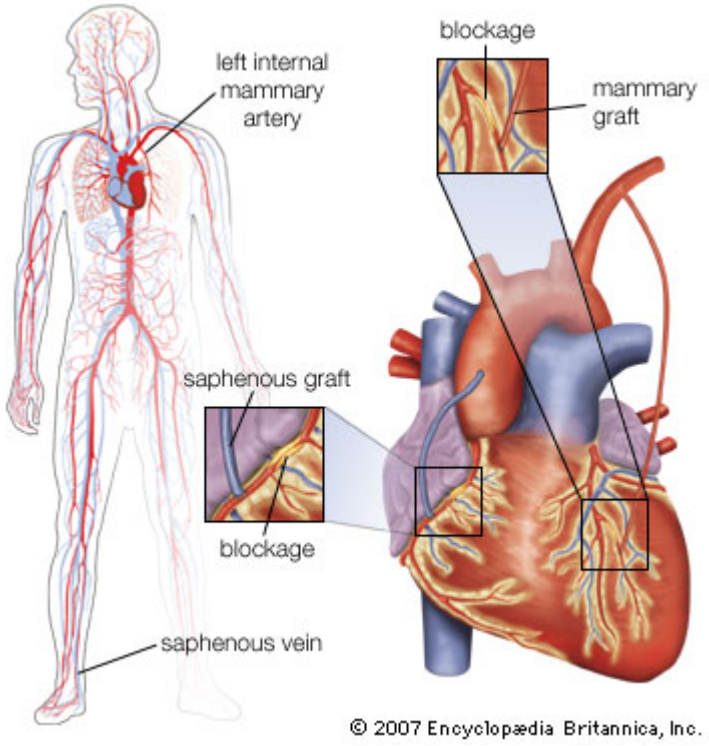

Figure 2.2. Coronary artery bypass graft. Figure 2.2 shows the common donor sites and vessels used in coronary artery bypass grafts. Reprinted with permission from Encyclopaedia Britannica[11].

Several decades ago, the standard for large diameter vascular grafts, expanded polytetrafluoroethylene (ePTFE), was evaluated for use in small diameter applications[6, 12]. In contrast to the outcomes observed in large diameter trials, small diameter grafts fabricated from ePTFE showed significant thrombosis, neointimal hyperplasia, and restenosis[3, 13-18]. Poly(ethylene terephthalate) (Dacron) has also been evaluated for use in small diameter vascular grafts[5, 19-20]. The outcome was similar to that of ePTFE.

In short term trials, these synthetic grafts perform favorably, however late term performance decreases rapidly, often attributed to poor luminal biocompatibility, low flows, and compliance mismatches, resulting in a chronic thrombogenesis, anastomotic intimal hyperplasia, and late stage failure from neointimal hyperplasia[5-6, 21-23]. Synthetic grafts demonstrate suboptimal patency rates of 30% after 5 years[24]. Both natural and synthetic small diameter vascular grafts have been under development, reporting varied degrees of success and patency[6, 8, 12].

In contrast, the saphenous vein grafts are significantly improved over synthetic grafts, with patency rates of 75% over 5 years[24]. However, the best available vascular graft for CABGs, to date, is the human internal mammary artery (IMA). The IMA demonstrates a 95.8% patency rate as compared to 75–82.4% patency rate for the saphenous vein after 5

years[5, 25]. Additionally, atherosclerosis is rare in the IMA, and speculations abound of its high elastin content being a significant contributing factor to its substantial patency rate[5, 26-27]. In spite of its successes, the IMA has its own complications, as the extensive surgery required during a bilateral IMA harvest can lead to an increased prevalence of complications during wound healing and donor site morbidity[5, 28]. Each of the vascular grafts presented above have been previously evaluated. However, a trend of increased patency rates with increasing elastin content, a seemingly key contributing factor to the graft's performance, might have been overlooked.

An ideal vascular graft would possess a native architecture closely mimicking the properties of the substituted vessel, maintain a blood contacting surface that was both non-thrombogenic and non-immunogenic, and originate from a readily available, easily replenished source. Shelf stability over extended time periods would make the vascular graft more adaptable to each individual patient and expedite the transition to clinical adoption.

2.3. Mechanisms of Small Diameter Vascular Graft Failure

Thrombosis is often the dominant failure mode during early stage (< 1 month) post-surgical recovery following surgical interventions utilizing small diameter vascular grafts[28]. Formation can occur either at the injury site or distally along the length of the vessel. Often, the underlying causes of the thrombotic response are attributed to the denudation of the endothelium or partial disruption of the endothelial monolayer, graft ischemia, and turbulent flow at the anastomoses due to a size or compliance mismatch[28].

Intimal or neointimal hyperplasia is an exaggerated healing process that occurs following injury to the vascular wall[7, 29]. Neointimal hyperplasia is generally initiated by injury to the vascular wall resulting in denudation of the endothelium, exposing the thrombogenic basement membrane and vSMCs to circulating blood[29]. Restenosis, or a reoccurrence of vascular stenosis, is often attributed to neointimal hyperplasia and is defined as a reduction in a vessel's luminal diameter of more than 50%[30-31].

Within seconds post-injury, the cascade towards intimal/neointimal hyperplasia first begins with platelet aggregation and adhesion to the underlying tissue, followed closely by fibrin deposition and thrombus formation[31]. Following platelet attachment, leukocyte chemotaxis and vSMC proliferation occur at the site of injury[29, 31]. Migration of vSMCs due to basic fibroblast growth factor (bFGF) exposure then occurs, followed by endothelial cell proliferation due to activated platelet derived factors[29, 31]. As vSMCs undergo a transition from the contractile state to the synthetic state, they migrate into the intimal layer and begin proliferating[31]. Under normal physiological conditions, the elastic laminae prevent vSMC migration into the intimal layer. Post-injury, ECM remodeling and collagen deposition allows cells to penetrate this barrier, forming the neointima[29, 31].

Onset of intimal hyperplasia often develops prior to thrombosis, and is considered a medium to long term event[1]. It is thought that the elastic mismatch between current grafts and the native architecture contributes to intimal hyperplasia, attributable to the resultant turbulent flow and shear stress[4, 23].

2.4. Classes of Small Diameter Vascular Grafts

Current research in the field of small diameter vascular graft fabrication has revealed several promising approaches to address some of the deficiencies in available technologies. Tissue engineered vascular grafts (TEVGs), decellularized constructs, electrospun vessels, and drug eluting polymeric vascular grafts are all under development.

One of the more prevalent techniques under development centers on the use of TEVGs. Three elements are required for TEVGs to work, deemed the tissue engineering triad: a biodegradable scaffold to promote neo-tissue formation, cells, and the signals required to promote differentiation and proper function[17, 32]. In this approach, an extracellular matrix based scaffold is fabricated with the intention of seeding and then culturing the patient's matching cells within the structure. A variation on this technique which has also shown some promise is the use of rolled cell sheets to form a tubular vessel[12, 33]. After a period of time, the graft becomes re-endothelialized and the specific cell types regain their original functions with the addition of humoral and mechanical signals imparted during fabrication. Re-endothelialization allows the vascular substitute to prevent post-implantation thrombosis through regulation of platelet adhesion[1].

As in native tissue, the structure and function of the vascular graft will be dependent on the organization and function of the individual components. Endothelial cells must re-endothelialize the lumen of the TEVG and remain attached, a critical aspect of thromboresistance and the prevention of neointimal formation through the suppression of smooth muscle cell proliferative factors and stimuli[17]. While the importance of a confluent monolayer is undisputed, fibroblasts and smooth muscle cells are critical to the formation and proper function of a TEVG[17]. Studies by Weinberg and Bell as well as Noishiki et al. revealed that graft seeding, regardless of cell type, accelerated endothelialization[17, 34]. Many groups are actively investigating the use of stem cells, where the ultimate goal of natural cellular differentiation based upon the local environment could create a universal source of cells[33].

In the physiological environment, oxygen maintains a diffusion limit of 200 μm^3. Thus, capillaries originating from the vasculature are required to supply oxygen and nutrients to surrounding tissue. Much like other organs and tissues, the vessels themselves must have a supply of oxygen and nutrients and rely on a network of vessels known as the vasa vasorum. The development of this support system has become a significant hurdle in the

development of cell sheet and tissue engineered vessels. Waste generated in the cells, such as CO_2, are also removed by the capillaries[3]. Some groups have developed methods of inducing angiogenesis in cell sheet and TEVG based synthetic grafts in an attempt to pre-vascularize the construct and optimize the growth and formation of the vessel during bioreactor perfusion. Eventually, these neo-vessels will connect to the patient's existing vasculature[3]. This can be accomplished through pre-vascularization of an *in vitro* construct, whereby a rudimentary vasculature is built into the underlying structure, or through the administration of angiogenic cytokines during *in vitro* culture[3].

A significant advantage in the use of stem cells comes from their ability to self-regenerate. In culture, biological and mechanical signals are required to begin cellular differentiation. In the absence of these signals, the cells would exist in a latent state. Induction of cellular differentiation could be initiated prior to implantation, allowing for excellent temporal control of the graft development[17]. While the theory behind this approach is solid and appears promising, the time required for fabrication of the grafts and their relatively delicate handling properties have shown limited *in vivo* and clinical successes.

Allogenic and xenogenic decellularized constructs are being investigated as scaffolds in the development of vascular grafts due to the ability to retain the native ECM architecture while providing preferential reorganizational capacity for a patient's native cells[6, 17]. The advantage of decellularized constructs over cell-synthesized, tissue engineered substrates comes from the natural, rather than cell-stimulated, organizational structure of the ECM. This structure can be retained through non-destructive processes such as protein or ECM digestion and decellularization. Additionally, decellularization removes any potential antigenic material which may provoke a stress immune response though the application of physical agitation, chemical digestion, surfactant washes, and enzymatic digestion[17]. Severe processing of decellularized scaffolds required to remove all of the antigenic material may cause excessive damage to the ECM components. Unfortunately, improving the mechanical properties of decellularized materials becomes more challenging than other tissue engineering approaches[17]. One of the significant criticisms of the decellularized constructs is the inherent lack of a suitable, non-thrombogenic, blood contacting surface[12]. Native elastin has been proposed as a potential solution to this deficiency[35-36].

Electrospinning was originally introduced in the 1930s as a novel method of textile manufacturing[28]. It has recently been adopted to fabricate nanoscale polymer fibers for medical use. Electrospinning provides an economical, rapid method to fabricate tubular constructs with minimal processing time that allows almost infinite tuning of the material, mechanical, and topographic properties of the finalized construct.

A basic electrospinning apparatus requires four components: a voltage supply, a grounded collector, a dissolved polymer solution, and a delivery mechanism (Figure 2.3). A typical electrospinner will have several additional components to control the alignment and distribution of the electrospun fibers. Generally, a polymer dissolved in an organic solvent is fed through a charged metal tube. This tube is elevated to a high potential, and placed over a grounded, static collector, generating an external electric field and imparting a charge imbalance to the system[28]. This charge imbalance results in the formation of a conical Taylor cone. As the charge imbalance of the electric field exceeds the surface tension of the polymer solution, a polymer jet is ejected from the opening of the tube. During the time required to reach the target, the solvent evaporates, forming a fibrous polymer mesh with no trend towards any specific fiber orientation. By rotating the collector, tubular constructs and aligned fibers can be formed[28].

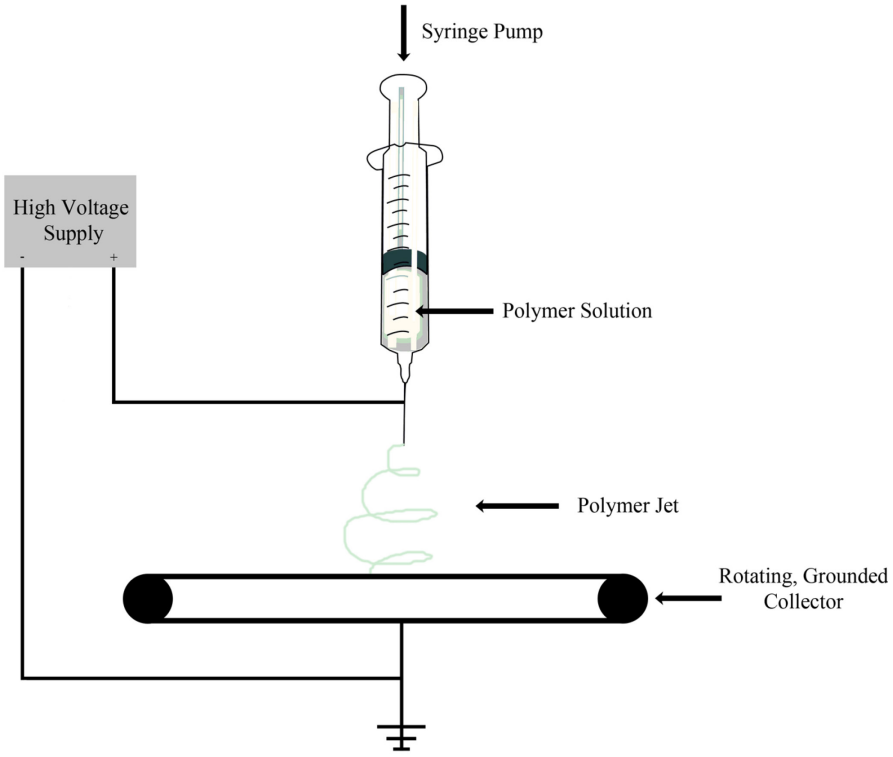

Figure 2.3. A diagram of a basic electrospinner. A typical electrospinner is shown in Figure 2.2, comprising of a syringe pump, high voltage power supply, polymer solution, and rotating collector.

Control over the electrospinning process requires careful consideration of many factors: the relative humidity of the electrospinning environment, the selected polymer and solvent, angular velocity of the collector, the accelerating voltage, and the length of the air gap. This is only a brief list of the elements that control the final product generated during electrospinning.

Electrospun fibers offer exceptional control over the material, mechanical properties, and morphology of a fabricated construct[17]. With fiber diameters ranging from the nanoscale to microscale, the mechanical properties of a vascular graft could conceivably be infinitely altered through materials selection, fiber morphology, fiber density, and fiber diameter. Due to the scale of the fibers, fabrication of nanotextured surfaces and the incorporation of mechano-chemical cues through electrospinning is possible[17]. The porosity of the fabricated construct can be tailored to match the application, and degradation properties of biodegradable scaffolds can be easily altered[37]. As many ECM proteins are deposited in fibrillar structures, it is possible for electrospun scaffolds to approximate this morphology to better mimic the native environment[38]. In fact, many groups have begun to electrospun native and synthetic ECM based materials in an attempt to replicate the native physiological architecture while maintaining some degree of control over the morphology and final chemical characteristics[39-44]. Anisotropic scaffolds can be fabricated through the use of aligned fibers, and aligned fibers have been shown to enhance endothelial cell migration[45-46].

Drug eluting grafts represent a directed approach to solving some of the many issues observed in small diameter vascular constructs. By incorporating one or more drugs into a construct, whether chemically or by mixing, several failings of current grafts may be addressed. Many groups have incorporated anti-thrombotic agents into polymeric constructs[28, 47-49], while others have incorporated anti-proliferative agents to reduce or prevent neointimal hyperplasia[50-52]. Incorporation of the drugs into polymer substrates has resulted in the fabrication of electrospun, drug eluting vascular grafts[28]. Localization of a drug within a construct would promote directed delivery, while tailored release rates, durations, and levels, would substantially increase its efficacy[28].

The fabrication time of any vascular substitute is critical in its evolution as a clinically viable solution. Typical fabrication times of electrospun scaffolds vary between 10 minutes to several hours, while TEVGs and cell sheet engineered products might require weeks to months[33, 53-59]. Eventually, a combination of electrospinning, 3D printing technology, and 3D imaging could be a promising approach for boutique, made while you wait, vascular grafts. Though graft fabrication time is important, storage stability and transport concerns are also a critical aspect in the fabrication of clinically viable vascular grafts. Incorporating materials which are easily stored and transported will lead to more rapid clinical acceptance than constructs with a finite lifespan.

2.5. Elastin as a Blood Contacting Surface

Elastin, a 67 kDa extracellular matrix protein, has previously demonstrated favorable properties as a blood contacting layer in small diameter vascular grafts[60]. Possessing biological properties such as low thrombogenicity, smooth muscle cell inhibitory

properties, and an endothelial cell favored surface, elastin is an ideal blood contacting layer in a small diameter vascular graft[5, 61]. However, native elastin is extremely insoluble and hydrophobic, leading to significant hurdles in its processing[62]. Synthetic elastin in the form of tropoelastin and synthetically produced elastin is cost prohibitive and its synthesis requires significant amounts of time[63-66]. Decellularization of native materials will maintain the chemical and mechanical architecture of the host tissue, improving the cellular integration and remodeling response, *in vivo*[24]. Due to elastin's favorable properties in vascular grafts, many groups have attempted to incorporate elastin into hybrid and synthetic constructs[22, 24, 60-61, 63, 65-66]. Figure 2.4 shows the location of the elastin containing elastic lamina within the arterial structure.

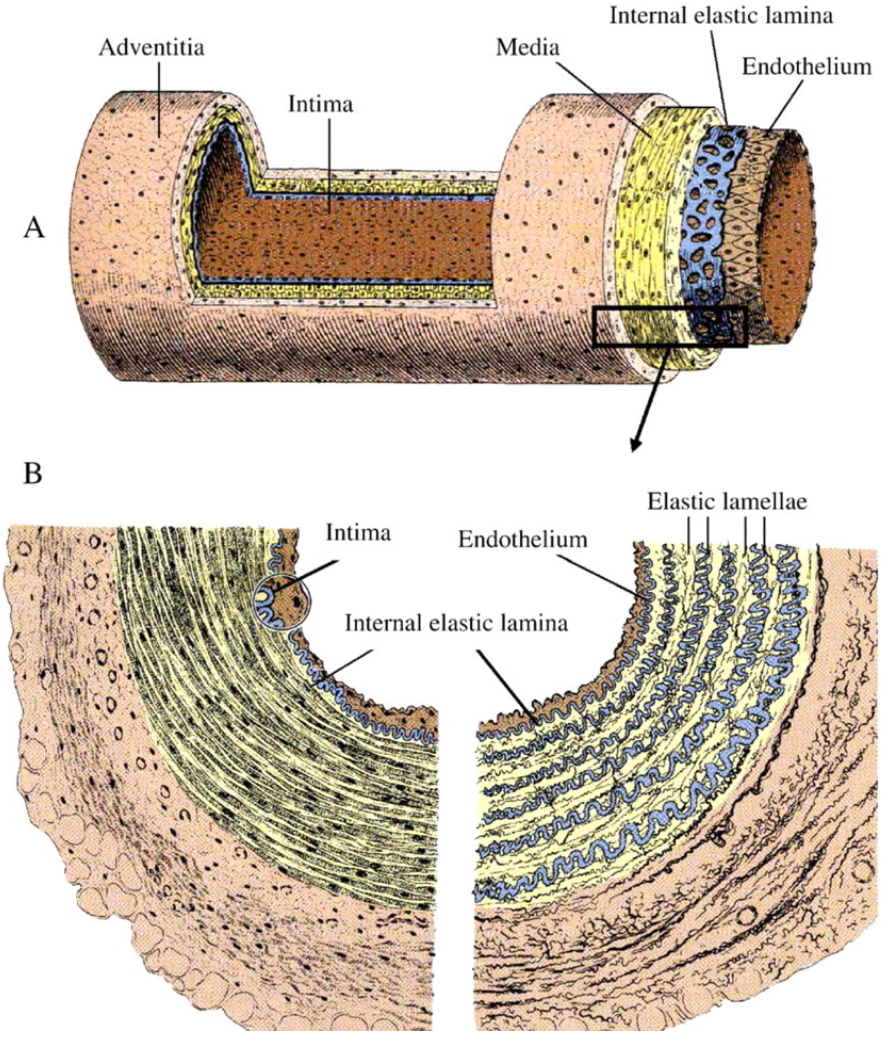

Figure 2.4. Elastin's location and structure within the artery. (A) denotes the location of the elastic lamina within the arterial structure. (B) shows the typical distribution of the elastic lamina in a muscular artery (left) and an elastic artery (right). Reprinted with permission from Oxford University Press[67].

Based on published research, native elastin provides an anti-thrombogenic and neointimal hyperplasia resistant blood contacting surface[35-36, 60, 68]. Thus, the quantity, organization, and location of native elastin within a vascular graft may have substantial effects on its performance.

The human saphenous vein is currently the most common graft utilized for CABG procedures. Collagen content of the saphenous vein is 65%, which is significantly higher than in arteries[69]. The presence of significant quantities of collagen will elicit improved mechanical properties, however may also contribute to thrombogenesis and neointimal hyperplasia. The human umbilical cord artery, in stark contrast to the saphenous vein and IMA, possesses a negligible quantity of elastin. However, its branch free length of 50 cm and a readily available supply of new tissue makes the umbilical cord artery desirable for vascular grafts fabrication[70].

In contrast, the human IMA contains between 25–40% collagen, while elastin accounts for the majority of the remaining tissue[69]. The IMA is most like the vessel show in the right side of Figure 2.4B. The high patency rate of the IMA makes it an ideal vascular graft, however the extensive surgical procedures and delicate properties of the vessel have hampered its acceptance as a widespread substitute. When the patency data is considered alongside the elastin content of each respective type of vessel, the IMA becomes a strong contender in the search for an ideal vascular substitute. A hybrid vascular construct utilizing native elastin may be superior to current approaches and address some of the key criteria of an ideal vascular graft presented earlier. Overcoming the difficulties and shortcomings of native elastin may prove fruitful in the search for a clinically viable small diameter vascular graft.

2.6. References

1. Sarkar, S.; Sales, K. M.; Hamilton, G.; Seifalian, A. M. Addressing Thrombogenicity in Vascular Graft Construction. *J Biomed Mater Res B Appl Biomater* **2007,** *82* (1), 100-108.
2. Stegemann, J. P.; Kaszuba, S. N.; Rowe, S. L. Review: Advances in Vascular Tissue Engineering Using Protein-Based Biomaterials. *Tissue Eng* **2007,** *13* (11), 2601-2613.
3. Novosel, E. C.; Kleinhans, C.; Kluger, P. J. Vascularization Is the Key Challenge in Tissue Engineering. *Advanced drug delivery reviews* **2011,** *63* (4), 300-311.
4. Sarkar, S.; Schmitz-Rixen, T.; Hamilton, G.; Seifalian, A. M. Achieving the Ideal Properties for Vascular Bypass Grafts Using a Tissue Engineered Approach: A Review. *Med Biol Eng Comput* **2007,** *45* (4), 327-336.
5. Byrom, M. J.; Ng, M. K.; Bannon, P. G. Biomechanics and Biocompatibility of the Perfect Conduit-Can We Build One? *Ann Cardiothorac Surg* **2013,** *2* (4), 435-443.
6. Wang, X.; Lin, P.; Yao, Q.; Chen, C. Development of Small-Diameter Vascular Grafts. *World J Surg* **2007,** *31* (4), 682-689.
7. de Mel, A.; Murad, F.; Seifalian, A. M. Nitric Oxide: A Guardian for Vascular Grafts? *Chem Rev* **2011,** *111* (9), 5742-5767.
8. Kannan, R. Y.; Salacinski, H. J.; Butler, P. E.; Hamilton, G.; Seifalian, A. M. Current Status of Prosthetic Bypass Grafts: A Review. *J Biomed Mater Res B Appl Biomater* **2005,** *74* (1), 570-581.
9. Nottelet, B.; Pektok, E.; Mandracchia, D.; Tille, J. C.; Walpoth, B.; Gurny, R.; Moeller, M. Factorial Design Optimization and in Vivo Feasibility of Poly (E-Caprolactone)-Micro-and Nanofiber-Based Small Diameter Vascular Grafts. *Journal of Biomedical Materials Research Part A* **2009,** *89* (4), 865-875.
10. Wang, X.; Lin, P.; Yao, Q.; Chen, C. Development of Small-Diameter Vascular Grafts. *World journal of surgery* **2007,** *31* (4), 682-689.
11. Coronary Artery Bypass. In *Encyclopaedia Britannica Online*, **2007**.
12. Nerem, R. M.; Seliktar, D. Vascular Tissue Engineering. *Annual review of biomedical engineering* **2001,** *3* (1), 225-243.
13. Wu, H.; Fan, J.; Chu, C.-C.; Wu, J. Electrospinning of Small Diameter 3-D Nanofibrous Tubular Scaffolds with Controllable Nanofiber Orientations for Vascular Grafts. *Journal of Materials Science: Materials in Medicine* **2010,** *21* (12), 3207-3215.
14. De Visscher, G.; Mesure, L.; Meuris, B.; Ivanova, A.; Flameng, W. Improved Endothelialization and Reduced Thrombosis by Coating a Synthetic Vascular Graft with Fibronectin and Stem Cell Homing Factor Sdf-1α. *Acta biomaterialia* **2012,** *8* (3), 1330-1338.
15. Hashi, C. K.; Derugin, N.; Janairo, R. R. R.; Lee, R.; Schultz, D.; Lotz, J.; Li, S. Antithrombogenic Modification of Small-Diameter Microfibrous Vascular Grafts. *Arteriosclerosis, thrombosis, and vascular biology* **2010,** *30* (8), 1621-1627.
16. Avci-Adali, M.; Ziemer, G.; Wendel, H. P. Induction of Epc Homing on Biofunctionalized Vascular Grafts for Rapid in Vivo Self-Endothelialization—a Review of Current Strategies. *Biotechnology advances* **2010,** *28* (1), 119-129.

17. Naito, Y.; Shinoka, T.; Duncan, D.; Hibino, N.; Solomon, D.; Cleary, M.; Rathore, A.; Fein, C.; Church, S.; Breuer, C. Vascular Tissue Engineering: Towards the Next Generation Vascular Grafts. *Advanced drug delivery reviews* **2011,** *63* (4), 312-323.
18. Nieponice, A.; Soletti, L.; Guan, J.; Hong, Y.; Gharaibeh, B.; Maul, T. M.; Huard, J.; Wagner, W. R.; Vorp, D. A. In Vivo Assessment of a Tissue-Engineered Vascular Graft Combining a Biodegradable Elastomeric Scaffold and Muscle-Derived Stem Cells in a Rat Model. *Tissue Engineering Part A* **2010,** *16* (4), 1215-1223.
19. Nerem, R. M.; Seliktar, D. Vascular Tissue Engineering. *Annu Rev Biomed Eng* **2001,** *3*, 225-243.
20. Desai, M.; Seifalian, A. M.; Hamilton, G. Role of Prosthetic Conduits in Coronary Artery Bypass Grafting. *Eur J Cardiothorac Surg* **2011,** *40* (2), 394-398.
21. Novosel, E. C.; Kleinhans, C.; Kluger, P. J. Vascularization Is the Key Challenge in Tissue Engineering. *Adv Drug Deliv Rev* **2011,** *63* (4-5), 300-311.
22. Wise, S. G.; Byrom, M. J.; Waterhouse, A.; Bannon, P. G.; Weiss, A. S.; Ng, M. K. A Multilayered Synthetic Human Elastin/Polycaprolactone Hybrid Vascular Graft with Tailored Mechanical Properties. *Acta Biomater* **2011,** *7* (1), 295-303.
23. Kapadia, M. R.; Popowich, D. A.; Kibbe, M. R. Modified Prosthetic Vascular Conduits. *Circulation* **2008,** *117* (14), 1873-1882.
24. McFetridge, P. S.; Daniel, J. W.; Bodamyali, T.; Horrocks, M.; Chaudhuri, J. B. Preparation of Porcine Carotid Arteries for Vascular Tissue Engineering Applications. *J Biomed Mater Res A* **2004,** *70* (2), 224-234.
25. Hayward, P. A.; Buxton, B. F. Contemporary Coronary Graft Patency: 5-Year Observational Data from a Randomized Trial of Conduits. *The Annals of thoracic surgery* **2007,** *84* (3), 795-799.
26. Barry, M. M.; Foulon, P.; Touati, G.; Ledoux, B.; Sevestre, H.; Carmi, D.; Laude, M. Comparative Histological and Biometric Study of the Coronary, Radial and Left Internal Thoracic Arteries. *Surg Radiol Anat* **2003,** *25* (3-4), 284-289.
27. Taggart, D. P. Bilateral Internal Mammary Artery Grafting: Are Bima Better? *Heart* **2002,** *88* (1), 7-9.
28. Han, J.; Lelkes, P. I. Drug-Eluting Vascular Grafts. **2014**, 405-427.
29. Ahanchi, S. S.; Tsihlis, N. D.; Kibbe, M. R. The Role of Nitric Oxide in the Pathophysiology of Intimal Hyperplasia. *J Vasc Surg* **2007,** *45 Suppl A*, A64-73.
30. Jimenez-Valero, S.; Moreno, R.; Sanchez-Recalde, A.; Galeote, G.; Calvo, L.; Viana, A.; Lopez de Sa, E.; Lopez-Sendon, J. Avoiding Restenosis: Is There a Role for Glucocorticoids in the Drug-Eluting Stent Era? *Ther Adv Cardiovasc Dis* **2008,** *2* (3), 137-146.
31. Hamid, H.; Coltart, J. 'Miracle Stents'-a Future without Restenosis. *McGill Journal of Medicine: MJM* **2007,** *10* (2), 105.
32. Bajpai, V. K.; Andreadis, S. T. Stem Cell Sources for Vascular Tissue Engineering and Regeneration. *Tissue Eng Part B Rev* **2012,** *18* (5), 405-425.
33. Peck, M.; Gebhart, D.; Dusserre, N.; McAllister, T. N.; L'Heureux, N. The Evolution of Vascular Tissue Engineering and Current State of the Art. *Cells Tissues Organs* **2012,** *195* (1-2), 144-158.

34. Noishiki, Y.; Yamane, Y.; Okoshi, T.; Tomizawa, Y.; Satoh, S. Choice, Isolation, and Preparation of Cells for Bioartificial Vascular Grafts. *Artificial organs* **1998,** *22* (1), 50-62.
35. Liu, S. Q.; Tieche, C.; Alkema, P. K. Neointima Formation on Vascular Elastic Laminae and Collagen Matrices Scaffolds Implanted in the Rat Aortae. *Biomaterials* **2004,** *25* (10), 1869-1882.
36. Liu, S. Q.; Alkema, P. K.; Tieche, C.; Tefft, B. J.; Liu, D. Z.; Li, Y. C.; Sumpio, B. E.; Caprini, J. A.; Paniagua, M. Negative Regulation of Monocyte Adhesion to Arterial Elastic Laminae by Signal Regulatory Protein Alpha and Src Homology 2 Domain-Containing Protein-Tyrosine Phosphatase-1. *J Biol Chem* **2005,** *280* (47), 39294-39301.
37. Greiner, A.; Wendorff, J. H. Electrospinning: A Fascinating Method for the Preparation of Ultrathin Fibers. *Angewandte Chemie International Edition* **2007,** *46* (30), 5670-5703.
38. Kumbar, S.; James, R.; Nukavarapu, S.; Laurencin, C. Electrospun Nanofiber Scaffolds: Engineering Soft Tissues. *Biomedical Materials* **2008,** *3* (3), 034002.
39. Wise, S. G.; Byrom, M. J.; Waterhouse, A.; Bannon, P. G.; Ng, M. K.; Weiss, A. S. A Multilayered Synthetic Human Elastin/Polycaprolactone Hybrid Vascular Graft with Tailored Mechanical Properties. *Acta Biomaterialia* **2011,** *7* (1), 295-303.
40. McKenna, K. A.; Hinds, M. T.; Sarao, R. C.; Wu, P.-C.; Maslen, C. L.; Glanville, R. W.; Babcock, D.; Gregory, K. W. Mechanical Property Characterization of Electrospun Recombinant Human Tropoelastin for Vascular Graft Biomaterials. *Acta biomaterialia* **2012,** *8* (1), 225-233.
41. Rnjak-Kovacina, J.; Wise, S. G.; Li, Z.; Maitz, P. K.; Young, C. J.; Wang, Y.; Weiss, A. S. Electrospun Synthetic Human Elastin: Collagen Composite Scaffolds for Dermal Tissue Engineering. *Acta biomaterialia* **2012,** *8* (10), 3714-3722.
42. Huang, C.; Chen, R.; Ke, Q.; Morsi, Y.; Zhang, K.; Mo, X. Electrospun Collagen–Chitosan–Tpu Nanofibrous Scaffolds for Tissue Engineered Tubular Grafts. *Colloids and Surfaces B: Biointerfaces* **2011,** *82* (2), 307-315.
43. Marelli, B.; Achilli, M.; Alessandrino, A.; Freddi, G.; Tanzi, M. C.; Farè, S.; Mantovani, D. Collagen-Reinforced Electrospun Silk Fibroin Tubular Construct as Small Calibre Vascular Graft. *Macromolecular bioscience* **2012,** *12* (11), 1566-1574.
44. Boland, E. D.; Matthews, J. A.; Pawlowski, K. J.; Simpson, D. G.; Wnek, G. E.; Bowlin, G. L. Electrospinning Collagen and Elastin: Preliminary Vascular Tissue Engineering. *Front Biosci* **2004,** *9* (1422), C1432.
45. Bouta, E. M.; McCarthy, C. W.; Keim, A.; Wang, H. B.; Gilbert, R. J.; Goldman, J. Biomaterial Guides for Lymphatic Endothelial Cell Alignment and Migration. *Acta biomaterialia* **2011,** *7* (3), 1104-1113.
46. Courtney, T.; Sacks, M. S.; Stankus, J.; Guan, J.; Wagner, W. R. Design and Analysis of Tissue Engineering Scaffolds That Mimic Soft Tissue Mechanical Anisotropy. *Biomaterials* **2006,** *27* (19), 3631-3638.
47. Taite, L. J.; Yang, P.; Jun, H. W.; West, J. L. Nitric Oxide-Releasing Polyurethane-Peg Copolymer Containing the Yigsr Peptide Promotes Endothelialization with Decreased Platelet Adhesion. *J Biomed Mater Res B Appl Biomater* **2008,** *84* (1), 108-116.
48. Zhai, W.; Qiu, L. j.; Mo, X. m.; Wang, S.; Xu, Y. f.; Peng, B.; Liu, M.; Huang, J. h.; Wang, G. c.; Zheng, J. h. Coaxial Electrospinning of P (Lla-Cl)/Heparin Biodegradable Polymer

Nanofibers: Potential Vascular Graft for Substitution of Femoral Artery. *Journal of Biomedical Materials Research Part B: Applied Biomaterials* **2013**.
49. Yao, Y.; Wang, J.; Cui, Y.; Xu, R.; Wang, Z.; Zhang, J.; Wang, K.; Li, Y.; Zhao, Q.; Kong, D. Effect of Sustained Heparin Release from Pcl/Chitosan Hybrid Small-Diameter Vascular Grafts on Anti-Thrombogenic Property and Endothelialization. *Acta biomaterialia* **2014,** *10* (6), 2739-2749.
50. Baek, I.; Hwang, J.; Park, J.; Kim, H.; Park, J.-S.; Kim, D. J. Paclitaxel Coating on the Terminal Portion of Hemodialysis Grafts Effectively Suppresses Neointimal Hyperplasia in a Porcine Model. *Journal of vascular surgery* **2015,** *61* (6), 1575-1582. e1571.
51. Masaki, T.; Rathi, R.; Zentner, G.; Leypoldt, J. K.; Mohammad, S. F.; Burns, G. L.; Li, L.; Zhuplatov, S.; Chirananthavat, T.; Kim, S.-J. Inhibition of Neointimal Hyperplasia in Vascular Grafts by Sustained Perivascular Delivery of Paclitaxel. *Kidney international* **2004,** *66* (5), 2061-2069.
52. Hu, Y.; Zou, Y.; Dietrich, H.; Wick, G.; Xu, Q. Inhibition of Neointima Hyperplasia of Mouse Vein Grafts by Locally Applied Suramin. *Circulation* **1999,** *100* (8), 861-868.
53. Inoguchi, H.; Kwon, I. K.; Inoue, E.; Takamizawa, K.; Maehara, Y.; Matsuda, T. Mechanical Responses of a Compliant Electrospun Poly(L-Lactide-Co-Epsilon-Caprolactone) Small-Diameter Vascular Graft. *Biomaterials* **2006,** *27* (8), 1470-1478.
54. Drilling, S.; Gaumer, J.; Lannutti, J. Fabrication of Burst Pressure Competent Vascular Grafts Via Electrospinning: Effects of Microstructure. *J Biomed Mater Res A* **2009,** *88* (4), 923-934.
55. Walpoth, B. H.; Bowlin, G. L. The Daunting Quest for a Small Diameter Vascular Graft. *Expert Rev Med Devices* **2005,** *2* (6), 647-651.
56. Rayatpisheh, S.; Heath, D. E.; Shakouri, A.; Rujitanaroj, P.-O.; Chew, S. Y.; Chan-Park, M. B. Combining Cell Sheet Technology and Electrospun Scaffolding for Engineered Tubular, Aligned, and Contractile Blood Vessels. *Biomaterials* **2014,** *35* (9), 2713-2719.
57. Zhao, J.; Liu, L.; Wei, J.; Ma, D.; Geng, W.; Yan, X.; Zhu, J.; Du, H.; Liu, Y.; Li, L.; Chen, F. A Novel Strategy to Engineer Small-Diameter Vascular Grafts from Marrow-Derived Mesenchymal Stem Cells. *Artif Organs* **2012,** *36* (1), 93-101.
58. Krawiec, J. T.; Vorp, D. A. Adult Stem Cell-Based Tissue Engineered Blood Vessels: A Review. *Biomaterials* **2012,** *33* (12), 3388-3400.
59. Hasan, A.; Memic, A.; Annabi, N.; Hossain, M.; Paul, A.; Dokmeci, M. R.; Dehghani, F.; Khademhosseini, A. Electrospun Scaffolds for Tissue Engineering of Vascular Grafts. *Acta Biomater* **2014,** *10* (1), 11-25.
60. Hinds, M. T.; Rowe, R. C.; Ren, Z.; Teach, J.; Wu, P. C.; Kirkpatrick, S. J.; Breneman, K. D.; Gregory, K. W.; Courtman, D. W. Development of a Reinforced Porcine Elastin Composite Vascular Scaffold. *J Biomed Mater Res A* **2006,** *77* (3), 458-469.
61. McClure, M. J.; Sell, S. A.; Simpson, D. G.; Walpoth, B. H.; Bowlin, G. L. A Three-Layered Electrospun Matrix to Mimic Native Arterial Architecture Using Polycaprolactone, Elastin, and Collagen: A Preliminary Study. *Acta Biomater* **2010,** *6* (7), 2422-2433.
62. Waterhouse, A.; Wise, S. G.; Ng, M. K.; Weiss, A. S. Elastin as a Nonthrombogenic Biomaterial. *Tissue Eng Part B Rev* **2011,** *17* (2), 93-99.

63. Blit, P. H.; McClung, W. G.; Brash, J. L.; Woodhouse, K. A.; Santerre, J. P. Platelet Inhibition and Endothelial Cell Adhesion on Elastin-Like Polypeptide Surface Modified Materials. *Biomaterials* **2011,** *32* (25), 5790-5800.
64. Srokowski, E. M.; Woodhouse, K. A. Surface and Adsorption Characteristics of Three Elastin-Like Polypeptide Coatings with Varying Sequence Lengths. *J Mater Sci Mater Med* **2013,** *24* (1), 71-84.
65. McKenna, K. A.; Hinds, M. T.; Sarao, R. C.; Wu, P. C.; Maslen, C. L.; Glanville, R. W.; Babcock, D.; Gregory, K. W. Mechanical Property Characterization of Electrospun Recombinant Human Tropoelastin for Vascular Graft Biomaterials. *Acta Biomater* **2012,** *8* (1), 225-233.
66. Dahl, S. L. M.; Koh, J.; Prabhakar, V.; Niklason, L. E. Decellularized Native and Engineered Arterial Scaffolds for Transplantation. *Cell Transplantation* **2003,** *12* (6), 659-666.
67. Patel, A.; Fine, B.; Sandig, M.; Mequanint, K. Elastin Biosynthesis: The Missing Link in Tissue-Engineered Blood Vessels. *Cardiovasc Res* **2006,** *71* (1), 40-49.
68. Simionescu, D. T.; Lu, Q.; Song, Y.; Lee, J. S.; Rosenbalm, T. N.; Kelley, C.; Vyavahare, N. R. Biocompatibility and Remodeling Potential of Pure Arterial Elastin and Collagen Scaffolds. *Biomaterials* **2006,** *27* (5), 702-713.
69. Aydin, S.; Aydin, S.; Nesimi Eren, M.; Sahin, I.; Yilmaz, M.; Kalayci, M.; Gungor, O. The Cardiovascular System and the Biochemistry of Grafts Used in Heart Surgery. *Springerplus* **2013,** *2*, 612.
70. Mallis, P.; Gontika, I.; Poulogiannopoulos, T.; Zoidakis, J.; Vlahou, A.; Michalopoulos, E.; Chatzistamatiou, T.; Papassavas, A.; Stavropoulos-Giokas, C. Evaluation of Decellularization in Umbilical Cord Artery. *Transplantation Proceedings* **2014,** *46* (9), 3232-3239.

Chapter 3: Overview of Project

Chapters 1 & 2 provided the necessary background information for the following chapters. These chapters provide a foundation for the fabrication of a hybrid, three component small diameter vascular graft which will significantly reduce thrombosis, inflammation, and late stage neointimal hyperplasia that commonly plagues current small diameter vascular grafts. This product is envisioned as follows.

The elastic lamina has been shown to reduce luminal thrombosis and migration of vSMCs, making it an ideal blood contacting material. Preservation of the native architecture through decellularization and decollagenization offers a viable process in the fabrication of small diameter, neointimal hyperplasia resistant vascular grafts. Combined with biostable or biodegradable polymeric coatings, the mechanical properties of the naturally weak elastic lamina can be sufficiently enhanced to create a viable vascular graft with good interfacial adhesion between layers. The development of this vascular graft is described in chapter 4.

NO, already known to act against the effects of thrombosis and neointimal hyperplasia, is readily incorporated into polymeric films and fibers. Current literature reports many S-nitrosothiols capable of controlled release of NO over periods of days to weeks. In clinical applications, NO release would ideally be extended over a time period of several months, during which time, a natural monolayer of endothelial cells can be deposited to restore the native vascular architecture. The NO donor described in chapter 5, SNAP-cyclam, has demonstrated long term stability and release of NO at physiologically relevant levels. As a component in the finalized hybrid graft, this material will be incorporated in the medial and adventitial layers.

To overcome the difficulty of controlled NO release *in vivo*, a novel method to generate NO was investigated. Transition metals are well known mediators of NO release from S-nitrosothiols, the most common of which are copper and iron. Chapter 6 presents results suggesting that Co^{2+}, Ni^{2+}, and Zn^{2+} also cause RSNO decomposition and release NO from SNAP. Recent developments of zinc based biomaterials and its physiological presence make zinc a favorable material for *in vivo* applications.

The envisioned graft will be a hybrid construct of the elements presented in chapters 4–6. Based on the structure of the artery shown in (Figure 2.1), the new graft will consist of a decellularized and partially decollagenized elastin blood contacting layer (intima). The media will be composed of alternating SNAP-cyclam doped polyether urethane electrospun fibers and zinc doped electrospun fibers. The adventitia of the proposed vascular graft would be composed of polyether urethane electrospun fibers.

Chapter 4: Fabrication and Short-Term *In Vivo* Performance of a Natural Elastic Lamina - Polymeric Hybrid Vascular Graft[1]

4.1. Abstract

Although significant advances have been made in the development of artificial vascular grafts, small diameter grafts still suffer from excessive platelet activation, thrombus formation, smooth muscle cell intimal hyperplasia, and high occurrences of restenosis. Recent discoveries demonstrating the excellent blood contacting properties of the natural elastic lamina have raised the possibility that an acellular elastic lamina could effectively serve as a patent blood contacting surface in engineered vascular grafts. However, the elastic lamina alone lacks the requisite mechanical properties to function as a viable vascular graft.

Here, we have screened a wide range of biodegradable and biostable medical grade polymers for their ability to adhere to the outer surface of the elastic lamina and allow cellular repopulation following engraftment in the rat abdominal aorta. We demonstrate a novel method for the fabrication of elastic lamina – polymeric hybrid small diameter vascular grafts and identify polyether urethane (PEU 1074A) as ideal for this purpose. *In vivo* results demonstrate graft patency over 21 days, with low thrombus formation, mild inflammation, and the general absence of smooth muscle cell hyperplasia on the graft's luminal surface.

The results provide a new direction for developing small diameter vascular grafts that are mass-producible and shelf stable; universally compatible due to a lack of immune response; and inhibit the in-graft restenosis response that is common to non-autologous materials.

4.2. Introduction

Small diameter blood vessels are required during coronary artery bypass grafting (CABG) to circumvent occluded coronary arteries. Currently, autologous arteries and veins used as grafts for the approximately 500,000 CABG procedures performed in the United States each year[1-2] represent the gold standard. However, a significant number of patients (~33%) are not able to make use of autologous vessels due to preexisting conditions[3]. Presently, there is no engineered vascular graft that is reliably able to replace autologous blood vessels in application.

[1]The material contained in this chapter has been previously published. Reprinted with permission from McCarthy, C. W.; Ahrens, D. C.; Joda, D.; Curtis, T. E.; Bowen, P. K.; Guillory, R. J.; Liu, S. Q.; Zhao, F.; Frost, M. C.; Goldman, J. Fabrication and Short-Term *in Vivo* Performance of a Natural Elastic Lamina–Polymeric Hybrid Vascular Graft. *ACS Appl. Mater. Interfaces* **2015,** *7* (30), 16202-16212. DOI: 10.1021/acsami.5b03892.

Both synthetic and natural vascular graft materials have been in use for several decades in large diameter arteries[2-4]. Synthetic examples include polymeric grafts fabricated from polytetrafluoroethylene (PTFE/ePTFE), poly(ethylene terephthalate) (Dacron), and polyurethanes[4-5]. However, small diameter synthetic vascular grafts are susceptible to high rates of failure due to thrombosis, intimal hyperplasia, and restenosis[6-12]. Natural, tissue engineered blood vessels (TEBVs) are under development and have achieved some clinical success[1, 13]. However, their expense, long fabrication time, short shelf life, and arduous regulatory pathway are expected to hinder their widespread clinical acceptance. Thus, there is a pressing need for small diameter vascular substitutes that can be mass-produced, are shelf stable over long time periods, and do not provoke excessive thrombosis or neointimal hyperplasia.

Decellularized elastic lamina, purified from the media layer of donor blood vessels, has recently been shown to possess anti-inflammatory and anti-thrombogenic properties. When exposed to arterial blood flow, the elastic lamina elicits lower platelet and monocyte activation, thrombosis, and smooth muscle cell proliferation than collagen-containing blood-contacting surfaces[14-17]. This has raised the prospect that the elastic lamina may substitute for a confluent endothelium in engineered acellular vascular grafts. However, despite highly promising early results with elastic lamina scaffolds, there has been a lack of progress incorporating this material into vascular grafts. This may be attributed to the high cost and low yields of synthetic elastin and recombinant tropoelastin[18-20]. Another significant hurdle is elastin's relative insolubility, precluding the polymerization of native elastin by common solvent deposition or electrospinning methods[21]. Recent studies on the inclusion of elastin in polymeric vascular grafts have focused on soluble human recombinant tropoelastin electrospun directly into the polymer fiber scaffold[20, 22] or soluble elastin derived from bovine ligamentum nuche[23], also electrospun directly into the scaffold. In the present study, we have purified native elastic lamina scaffolds from rat donor arteries, thereby circumventing these serious challenges while maintaining the native architecture and biological properties of the elastin matrix.

Unfortunately, the decellularized elastic lamina purified from donor arteries is easily torn, lacks mechanical strength, and retains regularly segmented holes due to side-branching. In this study, we have undertaken a materials selection process to identify polymeric materials that can adhere to the elastic lamina and provide mechanical integrity and structural support. We began our development work by employing polyglycolic acid (PGA) and poly(L-lactic acid) (PLLA) polymers, which are widely used and well characterized[24-28], as a proof-of-concept. Both PGA and PLLA are biodegradable aliphatic polyesters. PGA has a degradation time of approximately 2 to 4 weeks, while PLLA will degrade over a period of several months to several years. Both PGA (45–55%) and PLLA (37%) are considered semi-crystalline materials[25, 28-29].

Subsequently, polycaprolactone (PCL), polyether urethanes (PEUs), and polycarbonate-urethanes (PCUs) were selected for evaluation due to their well-accepted biocompatibility, hydrophobicity similar to that of the elastic lamina, and mechanical properties similar to those of the arterial tissue of the host (Table 4.1[30-36])[37-42]. We then evaluated the best performing hybrid vascular graft out to 21 days, *in vivo*.

Table 4.1. Properties for hybrid vascular graft polymer selection. Summary of properties for selected polymers. Standard deviations are given in parenthesis when the data was available. NDA signifies that no data were available. Where there are no references listed, values were obtained from the manufacturer's data sheet.

	Structure	Ultimate Tensile Strength (MPa)	Ultimate Elongation (%)	Wetting Angle (degrees)
PGA	Aliphatic	60–99.7[33]	1.5–20[33]	70.3[34]
PLLA	Aliphatic	50(2.4)–55(0.5)[30-31]	2.1(0.1)–8.0(0.2)[30-31]	82(2.3)[32]
PCL	Aliphatic	25.1[35]	>450[35]	69[37]
PCU 3585A	Aliphatic	57.23	425	82.1[43]
PCU 4085A	Aliphatic	62.05	400	82.1[43]
PEU SG80A	Aliphatic	39.99[39]	660[39]	NDA
PEU 1074A	Aromatic	41.37	550	82[36]
PEU 1085A	Aromatic	48.26	450	NDA

4.3. Materials & Methods

4.3.1. Aorta Specimen Collection

All animal work was approved by Michigan Technological University's Internal Animal Care and Use Committee (IACUC; #380482-12). Rat thoracic aortas used as donor tissue were collected from Sprague Dawley rats (Harlan Laboratories; Indianapolis, IN) euthanized with 5% inhaled isoflurane. The diaphragms were punctured, and the hearts were removed to ensure death. Thoracic aorta segments of ~30 mm in length were isolated, excised, and stored in phosphate buffered saline (PBS) (pH 7.4) at 4°C for later use.

4.3.2. Polymers & Solvents

PGA was purchased from Polysciences, Inc. (Warrington, PA). PLLA was purchased from NatureWorks LLC (Blair, NE). All polyurethanes used were from the Lubrizol LifeSciences (Wickliffe, OH) polymer family and are biostable[43-44] thermoplastic polyurethanes. These included polyether urethanes Tecothane 1074A and 1085A as well as Tecoflex SG80A. The polycarbonate urethane compounds used in this project were also from the Lubrizol LifeSciences polymer family and included Carbothane 3585A and 4085A. PBS, hexafluoro-2-propanol (HFIP), chloroform, dichloromethane, N,N-

dimethylacetamide, acetone, Dulbecco's modified Eagle's medium (DMEM), fetal bovine serum (FBS), penicillin-streptomycin (P/S), and sodium hydroxide (NaOH) were all purchased from Sigma-Aldrich (St. Louis, MO).

4.3.3. Decellularization and UV Treatment of the Elastic Lamina

Aortic specimens were processed to remove all non-elastin matrixes, leaving a purified and decellularized elastic lamina. Briefly, the aortic specimens were placed in a 50 mL conical tube immersed in PBS (pH 7.4). NaOH was added to the solution to make a basic PBS solution (pH 12.7)[14-15]. They were then placed into an ultrasonic bath for 4 hours at 37°C, changing the solution every hour. The aortic specimens were rinsed in PBS (pH 7.4) to remove residual NaOH. They were then washed in DMEM with 10% (v/v) FBS and 1% (v/v) P/S for 48 hours at 4°C to remove cellular fragments and residual DNA material.

The elastic lamina matrix was modified by irradiating the outer matrix layer with ultraviolet (UV) light. UV treatment to cross-link natural matrixes has been described previously[45]. Contrary to chemical methods of cross-linking, irradiation based treatment does not incorporate cytotoxic compounds into the matrix[46]. Some groups have reported limited degradation of matrix components after UV treatment[47]. Processed segments were mounted on 304 stainless steel mandrels (outer diameter of 1.65 mm) and UV irradiated with 380 ± 20 nm radiation at 1.5 W/cm^2 (Phoseon Technology; Hillsboro, OR) for 2 hours. The UV source was placed 6 cm above the specimens. The specimens were rotated 90 degrees every 30 minutes to ensure even exposure. A PBS (pH 7.4) bath was used to keep the specimens hydrated. The elastic lamina scaffolds were allowed to dry for 48 hours after UV treatment.

4.3.4. Polymer Coating of the Elastic Lamina

The UV-treated elastic lamina scaffolds were coated in 1% (w/w) solutions of the selected solvent/polymer combination, listed in Table 4.2. An airbrush (Iwata Eclipse; Portland, OR) was used to spray-coat the scaffold with the chosen polymer solution. The airbrush was fed at 15 psi from a dry, compressed air source. The scaffold was coated with 500 μL of polymer solution at a distance of 10 cm from the brush tip. The vessels were allowed to dry overnight prior to electrospinning. Polymer adhesion to the elastic lamina was evaluated by spray coating a sample of the UV-treated elastic lamina with each polymer and soaking the samples in PBS (pH 7.4) for 5 days at room temperature. The PBS-immersed specimens were qualitatively examined under a stereomicroscope to identify the presence of delamination.

Table 4.2. List of polymers and solvents used in the fabrication of hybrid grafts. Summary of polymer/solvent combinations used throughout chapter 4.

	Polymer	Solvent	Polymer Weight (%, w/w)
Vessel Coating	PGA	Hexafluoro-2-propanol	**1**
Vessel Coating	PCL	Acetone	**1**
Vessel Coating	PEU 1074A	N,N-Dimethylacetamide	**1**
Vessel Coating	PEU 1085A	N,N-Dimethylacetamide	**1**
Vessel Coating	PEU SG80A	N,N-Dimethylacetamide	**1**
Vessel Coating	PCU 3585A	N,N-Dimethylacetamide	**1**
Vessel Coating	PCU 4085A	N,N-Dimethylacetamide	**1**
Electrospinning	PLLA	Chloroform/Dichloromethane	**8**
Electrospinning	PEU 1074A	Hexafluoro-2-propanol	**5**

To provide structural support, electrospun fibers were deposited over the polymer coated elastic lamina scaffolds. Electrospinning needles were purchased from Beckton, Dickinson & Co (Franklin Lakes, NJ). For the constructs coated in PLLA, an 8% (w/w) solution of PLLA was prepared in equal masses of chloroform and dichloromethane. For the samples coated in the polyurethane based materials, a 5% (w/w) solution of PEU 1074A dissolved in HFIP was used. Electrospinning of the PLLA fibers was performed between 33% and 37% relative humidity, with a solution feed of 2 mL/h through a 22 gauge needle at a distance of 4.5 cm from the needle tip. The accelerating voltage used was 17 kV, and the 1.65 mm diameter mandrel rotated at 2,500 rpm during collection. The polyether urethane samples had similar parameters, however the flow rate was decreased to 0.5 mL/h due to the change in solvent to HFIP. The samples were electrospun for 10 minutes to create the specific layer thickness and fiber density. The samples were treated with ethylene oxide for 12 hours in an Anprolene AN74i sterilizer (Haw River, NC) prior to implantation. All samples were hydrated in sterile saline for ~5 minutes prior to surgery to prevent fractures during manipulation.

4.3.5. Electron Microscopy

Field emission scanning electron microscopy (FESEM) was used to examine the processed elastic lamina scaffolds and engineered vascular grafts using a Hitachi S-4700 field emission electron microscope (5kV accelerating voltage; 10 μA beam current; Tokyo, Japan). Specimens were prepared for imaging by allowing them to air dry. Final dehydration was accomplished while under vacuum in the sputter coater. Specimens were

sputter coated with 5 nm of Pt/Pd on a Hummer 6.2 sputter coater (Anatech, Ltd.; Denver, NC), and were stored in a desiccator prior to imaging.

4.3.6. Electrospun Fiber Characterization

Electrospun fibers (n = 3) were characterized manually using NIH ImageJ software after imaging on the electron microscope. Fiber diameters were determined by manually measuring individual fibers under high magnification. Fiber densities were determined by drawing a horizontal line in the image and counting the number of fibers present over the total length of the line.

4.3.7. Burst Pressure Testing

Vascular graft samples (n = 4) were mechanically tested to failure through burst pressure measurement. To perform the burst pressure testing, samples were fixed to hollow 304 stainless steel mandrels (1.65 mm outside diameter) with Dow Corning Silastic tubing (0.3 mm i.d., 0.64 mm o.d.; Midland, MI). The far end of the distal mandrel was capped following the removal of air from the apparatus. The hydrostatic pressure was recorded on a Fisher Scientific vacuum gauge (Pittsburgh, PA), while videos of the vessels during the test were recorded on a Nikon D3200 DSLR camera (Melville, NY). PBS (pH 7.4) was pumped into the vessel at a fixed rate of 300 μL/min by a syringe pump (Kent Scientific Genie Plus; Torrington, CT).

4.3.8. Mechanical Analysis

The electrospun polymer layers of the vascular grafts were mechanically tested in monotonic tension in the longitudinal direction on a Bose Electroforce 3200 series III (Eden Prairie, MN) frame with a 2 kg (19.6 N) load cell. Tubular samples were cut open longitudinally to produce sheets, which were fixed in Bose low force grips. The Bose Electroforce 3200 used in this work had a 6 mm travel limit during tensile testing. Thus, PLLA electrospun samples were tested to failure while the highly elastic PEU 1074A electrospun fibers were tested up to the limit of the testing frame. Values affected by these limitations are denoted within the paper. Mechanical data are presented as an average of six samples ± standard deviations. Data were analyzed in Matlab R2014a (Mathworks; Natick, MA).

4.3.9. Surgical Procedure

Sprague Dawley rats (Harlan Laboratories; Indianapolis, IN) anesthetized with 2.1% inhaled isoflurane in oxygen gas were implanted with ~ 6–8 mm long engineered vessels, as interpositional vascular grafts, using an end-to-end anastamotic technique described previously[38]. Briefly, the abdominal aorta was carefully isolated and the proximal and distal ends were clamped to prevent blood flow. Side branches were identified and tied off to prevent blood flow within the clamped aortic segment, prior to the artery being severed midway between the two clamps. For the PLLA scaffolds that were evaluated at

1 hour and 3 days (n = 1), both distal and proximal ends of the exposed, severed artery were treated with heparin in PBS (pH 7.4; 0.5 unit in ~2 μL saline) to reduce blood coagulation at the exposed collagen containing arterial wall. However, no heparin or any other anti-coagulant was used when the polyurethane based scaffold was implanted for either 3 (n = 1) or 21 (n = 5) days. The vessel constructs were engrafted with 15–20 interrupted suture stitches (10-0 nylon suture) at each end. Blood flow was reestablished, and the grafts were evaluated for leakage. Upon re-establishment of blood flow, pulsation was observed in the host artery, both proximally and distally to the implant. The abdomen was either kept open, in the case of the 1 hour PLLA specimen, or closed using a combination of sutures (for muscle) and staples (for skin), and the rat was allowed to recover for 3 or 21 days. The rats were observed for several minutes following recovery to confirm normal mobility in the hind quarters, which further indicated graft patency.

Animals were sacrificed at the designated end points by increasing the inhaled isoflurane concentration from 2.1% to 5% after the animals were fully anesthetized. The implant site was carefully isolated, and the vessels were evaluated for vascular tone and blood flow. Again, pulsation was observed in the host artery surrounding the graft. Then, under deep anesthesia, the diaphragms were punctured, the chest cavity was opened, and the heart was removed to ensure death. The grafts were collected with host artery connected at both the distal and proximal ends. A longitudinal cut was made in the collected graft to expose the internal lumen for imaging the graft surface for the single 1 hour and two 3 day grafts. The five 21 day grafts were left intact and gently syringe perfused with freezing medium to both confirm patency and facilitate cryo-sectioning. The samples were surrounded with Polyfreeze freezing medium (Sigma Aldrich; St. Louis, MO), snap frozen in liquid nitrogen, and stored at -80°C until cryo-sectioning. A 21 day implant duration reflects the standard practice for early phase vascular graft development[22].

4.3.10. Histological Preparation and Imaging

Processed elastic lamina scaffolds were imaged on an Olympus BX-51 microscope (Waltham, MA) to confirm decellularization and decollagenization prior to UV treatment, using both a fluorescent 4',6-diamidino-2-phenylindole (DAPI) nuclear stain and a Verhoeff's - Van Gieson (VVG) stain. Explanted samples were additionally stained with hematoxylin & eosin (H&E). All components for staining were purchased from Sigma-Aldrich (St. Louis, MO), with the exception of the Gill's #3, which was purchased from Leica Biosystems (Buffalo Grove, IL). Specimens were sectioned on a Microm HM550 cryostat (Microm International GmbH; Walldorf, Germany) at a thickness of 10 μm and fixed in ethanol for 60 seconds.

The samples were rinsed in PBS (pH 7.4) three times prior to undergoing staining for DAPI imaging or VVG staining. For DAPI staining of cell nuclei, 3 μL (5 mg/mL) of

diluted DAPI was added to the samples in 1 mL of PBS (pH 7.4). The VVG staining procedure followed a protocol published by the American Society of Clinical Pathologists[48]. Verhoeff's solution was prepared by mixing 30 mL of hematoxylin (Gills #3), 12 mL of 10% (m/v) ferric chloride, and 12 mL of Lugol's iodine. Gills #3 turns the elastic lamina brown. The Verhoeff's solution that was used produced a brown color change specific to elastin-containing matrixes. Tissue sections were placed into Verhoeff's solution for one hour, and then rinsed twice with deionized water. Sections were then differentiated in a 2% (m/v) ferric chloride solution. The sections were again rinsed with distilled water, treated with 5% (m/v) sodium thiosulfate for one minute, and rinsed in tap water three times. Sections were counterstained in Van Gieson's solution for 30 seconds, differentiated in 95% alcohol, dehydrated with absolute ethanol, and cleared in xylene substitute before mounting and imaging.

Explanted samples were additionally stained by H&E. Ethanol fixed cross sections were washed in three changes of PBS (pH 7.4) for 5 minutes each, followed by a wash in deionized water for 5 minutes. The samples were then placed in Gills #3 for 5 minutes to fully stain the sections. The slides were then differentiated by dipping five times into a solution of hydrochloric acid in deionized water (pH 2). Once differentiated, the slides were placed into deionized water for 1 minute to blue them. The blued samples were placed into two changes of 95% ethanol for 5 minutes per change. Eosin Y (0.25%) was then used to counterstain the sections for 30 seconds, after which they were dehydrated in absolute ethanol and cleared in xylene substitute. The samples were then mounted and imaged.

4.4. Results

4.4.1. Decellularization and Stabilization of Elastic Lamina

Histological analysis of the processed aortic specimens demonstrated successful isolation of the elastic lamina. The elastic lamina was clearly defined (shown as brown fibers) with no collagen-bearing matrixes observed between the layers of elastic lamina or inner/outer vascular layers (Figure 4.1A, B). The processed specimens were found to be completely devoid of cell nuclei (Figure 4.1C, D). Success of the decellularization processing was further confirmed by electron microscopy. FESEM images of the processed elastic lamina depict an intact elastic lamina matrix composed of several layers, with interconnecting fibers (Figure 4.2). The internal surface of the elastic lamina is irregular, with many crevices. The thickness of the elastic lamina varied between 40 and 80 μm.

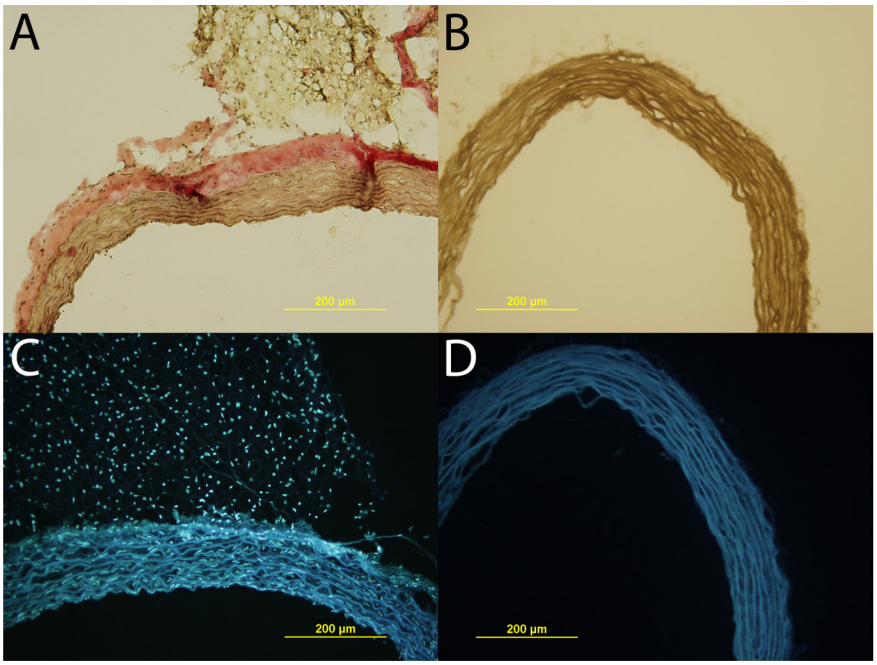

Figure 4.1. Decellularization of rat thoracic aortas. Representative images for native and decellularized/decollagenized arterial cross-sections. (A, B) The elastic lamina stained with VVG to show collagens present in the unprocessed vessel (A) and their absence in the processed tissue (B). (C, D) Cell nuclei were stained with DAPI to show cellularization of the elastic lamina and adventitial layers of the native artery (C) and the absence of cell nuclei after decellularization (D). The blue fibers in (C) and (D) are due to inherent fluorescence from the elastic lamina, not from DAPI staining.

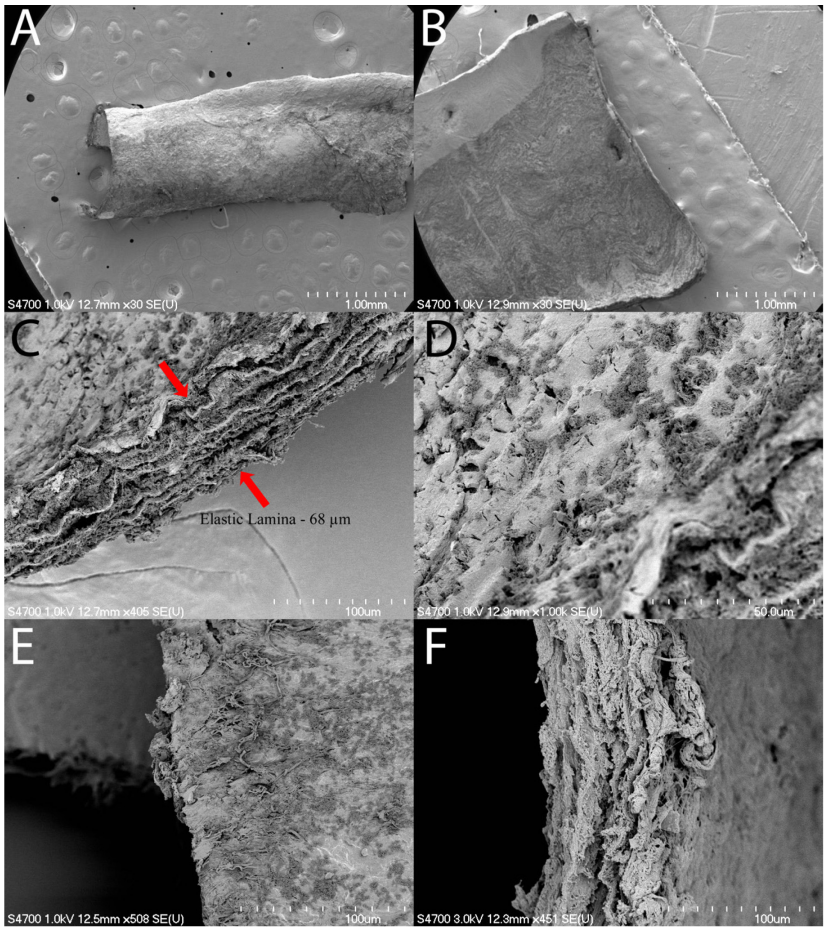

Figure 4.2. Images of decellularized elastin products. FESEM images of the decellularized elastin scaffold. (A) External view. (B) Internal view. (C) Internal surface/scaffold wall. (D) Magnified image of the internal surface from window C. (E) Magnified image of the external surface and scaffold edge. (F) Magnified image of the external surface/scaffold wall.

Elastic lamina matrixes that were UV-treated for two hours exhibited more favorable mechanical properties relative to the non-treated matrixes. After treatment, the decellularized elastin vessels were able to support themselves partially open.

4.4.2. Aortic Engraftment Using Only UV-Treated Elastic Lamina

After determination that UV treatment for 2 hours improved the material handling properties and mechanical strength, an early attempt was made to engraft a segment into the rat abdominal aorta, without polymeric support. Unfortunately, as the sutures were placed and tightened, tears appeared in the elastic lamina scaffold (data not shown). This result suggested the treatment decreased the elastic lamina's resistance to tearing.

4.4.3. Early Hybrid Grafts

This early engraftment demonstrated the need for external mechanical support of the elastin matrix via polymer coating. To accomplish this, a spray-coated layer of PGA in HFIP was deposited on the external elastic lamina surface. PGA acted as a transitional layer to connect an electrospun PLLA scaffold to the elastic lamina, while improving the graft's mechanical properties. Once dried, PLLA electrospun fibers were deposited over the PGA surface. These fibers were found to be unaligned. The fibers were found to have widely varying diameters and orientations, which promotes suturability and mechanical isotropy in the electrospun fiber layer. The innermost fiber layer contained relatively small diameter fibers with few defects. The outermost layer generally contained larger diameter fibers, with significant necking and branching, indicative of poor grounding of the mandrel due to fiber buildup. Pore sizes between the fibers appeared to vary on the basis of the layer in which they were deposited (Figure 4.3A-C). Large pores between fibers are anticipated to permit cellular infiltration.

An FESEM image of the fabricated construct demonstrated sufficient adhesion to promote graft stability between the deposited PGA layer and the PLLA fibers, even after several cycles of hydration and dehydration (Figure 4.3C). It is important to note that the FESEM sample preparation caused slight delamination of the PGA layer from the elastic lamina surface due to the requisite dehydration (Figure 4.3D). This effect was not observed during processing or surgery, but suggests the adhesion between these layers could be improved. Despite this shortcoming, the overall mechanical integrity of the hybrid construct was much preferable relative to that of the only UV-treated elastic lamina.

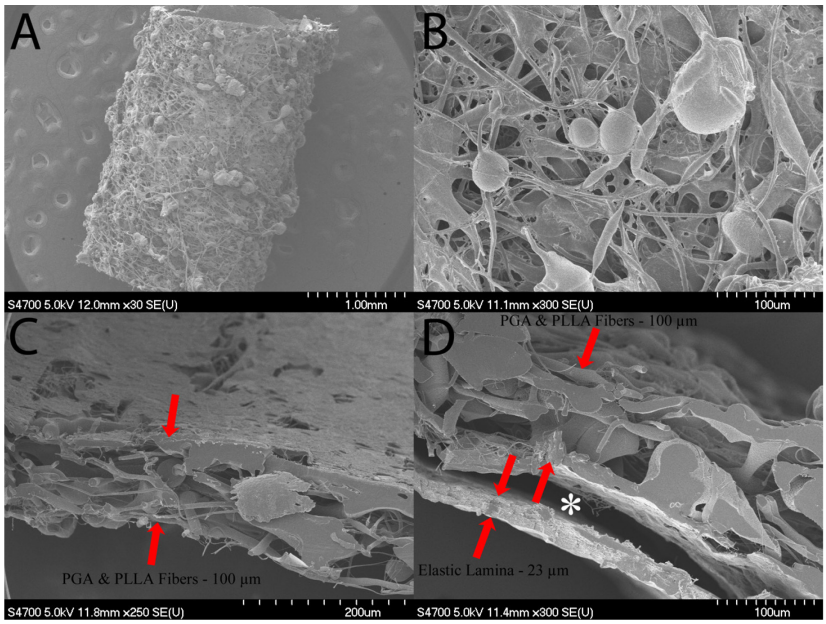

Figure 4.3. Images of an early elastin hybrid graft. FESEM images showing the fiber morphology of the PGA/PLLA vascular graft. (A) Wide view of the intact graft. (B) Magnified view of the graft. (C) Image of the elastic lamina contacting side of the fiber layer without the elastic lamina. (D) Edge view of the assembled graft with polymer layers and elastic lamina. Asterisks (*) denote delamination due to the FESEM preparation protocol. n = 2.

4.4.4. Aortic Engraftment of PGA/PLLA Hybrid Constructs

After observation of good suturability and layer adhesion, the PGA/PLLA/elastic lamina constructs were interposed and sutured into the rat abdominal aorta. The luminal elastic lamina surface of a representative graft prior to implantation is shown in Figure 4.4A–B. The graft was collected for analysis after either one hour (Figure 4.4C–D) or 3 days (Figure 4.5) post implantation (n = 1 per time point). The one hour sample was free from obvious signs of blood coagulation. The 3 day vessel also showed no obvious signs of blood coagulation. Staining confirmed the absence of cellular infiltrates into the elastic lamina matrix (Figure 4.5C–G). A comparison between the 3 day graft and the native artery at the graft/artery interface demonstrates the absence of cell nuclei in the fabricated grafts as compared to the native artery, as well as the continuous surface of the elastic lamina up to the endothelialized host artery (Figure 4.5G, H). There was evidence of modest blood coagulation at the suture line, which is attributable to blood contact with either the suture material or PGA/PLLA that became exposed during suturing.

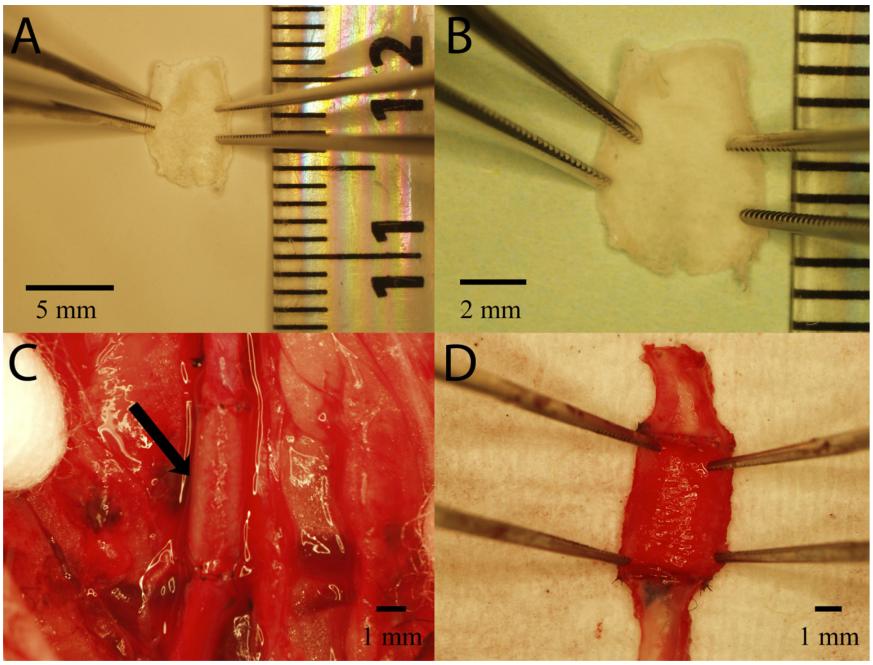

Figure 4.4. Implantation of a preliminary elastin hybrid vascular graft. (A, B) Luminal view of the PGA/PLLA graft prior to implantation. (C) The PGA/PLLA vascular graft is shown prior to harvest, at 1 hour post-surgery. (D) The collected graft's luminal surface is exposed to show absence of obvious coagulated blood.

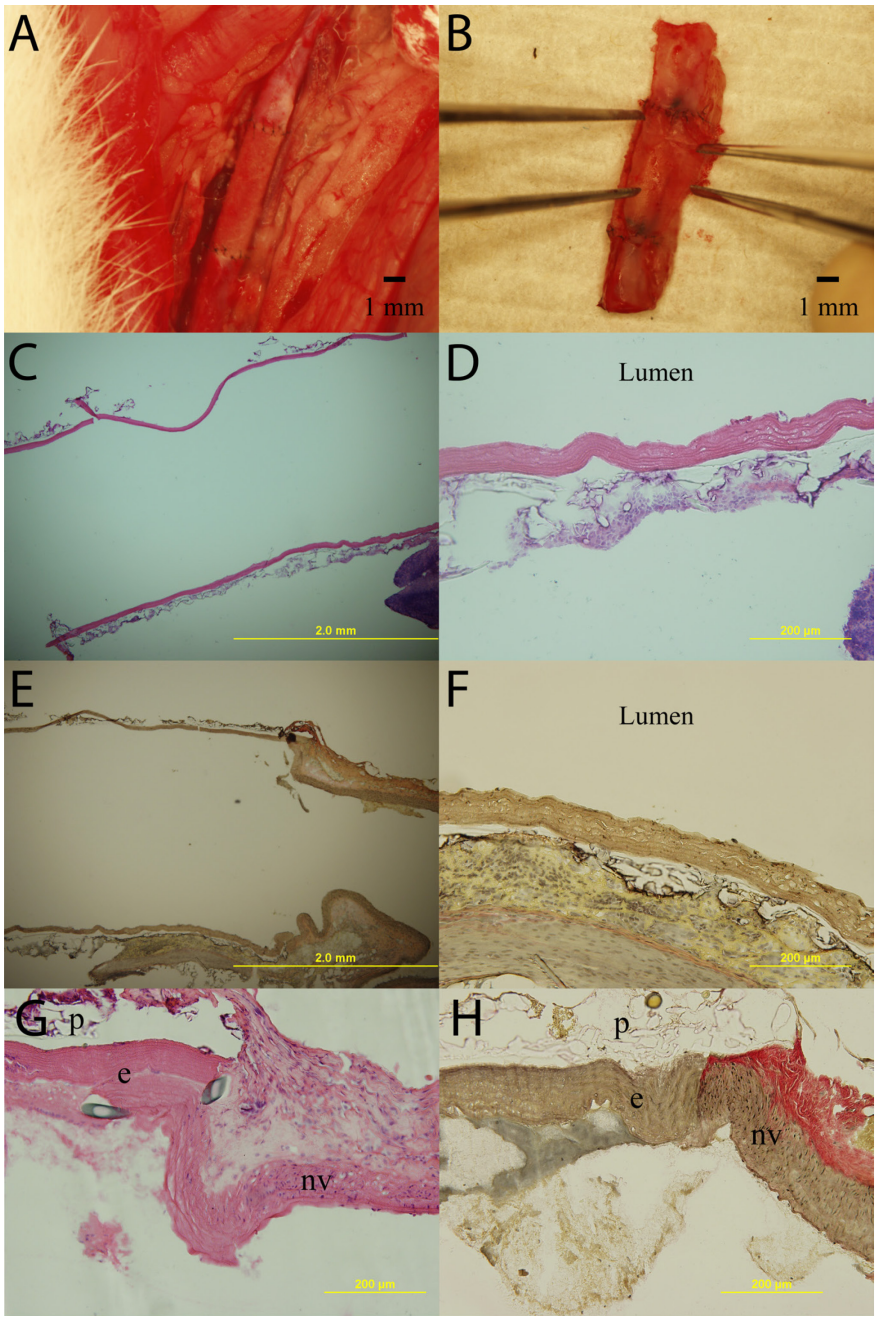

Figure 4.5. Histology of a preliminary elastin hybrid graft. Imaging and characterization of the 3 day PGA/PLLA vascular graft. (A) Depiction of the vessel prior to collection at 3 days post-surgery. (B) The graft's luminal surface is exposed to demonstrate absence of obvious signs of blood coagulation. (C, D) H&E staining of the cross sectioned vessel, showing open lumen with minimal thrombus, as well as absence of cellular infiltration into the elastic lamina and polymer layers. (E, F) Verhoeff's Van-Gieson staining of the cross sectioned vessel identifying the location of the processed elastic lamina and demonstrating continued absence of cells. (G) H&E staining at the graft-vessel junction. (H) Verhoeff's Van-Gieson staining at the graft-vessel junction. In G and H,

'e' identifies the acellular elastic lamina of the engineered graft, 'nv' identifies the cellularized elastic lamina of the native vessel, and 'p' identifies the acellular polymeric material.

Although the PGA/PLLA/elastic lamina graft performed well overall, the graft was found to be excessively brittle, as the PLLA layer cracked and flaked to some extent during suturing. Furthermore, adhesion defects revealed by SEM processing (Figure 4.3D) suggested that the PGA layer was not able to strongly adhere to the elastic lamina. For this reason, it was necessary to explore other polymeric biomaterials that could better serve as mechanical reinforcement to the elastic lamina.

4.4.5. Fabrication and Performance of Improved Hybrid Grafts

Polymer selection to identify materials with superior performance began by identifying well-characterized polymers with lower crystallinity and higher elastic moduli relative to PGA and PLLA. Table 4.1 lists the relevant properties of the considered materials. Most of the selected materials were hydrophobic to some degree, and all possessed high elongations to failure (≥ 400%). The hydrophobicity of some materials was anticipated to assist in adhesion to the hydrophobic elastic lamina. High elongations to failure implied that these materials were less likely to crack during processing and surgical implantation.

Polymer coated samples were examined for delamination after hydration in PBS (Figure 4.6). Both PCL and PEU SG80A suffered from severe delamination and were therefore eliminated from consideration. Further delamination analysis was performed by dehydrating the hybrid grafts and examining an example of each in cross section (Figure 4.7). Again, PCL and PEU SG80A scaffolds were found to adhere poorly to the elastic lamina. Minor delamination was also seen with PCU 4085A. Magnified images of scaffolds were collected for closer inspection of the polymer/elastic lamina interface (Figure 4.8). PCL was completely delaminated from the elastic lamina layer. PEU 1085A exhibited adequate adhesion between the polymer/elastin layers. PEU SG80A was completely delaminated (elastic lamina shown in Figure 4.8C and separated polymer coating shown in Figure 4.8D). PCU 3585A was well adhered to the elastic lamina. In this case, the polymer layer was difficult to distinguish from the elastin. PCU 4085A was delaminated in several areas of the sample. Due to this result, PCU 4085A was eliminated from further evaluation. PEU 1074A was found to have excellent adhesion to the elastic lamina matrix.

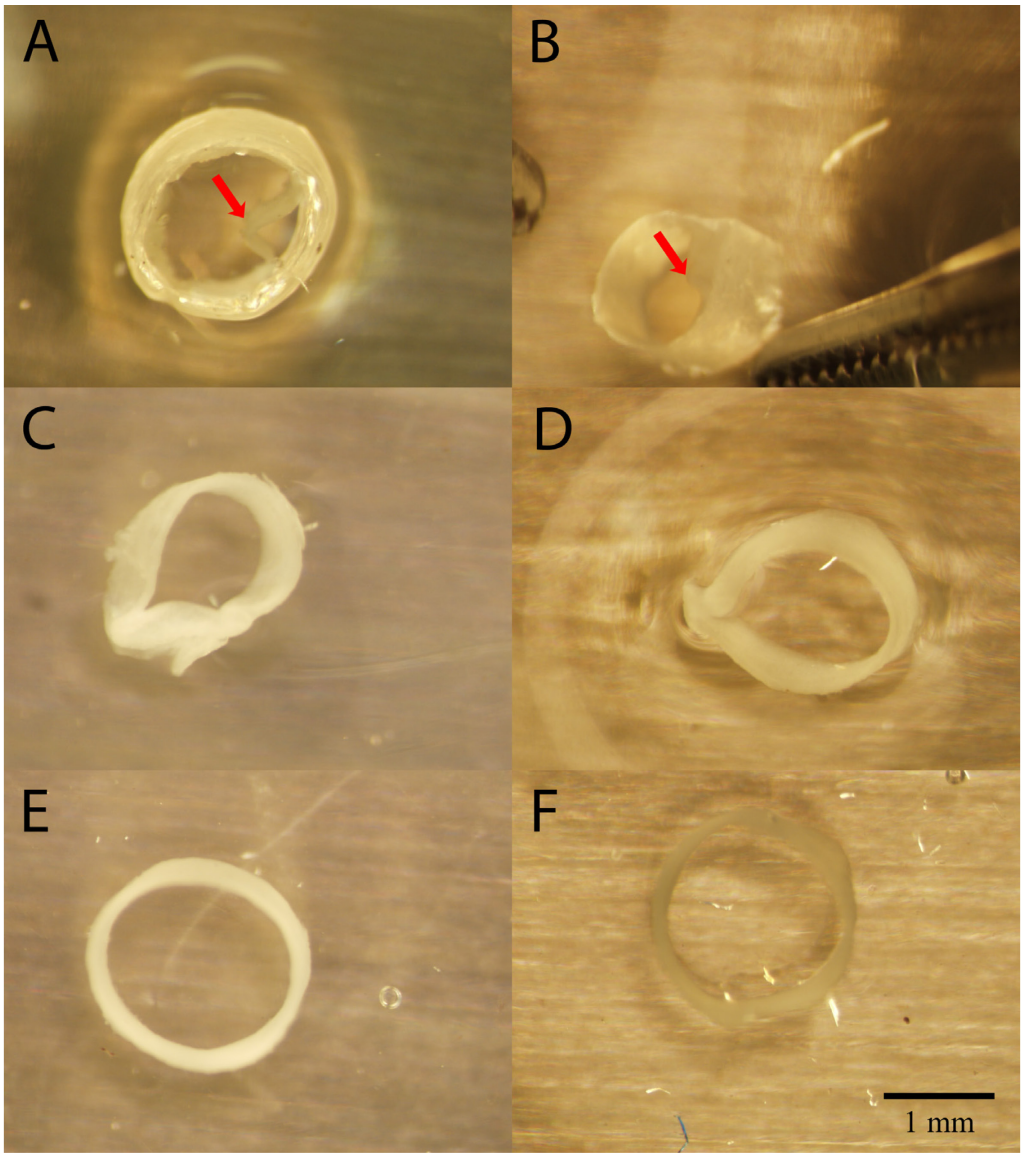

Figure 4.6. Evaluation of polymer delamination in elastin hybrid grafts. Polymer coated elastic lamina cross sections immersed in PBS solution and imaged with a stereoscope. (A) PCL. (B) PEU SG80A. (C) PCU 4085A. (D) PEU 1085A. (E) PCU 3585A. (F) PEU 1074A. Red arrows in A and B identify sites of delamination between the elastic lamina and polymer coating. n = 2 per polymer coating.

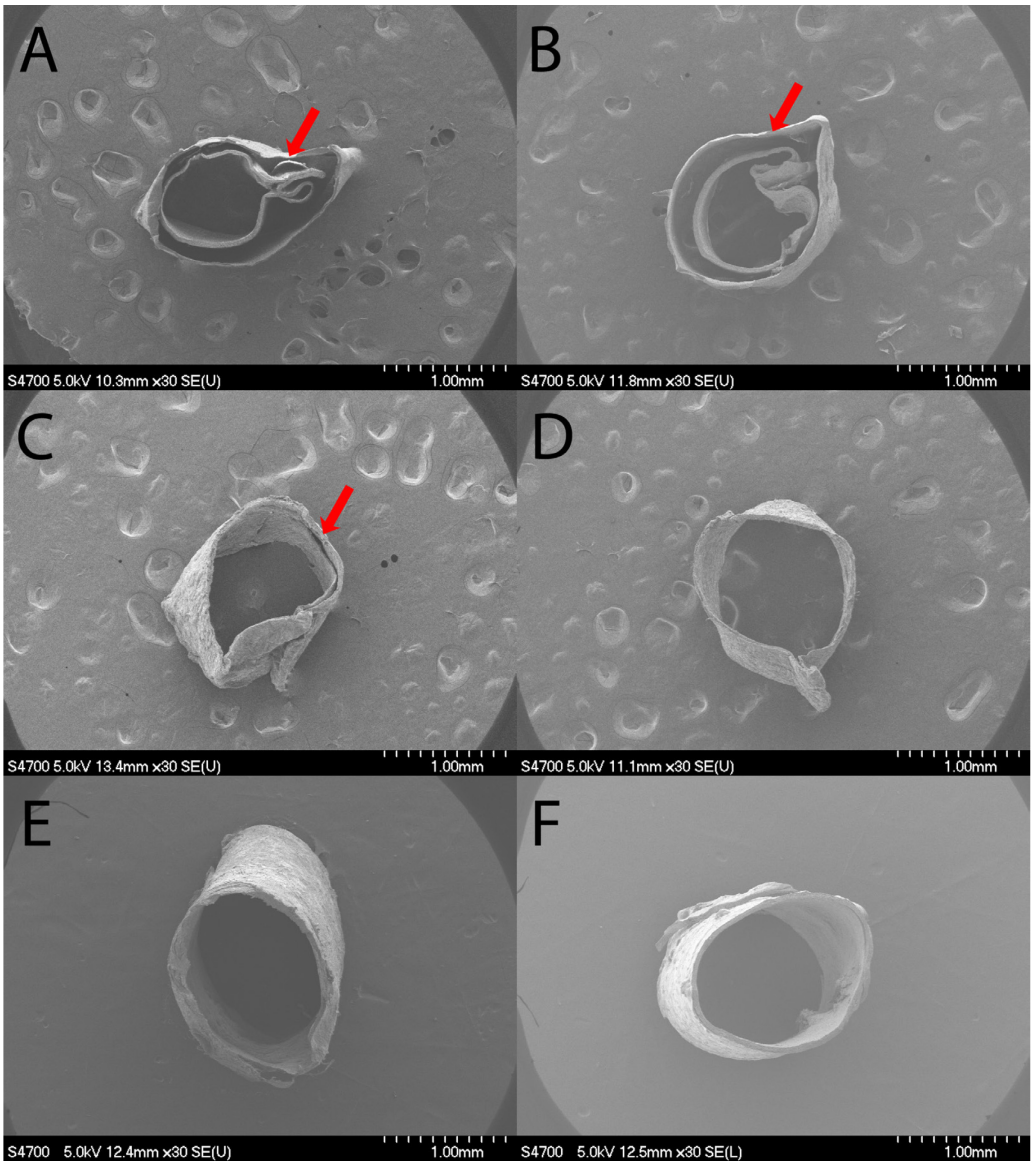

Figure 4.7. Images of polymer delamination on elastin hybrid vascular grafts. FESEM images of polymer coated elastic lamina specimens. (A) PCL. (B) PEU SG80A. (C) PCU 4085A. (D) PEU 1085A. (E) PCU 3585A. (F) PEU 1074A. Red arrows in A, B, and C identify sites of delamination between the elastin and polymer coating. n = 2 per polymer coating.

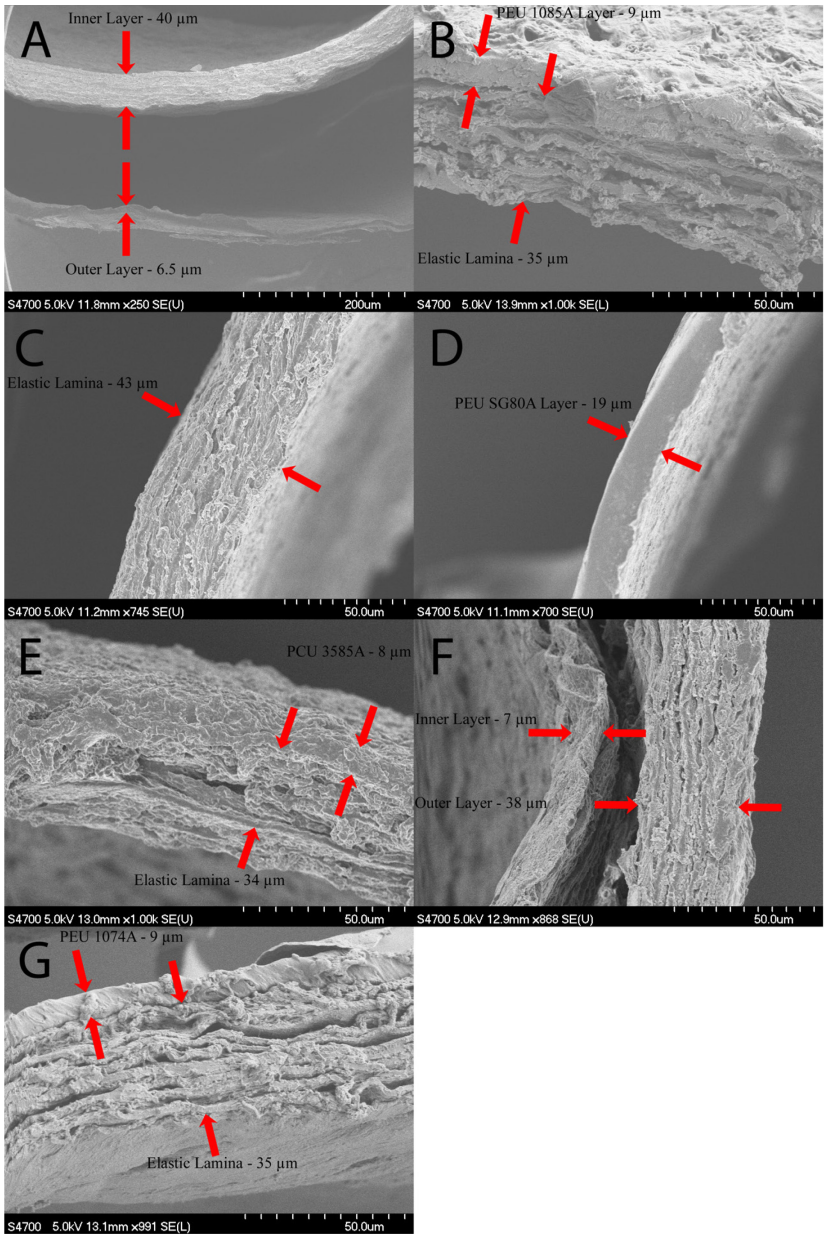

Figure 4.8. Images of various polymer/elastin interfaces. High magnification FESEM images of the polymer/elastic lamina interface for (A) PCL, (B) PEU 1085A, (C, D) PEU SG80A, (E) PCU 3585A, (F) PCU 4085A and (G) PEU 1074A. The thickness of each layer is labeled in each panel. n = 2 per polymer coating.

The successful polymers (PEU 1074A, PEU 1085A, and PCU 3585A) were then evaluated in a suture pullout test to provide information on how they would perform during suturing. The elastic lamina was spray coated with the three remaining polymers and electrospun with PLLA fibers and underwent a suture pullout event followed by FESEM imaging of the failure surfaces (data not shown). An ideal suture pullout should

reveal good elasticity and plastic deformation, but also good resistance to suture pullout. PEU 1074A resisted suture pullout without exhibiting brittle fracture. PEU 1085A failed with low resistance and was consequently dismissed from consideration. PCU 3585A failed by brittle fracture and was also removed from further consideration. Therefore, PEU 1074A was deemed the best material of those considered for this application.

4.4.6. Polyether urethane (PEU 1074A) Hybrid Graft Implantation

Prior to implantation, the PEU 1074A/elastic lamina conduit was further improved by electrospinning fibers using PEU 1074A dissolved in HFIP (Figure 4.9) in place of the electrospun PLLA fibers used in previous tests. This modification was found to vastly improve the interfacial adhesion between the polymer layers, and also resulted in better quality fibers in the fully assembled vascular graft. After three days post-implantation (n = 1), the graft was excised and characterized histologically (Figure 4.10). A longitudinal cut made to expose the luminal graft surface revealed a small region with attached coagulated blood. This material was loosely adhered to the suture line at the distal end of the graft but was not attached to the elastic lamina surface. An H&E stain showed significant cellular infiltration into the electrospun PEU 1074A fibers, as well as a thin thrombus layer near the suture site. The thrombus layer thickness was well below 10 µm at most locations away from the suture line.

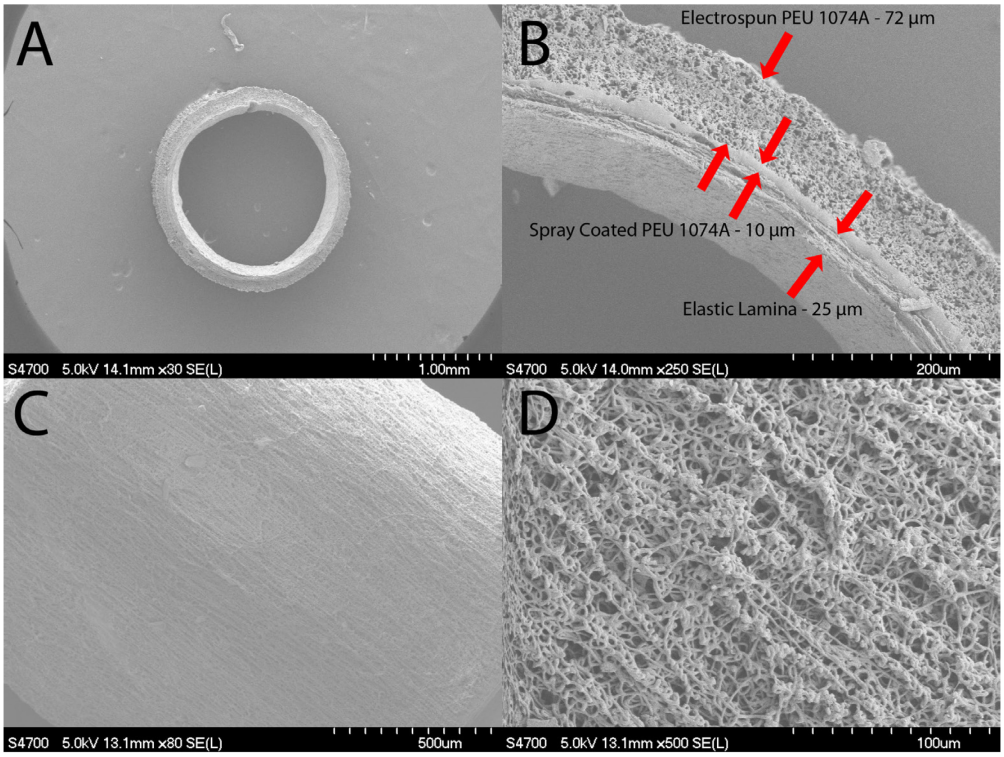

Figure 4.9. Images of a finalized hybrid elastin vascular graft. Elastic lamina coated in PEU 1074A with electrospun PEU 1074A fibers deposited externally. (A, B) Cross sectional view of the pre-

implantation specimen, demonstrating good adhesion between the layers. (C, D) Longitudinal view of the pre-implantation specimen's fibers, showing unexpected partial longitudinal fiber alignment. Both polymers were dissolved in HFIP for coating. n = 2.

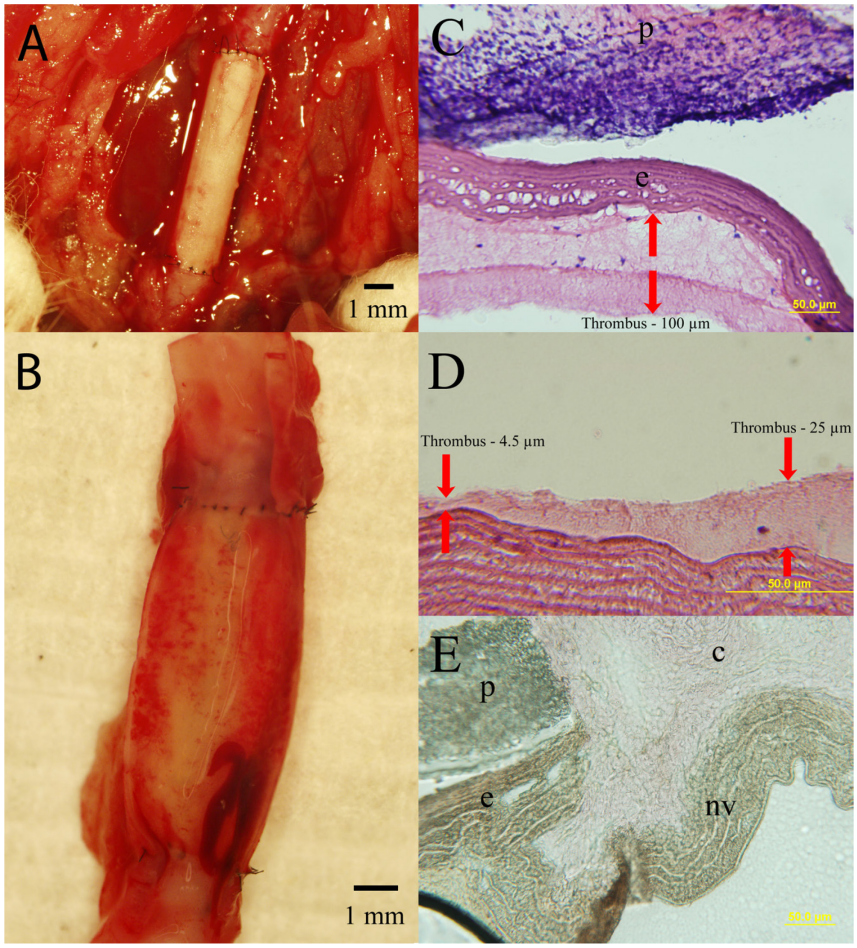

Figure 4.10. Histology of short-term hybrid elastin vascular grafts. Characterization of the 3 day PEU 1074A vascular graft. (A) The PEU 1074A graft is shown prior to collection. (B) The excised graft is opened to expose the luminal surface, showing near complete absence of obvious blood coagulation. (C) H&E staining of a vessel section near the suture site demonstrates modest thrombus formation and an extensive cellular infiltration into the polymer layer 'p', whereas the elastic lamina 'e' remains acellular. (D) Magnified view of a more representative thrombus layer, collected from a location midway along the vessel. (E) Verhoeff's Van-Gieson staining of the explanted vessel shows the graft-vessel junction. 'nv' represents the native vessel, 'e' represents the elastin graft, 'p' shows the polymer, and 'c' is the collagenous layer. A continuous elastic lamina layer is present up to the host artery.

After 21 days post-implantation (n = 5), the grafts were excised and characterized (Figure 4.11). All five grafts were patent, with clear signs of arterial pulsation evident at both distal and proximal host locations. H&E stains verified patent lumens as well as the formation of a relatively thin neointima on the luminal surface of the grafts (Figure

4.11B). Some wrinkling of the elastic lamina and artificial detachment of the polymer coating due to cross sectioning is evident. Typical low (Figure 4.11C) and high (Figure 4.11D) neointimal tissue thicknesses are shown. Delamination of the polymer coating from the elastic lamina was commonly detected post cross sectioning (Figure 4.11B, D). However, delamination is unlikely to have been a dominant factor *in situ*, as excellent interfacial adhesion was seen at the sites of pores within the elastic lamina (Figure 4.11E). These sites provide direct contact between the polymer and blood flow/pressure and are therefore natural nucleation sites for delamination, if it were to occur. In rare cases, cells could be seen residing within the elastic lamina (Figure 4.11D). Sites of wrinkling (Figure 4.11B) and pores (Figure 4.11E) were associated with an increased neointimal thickness.

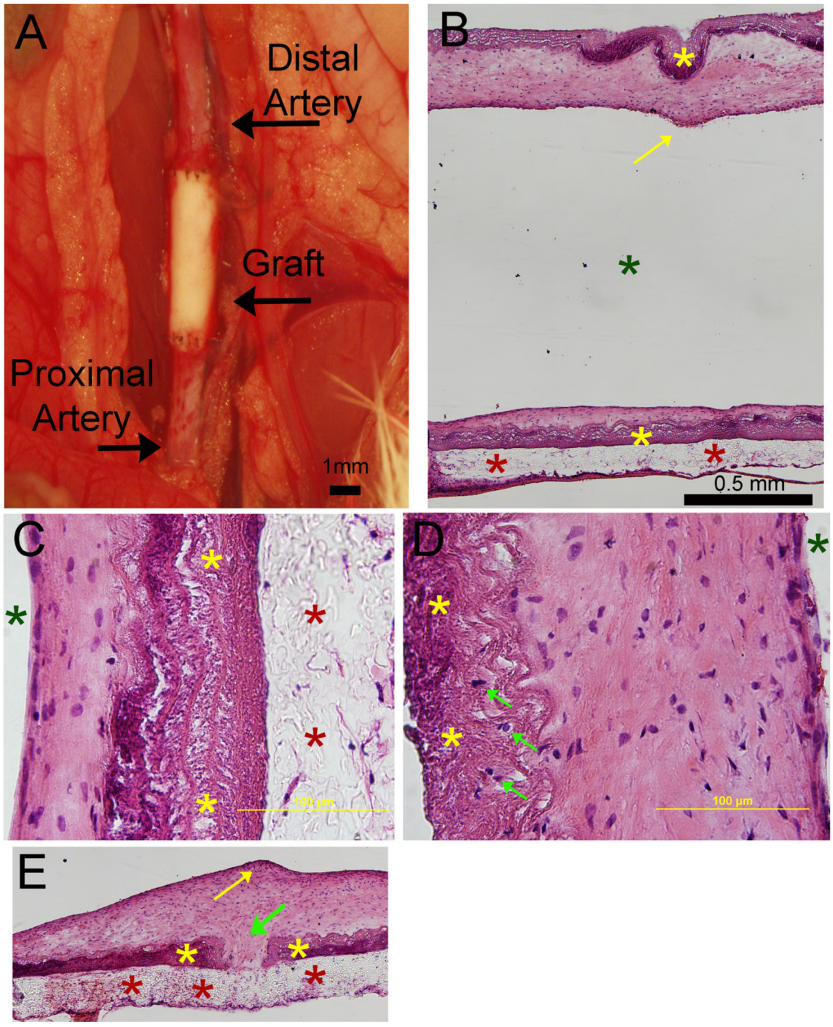

Figure 4.11. Histology of long-term hybrid elastin vascular grafts. Characterization of the 21 day PEU 1074A vascular graft. (A) The PEU 1074A graft is shown prior to collection. (B) H&E staining of a vessel transverse section demonstrates modest neointimal formation on both sides of the graft

(top and bottom of image) and an open lumen. (C) Magnified view of a representative low thickness neointimal layer. Polymer coating can be seen adhering to the elastic lamina. (D) Magnified view of a representative high thickness neointimal layer. Cell nuclei can be seen to have migrated into the elastic lamina. Dark green stars identify lumen, red stars identify polymer, and yellow stars in images identify elastic lamina. Light green arrows identify cells within the elastic lamina in (D). The light green arrow in E identifies a pore in the elastic lamina, which is created by arterial side branching at the donor site. Yellow arrows in B and E identify protrusion of the neointimal layer into the lumen due to elastic lamina defects. Blood flow proceeds left to right in (B) and (E). The scale bar shown in (B) is the same for (E).

4.4.7. Mechanical Evaluation of Hybrid Vascular Grafts

Characterization of the electrospun PEU 1074A fibers and mechanical properties of the graft are shown in (Table 4.3). We found burst pressures to be well in excess of physiological demands and in accordance with other experimental vascular grafts[49-51]. In one specimen, the elastic lamina was seen to delaminate from the reinforcing polymer at ~800 mmHg, prior to burst failure of the polymer layer. Notably, the elastic lamina did not delaminate from any of the other specimens, despite the presence of large pores in this layer due to extensive arterial side-branching at the donor site. Thus, the elastic lamina and polymer layers exhibited excellent interfacial adhesion.

Table 4.3. Comparison of hybrid elastin vascular graft properties. Table 4.3 summarizes the physical properties of the vessels and provides data for the native saphenous vein for comparison purposes. Values are reported with standard deviations where available. n = 4 for burst pressure and wall thickness measurements. n = 3 for fiber diameter and density measurements.

	Wall Thickness (µm)	Burst Pressure (mmHg)	Fiber Diameter (µm)	Fiber Density (fibers/mm)
PEU Coated Elastin	N/A	200 ± 29	N/A	N/A
Vascular Grafts	106 ± 42	990. ± 110	1.7 ± 0.7	200 ± 80
Saphenous Vein	250[52]	1600–2500[52]	N/A	N/A

Due to the negligible contributions of both the elastic lamina and spray-coated layer to the mechanical properties of the vessel, tensile testing was restricted to the two different electrospun fibers used to construct all of the hybrid vascular grafts. A representative stress-strain plot for both the electrospun PLLA and PEU 1074A fibers can be seen in Figure 4.12. While the relatively brittle character of the PLLA fibers allowed all samples to be evaluated to failure, the exceptional elasticity of the PEU 1074A fibers prevented the collection of failure data for this material. The average elastic modulus of the electrospun fibers was 64 ± 35 MPa for the PLLA samples and 1.4 ± 0.80 MPa for the PEU 1074A samples. The elongation to failure for PLLA was 10. ± 4.1%. The average observed elongation of the PEU 1074A without failure was 200 ± 24%. These data are summarized in Table 4.4.

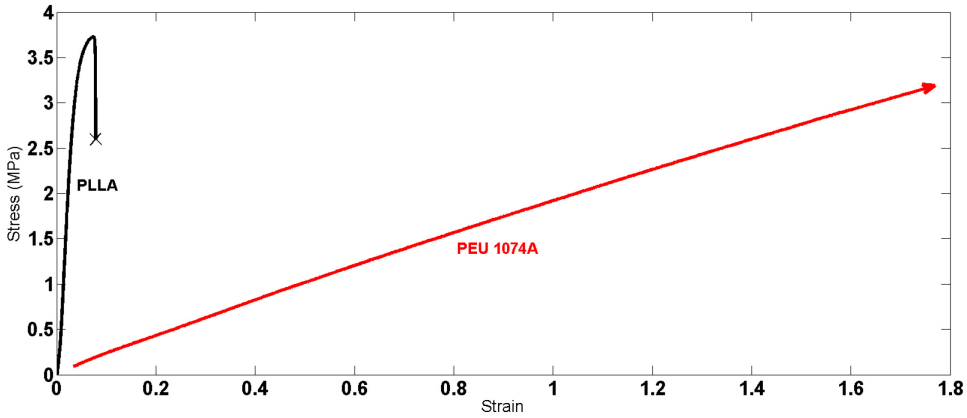

Figure 4.12. Mechanical testing of hybrid elastin vascular grafts. The representative plots of stress vs. strain for both the electrospun PLLA (black) and PEU 1074A (red) can be seen above. Due to the limits of the mechanical tester, the PEU 1074A samples were not able to be evaluated to failure.

Table 4.4. Summary of hybrid elastin vascular graft mechanical testing. Table 4.4 summarizes the mechanical properties of the electrospun PLLA and PEU 1074A fibers.

	Observed Elastic Modulus (MPa)	Observed Elongation (%)
Poly (L-lactic acid)	64 ± 35	10. ± 4.1
Polyether Urethane 1074A	1.4 ± 0.8	200 ± 24
Native Saphenous Vein	1.6 ± 0.057[53]	17[54]

4.5. Discussion

Here, we have constructed a novel vascular graft by supporting an elastic lamina blood-contacting surface with polymeric materials. The graft was easy to manipulate and suture. Importantly, the graft avoided significant inflammatory responses and progressive intimal hyperplasia, both widely recognized as mediating factors in restenosis. The elastic lamina appears to exert suppressive effects on resident cells. This requires receptor-mediated signaling mechanisms, which employ a ligand with precise protein structure and electrostatic activity[15]. Thus, it seems that the processing conditions used to construct the graft (e.g. NaOH decellularization, UV irradiation, and ethylene oxide treatments) did not substantially alter the chemical composition of the elastic lamina.

An ideal vascular graft should match the mechanical characteristics of the native artery. Concurrently, viable vascular grafts must mimic the properties of a native endothelium at the blood contacting surface, not provoke an inflammatory response, remain shelf stable over extended time periods prior to use, and be easy to handle and suture. The latter requirement precludes the presence of cellular fragments or DNA from the donor. It has been challenging thus far for the scientific and industrial community to develop a graft

that possesses all of these ideal properties. This is mainly due to the challenge of mimicking a confluent endothelium on the luminal surface of acellular materials and the difficulties in generating universally compatible implant materials from cellularized constructs.

The grafts developed here have a wall thickness and burst pressure similar to those of the native saphenous vein, which is a widely used autologous conduit for coronary artery bypass grafting. Specifically, the native saphenous vein has a burst pressure of 1600 - 2500 mmHg and a wall thickness of 250 μm[52]. While the present vascular grafts exhibit a slightly lower average burst pressure of 990. ± 112 mmHg, their wall thickness is less than half that of the saphenous vein at 106 ± 42.0 μm. These data would suggest a similar mechanical strength for the bulk material.

Tensile evaluation of the PLLA and PEU 1074A electrospun polymers revealed a clear difference in their mechanical properties as the brittle behavior of the PLLA was evident. The relative brittleness of PLLA is consistent with tabulated mechanical data presented in Table 4.1, which lists PLLA as having among the lowest elongations to failure. In contrast, the final polymer used in this work, PEU 1074A, exhibited exceptional elastic behavior in both burst pressure and tensile tests. Ideally, the selected reinforcing polymer for the vascular graft should possess mechanical properties similar to those of native blood vessels. The elastic modulus of a typical, non-diseased human coronary artery is 1.48 MPa[55], while the elongation to failure of the human carotid artery is reported as 105%[20]. The native saphenous vein demonstrates an elastic modulus of 1.6 ± 0.057 MPA and an observed elongation of 17%[53-54]. Thus, PEU 1074A matches or exceeds the mechanical properties of a native small diameter human artery and the current standard for their replacement.

In the case of the present hybrid graft, the main function of the polymeric biomaterials (either the biodegradable PLLA or biostable PEU 1074A) is to provide mechanical support. In this role, polymeric supporting materials can be optimized with fewer concerns for blood-contacting properties, and allow development to move toward matching their mechanical characteristics to the native artery. Meanwhile, the elastic lamina provides an excellent acellular blood contacting layer, which has been a serious limitation of acellular materials to date. Conversely to the polymer materials, the elastic lamina may be harvested and processed with little concern for its mechanical performance. Thus, the multilayered design of the present engineered acellular vascular graft, with a biological layer and a synthetic layer that are each optimized for different functions, makes it more feasible to achieve the overall performance goals. Such a graft, because it is acellular, can be developed specifically as a xenograft from the artery of any donor animal and be implanted into any recipient. It is also shelf stable and can be

quickly hydrated in the operating room, and therefore can be stocked to meet the urgent needs of surgeons and patients.

During the course of evaluation, a number of defects in these experimental grafts became evident. These included rare cases of cell migration into the elastic lamina and regions of delamination between the different polymers and elastic lamina. Although we have achieved excellent results with the present processing conditions, the processing steps are amenable to improvements. Further refinement may result in a reduced neointimal tissue development relative to what was found here. For example, alternative techniques to decellularize and purify the elastic lamina could be employed to better preserve the structural and chemical integrity of its constituent proteins, which serve as ligands for the receptor-mediated signaling events that suppress cellular activity. The presence of cells within the elastic lamina at rare sites in the 21 day grafts suggests that processing conditions may have locally altered the chemical structure of the elastic lamina. Altering the molecular weight or solvent concentration in polymer processing may improve adhesion between the PLLA and elastic lamina and provide a testable, biodegradable graft to compare at longer times with the biostable PEU 1074A graft. In addition, consistency between batches of vascular grafts would benefit from more automated and controlled processing and fabrication conditions.

While characterizing the hybrid grafts, we observed longitudinal alignment of electrospun fibers in the PEU 1074A graft. This fiber orientation will cause the material to be resilient when stretched along the longitudinal direction, but may create deficiencies in resisting large hoop stresses. While this introduces some concerns, the grafts were still able to resist arterial pulsatile pressure and retain sutures for up to 21 days. Future work with this material will aim to provide a more uniform distribution of fiber alignment with the ultimate goal of achieving mechanical isotropy in the structural coating.

It is important to note that the low degree of thrombus formation in the elastic lamina/PEU 1074A graft was similar to that of the elastic lamina/PGA/PLLA graft at the 3 day time point. This is likely due to the excellent hemocompatibility of the elastic lamina, and confirms that the hybrid conduit design offers flexibility in polymer selection. Surprisingly, although the PLLA electrospun fiber layer was thicker than that of the PEU 1074A fibers, there was markedly more cellular infiltration seen within the PEU 1074A fibers. This is likely due to a combination of differences in porosity, pore size distribution, fiber diameter, hydrophobicity/hydrophilicity, and the associated degree of swelling between the two constructs. Because cellular infiltration into the graft is necessary for integration of the material, the ability of cells to infiltrate and the type of cell infiltrates represent an additional consideration for polymer selection and modification, especially if biodegradable constructs are being considered.

Future work aimed at improving the performance of the vascular graft could be directed toward clarifying the key factors that regulate interfacial adhesion between the polymer and elastic lamina. Such an assessment may reduce the reliance upon bulk properties for material selection. Future experiments with longer term *in vivo* implantations (between 6 months and 1 year) will enable a more thorough characterization of the long-term biocompatibility of the graft. Lastly, optimization of the donor artery processing conditions may reduce chemical and physical alterations of the elastic lamina from its native state and better preserve the cell suppressive properties that make this material an excellent blood contacting layer.

4.6. Conclusion

This work has demonstrated an effective approach for the construction of hybrid vascular grafts with natural elastic lamina as blood contacting surfaces. Using simple tissue engineering techniques and fabrication methods, a vascular construct has been devised that demonstrates promising short term performance as a vascular graft, *in vivo*. The vessel fabricated in this work improves upon current small diameter vascular grafts by making use of an elastic lamina blood-contacting layer, which has been shown to be non-thrombogenic, non-immunogenic, and neointimal hyperplasia resistant. As compared to experimental vascular grafts that rely upon synthetic elastin or elastin-like polypeptides, our approach decellularizes widely available donor tissue. The arteries of larger animals could serve as donors for human applications. This approach minimizes the costs, simplifies the fabrication process, and preserves the native architecture and biological properties of the elastic lamina. The use of synthetic polymers to provide mechanical reinforcement is another innovative feature that allows for extensive refinement of the mechanical properties in the final product. Further innovation may involve the incorporation of drug releasing components into the polymeric material.

The positive results of this work open the door for further development of the decellularization methods, polymers, coating techniques, and electrospinning process. A shelf-stable vascular graft containing a natural and intact elastic lamina that reduces the natural tendency of the host environment to respond to vascular engraftment with platelet activation, excessive thrombogenesis, and intimal hyperplasia may provide a new direction for developing small diameter vascular grafts, particularly for coronary artery bypass procedures.

4.7. Acknowledgements

This work was supported by National Institutes of Health Contract Grant R15-HL-113954 (the contract grant sponsors were Jon Stinson and Peter Edelman, Boston Scientific Corp.). F.Z. was supported by NIH grant 1R15HL115521-01A1. P.K.B. was

supported by an American Heart Association predoctoral fellowship. The authors would like to thank David Rosen for his help with the Bose Electroforce 3200.

4.8. References

1. Nottelet, B.; Pektok, E.; Mandracchia, D.; Tille, J. C.; Walpoth, B.; Gurny, R.; Moller, M. Factorial Design Optimization and in Vivo Feasibility of Poly(Epsilon-Caprolactone)-Micro- and Nanofiber-Based Small Diameter Vascular Grafts. *J Biomed Mater Res A* **2009,** *89* (4), 865-875.
2. Wang, X.; Lin, P.; Yao, Q.; Chen, C. Development of Small-Diameter Vascular Grafts. *World J Surg* **2007,** *31* (4), 682-689.
3. Kannan, R. Y.; Salacinski, H. J.; Butler, P. E.; Hamilton, G.; Seifalian, A. M. Current Status of Prosthetic Bypass Grafts: A Review. *J Biomed Mater Res B Appl Biomater* **2005,** *74* (1), 570-581.
4. Nerem, R. M.; Seliktar, D. Vascular Tissue Engineering. *Annu Rev Biomed Eng* **2001,** *3*, 225-243.
5. Desai, M.; Seifalian, A. M.; Hamilton, G. Role of Prosthetic Conduits in Coronary Artery Bypass Grafting. *Eur J Cardiothorac Surg* **2011,** *40* (2), 394-398.
6. Wu, H.; Fan, J.; Chu, C.-C.; Wu, J. Electrospinning of Small Diameter 3-D Nanofibrous Tubular Scaffolds with Controllable Nanofiber Orientations for Vascular Grafts. *Journal of Materials Science: Materials in Medicine* **2010,** *21* (12), 3207-3215.
7. De Visscher, G.; Mesure, L.; Meuris, B.; Ivanova, A.; Flameng, W. Improved Endothelialization and Reduced Thrombosis by Coating a Synthetic Vascular Graft with Fibronectin and Stem Cell Homing Factor Sdf-1α. *Acta biomaterialia* **2012,** *8* (3), 1330-1338.
8. Hashi, C. K.; Derugin, N.; Janairo, R. R. R.; Lee, R.; Schultz, D.; Lotz, J.; Li, S. Antithrombogenic Modification of Small-Diameter Microfibrous Vascular Grafts. *Arteriosclerosis, thrombosis, and vascular biology* **2010,** *30* (8), 1621-1627.
9. Avci-Adali, M.; Ziemer, G.; Wendel, H. P. Induction of Epc Homing on Biofunctionalized Vascular Grafts for Rapid in Vivo Self-Endothelialization—a Review of Current Strategies. *Biotechnology advances* **2010,** *28* (1), 119-129.
10. Novosel, E. C.; Kleinhans, C.; Kluger, P. J. Vascularization Is the Key Challenge in Tissue Engineering. *Adv Drug Deliv Rev* **2011,** *63* (4-5), 300-311.
11. Naito, Y.; Shinoka, T.; Duncan, D.; Hibino, N.; Solomon, D.; Cleary, M.; Rathore, A.; Fein, C.; Church, S.; Breuer, C. Vascular Tissue Engineering: Towards the Next Generation Vascular Grafts. *Advanced drug delivery reviews* **2011,** *63* (4), 312-323.
12. Nieponice, A.; Soletti, L.; Guan, J.; Hong, Y.; Gharaibeh, B.; Maul, T. M.; Huard, J.; Wagner, W. R.; Vorp, D. A. In Vivo Assessment of a Tissue-Engineered Vascular Graft Combining a Biodegradable Elastomeric Scaffold and Muscle-Derived Stem Cells in a Rat Model. *Tissue Engineering Part A* **2010,** *16* (4), 1215-1223.
13. Uttayarat, P.; Perets, A.; Li, M.; Pimton, P.; Stachelek, S. J.; Alferiev, I.; Composto, R. J.; Levy, R. J.; Lelkes, P. I. Micropatterning of Three-Dimensional Electrospun Polyurethane Vascular Grafts. *Acta biomaterialia* **2010,** *6* (11), 4229-4237.
14. Liu, S. Q.; Tieche, C.; Alkema, P. K. Neointima Formation on Vascular Elastic Laminae and Collagen Matrices Scaffolds Implanted in the Rat Aortae. *Biomaterials* **2004,** *25* (10), 1869-1882.

15. Liu, S. Q.; Alkema, P. K.; Tieché, C.; Tefft, B. J.; Liu, D. Z.; Li, Y. C.; Sumpio, B. E.; Caprini, J. A.; Paniagua, M. Negative Regulation of Monocyte Adhesion to Arterial Elastic Laminae by Signal Regulatory Protein A and Src Homology 2 Domain-Containing Protein-Tyrosine Phosphatase-1. *Journal of Biological Chemistry* **2005,** *280* (47), 39294-39301.
16. Hinds, M. T.; Rowe, R. C.; Ren, Z.; Teach, J.; Wu, P. C.; Kirkpatrick, S. J.; Breneman, K. D.; Gregory, K. W.; Courtman, D. W. Development of a Reinforced Porcine Elastin Composite Vascular Scaffold. *J Biomed Mater Res A* **2006,** *77* (3), 458-469.
17. Simionescu, D. T.; Lu, Q.; Song, Y.; Lee, J. S.; Rosenbalm, T. N.; Kelley, C.; Vyavahare, N. R. Biocompatibility and Remodeling Potential of Pure Arterial Elastin and Collagen Scaffolds. *Biomaterials* **2006,** *27* (5), 702-713.
18. Blit, P. H.; McClung, W. G.; Brash, J. L.; Woodhouse, K. A.; Santerre, J. P. Platelet Inhibition and Endothelial Cell Adhesion on Elastin-Like Polypeptide Surface Modified Materials. *Biomaterials* **2011,** *32* (25), 5790-5800.
19. Srokowski, E. M.; Woodhouse, K. A. Surface and Adsorption Characteristics of Three Elastin-Like Polypeptide Coatings with Varying Sequence Lengths. *J Mater Sci Mater Med* **2013,** *24* (1), 71-84.
20. McKenna, K. A.; Hinds, M. T.; Sarao, R. C.; Wu, P.-C.; Maslen, C. L.; Glanville, R. W.; Babcock, D.; Gregory, K. W. Mechanical Property Characterization of Electrospun Recombinant Human Tropoelastin for Vascular Graft Biomaterials. *Acta biomaterialia* **2012,** *8* (1), 225-233.
21. Waterhouse, A.; Wise, S. G.; Ng, M. K.; Weiss, A. S. Elastin as a Nonthrombogenic Biomaterial. *Tissue Eng Part B Rev* **2011,** *17* (2), 93-99.
22. Wise, S. G.; Byrom, M. J.; Waterhouse, A.; Bannon, P. G.; Weiss, A. S.; Ng, M. K. A Multilayered Synthetic Human Elastin/Polycaprolactone Hybrid Vascular Graft with Tailored Mechanical Properties. *Acta Biomater* **2011,** *7* (1), 295-303.
23. McClure, M. J.; Simpson, D. G.; Bowlin, G. L. Tri-Layered Vascular Grafts Composed of Polycaprolactone, Elastin, Collagen, and Silk: Optimization of Graft Properties. *Journal of the mechanical behavior of biomedical materials* **2012,** *10*, 48-61.
24. Cheung, H.-Y.; Lau, K.-T.; Lu, T.-P.; Hui, D. A Critical Review on Polymer-Based Bio-Engineered Materials for Scaffold Development. *Composites Part B: Engineering* **2007,** *38* (3), 291-300.
25. Guo, B.; Ma, P. X. Synthetic Biodegradable Functional Polymers for Tissue Engineering: A Brief Review. *Science China Chemistry* **2014,** *57* (4), 490-500.
26. Dhandayuthapani, B.; Yoshida, Y.; Maekawa, T.; Kumar, D. S. Polymeric Scaffolds in Tissue Engineering Application: A Review. *International Journal of Polymer Science* **2011,** *2011*.
27. Lasprilla, A. J.; Martinez, G. A.; Lunelli, B. H.; Jardini, A. L.; Maciel Filho, R. Poly-Lactic Acid Synthesis for Application in Biomedical Devices—a Review. *Biotechnology advances* **2012,** *30* (1), 321-328.
28. Maurus, P. B.; Kaeding, C. C. Bioabsorbable Implant Material Review. *Operative Techniques in Sports Medicine* **2004,** *12* (3), 158-160.
29. Oksman, K.; Skrifvars, M.; Selin, J.-F. Natural Fibres as Reinforcement in Polylactic Acid (Pla) Composites. *Composites science and technology* **2003,** *63* (9), 1317-1324.

30. Plackett, D.; Andersen, T. L.; Pedersen, W. B.; Nielsen, L. Biodegradable Composites Based on L-Polylactide and Jute Fibres. *Composites Science and Technology* **2003,** *63* (9), 1287-1296.
31. Ma, Z.; Gao, C.; Gong, Y.; Shen, J. Chondrocyte Behaviors on Poly-L-Lactic Acid (Plla) Membranes Containing Hydroxyl, Amide or Carboxyl Groups. *Biomaterials* **2003,** *24* (21), 3725-3730.
32. Vieira, A.; Vieira, J.; Guedes, R.; Marques, A. Experimental Degradation Characterization of Pla-Pcl, Pga-Pcl, Pdo and Pga Fibres. *International Committee on Composite Materials (ICCM). Edinburgh* **2009**, 27-31.
33. Yoon, J. S.; Jung, H. W.; Kim, M. N.; Park, E. S. Diffusion Coefficient and Equilibrium Solubility of Water Molecules in Biodegradable Polymers. *Journal of applied polymer science* **2000,** *77* (8), 1716-1722.
34. Matzinos, P.; Tserki, V.; Kontoyiannis, A.; Panayiotou, C. Processing and Characterization of Starch/Polycaprolactone Products. *Polymer Degradation and Stability* **2002,** *77* (1), 17-24.
35. Yang, M.; Zhang, Z.; Hahn, C.; Laroche, G.; King, M. W.; Guidoin, R. Totally Implantable Artificial Hearts and Left Ventricular Assist Devices: Selecting Impermeable Polycarbonate Urethane to Manufacture Ventricles. *Journal of biomedical materials research* **1999,** *48* (1), 13-23.
36. Marletta, G.; Ciapetti, G.; Satriano, C.; Pagani, S.; Baldini, N. The Effect of Irradiation Modification and Rgd Sequence Adsorption on the Response of Human Osteoblasts to Polycaprolactone. *Biomaterials* **2005,** *26* (23), 4793-4804.
37. Chen, R.; Huang, C.; Ke, Q.; He, C.; Wang, H.; Mo, X. Preparation and Characterization of Coaxial Electrospun Thermoplastic Polyurethane/Collagen Compound Nanofibers for Tissue Engineering Applications. *Colloids and Surfaces B: Biointerfaces* **2010,** *79* (2), 315-325.
38. Goldman, J.; Zhong, L.; Liu, S. Q. Negative Regulation of Vascular Smooth Muscle Cell Migration by Blood Shear Stress. *Am J Physiol-Heart C* **2007,** *292* (2), H928-H938.
39. Gunatillake, P. A.; Adhikari, R. Biodegradable Synthetic Polymers for Tissue Engineering. *Eur Cell Mater* **2003,** *5* (1), 1-16.
40. Labet, M.; Thielemans, W. Synthesis of Polycaprolactone: A Review. *Chemical Society Reviews* **2009,** *38* (12), 3484-3504.
41. Williamson, M. R.; Black, R.; Kielty, C. Pcl–Pu Composite Vascular Scaffold Production for Vascular Tissue Engineering: Attachment, Proliferation and Bioactivity of Human Vascular Endothelial Cells. *Biomaterials* **2006,** *27* (19), 3608-3616.
42. Tanzi, M. C.; Mantovani, D.; Petrini, P.; Guidoin, R.; Laroche, G. Chemical Stability of Polyether Urethanes Versus Polycarbonate Urethanes. *Journal of biomedical materials research* **1997,** *36* (4), 550-559.
43. Guo, J.; Feng, Y.; Ye, Y.; Zhao, H. Construction of Hemocompatible Polycarbonate Urethane with Sulfoammonium Zwitterionic Polyethylene Glycol. *Journal of Applied Polymer Science* **2011,** *122* (2), 1084-1091.

44. Tatai, L.; Moore, T. G.; Adhikari, R.; Malherbe, F.; Jayasekara, R.; Griffiths, I.; Gunatillake, P. A. Thermoplastic Biodegradable Polyurethanes: The Effect of Chain Extender Structure on Properties and in-Vitro Degradation. *Biomaterials* **2007,** *28* (36), 5407-5417.
45. Lee, C.; Grodzinsky, A.; Spector, M. The Effects of Cross-Linking of Collagen-Glycosaminoglycan Scaffolds on Compressive Stiffness, Chondrocyte-Mediated Contraction, Proliferation and Biosynthesis. *Biomaterials* **2001,** *22* (23), 3145-3154.
46. Berglund, J. D.; Mohseni, M. M.; Nerem, R. M.; Sambanis, A. A Biological Hybrid Model for Collagen-Based Tissue Engineered Vascular Constructs. *Biomaterials* **2003,** *24* (7), 1241-1254.
47. Weadock, K. S.; Miller, E. J.; Bellincampi, L. D.; Zawadsky, J. P.; Dunn, M. G. Physical Crosslinking of Collagen Fibers: Comparison of Ultraviolet Irradiation and Dehydrothermal Treatment. *Journal of biomedical materials research* **1995,** *29* (11), 1373-1379.
48. Mallory; Sheehan; Hrapchak, *Histotechnology - a Self-Instructional Text*. American Society of Clinical Pathologists (ASCP) Press: Chicago, IL, **1990**.
49. Khait, L.; Birla, R. Bypassing the Patient: Comparison of Biocompatible Models for the Future of Vascular Tissue Engineering. *Cell transplantation* **2012,** *21* (1), 269-283.
50. Tondreau, M. Y.; Laterreur, V.; Gauvin, R.; Vallières, K.; Bourget, J.-M.; Lacroix, D.; Tremblay, C.; Germain, L.; Ruel, J.; Auger, F. A. Mechanical Properties of Endothelialized Fibroblast-Derived Vascular Scaffolds Stimulated in a Bioreactor. *Acta biomaterialia* **2015,** *18*, 176-185.
51. Browning, M.; Dempsey, D.; Guiza, V.; Becerra, S.; Rivera, J.; Russell, B.; Höök, M.; Clubb, F.; Miller, M.; Fossum, T. Multilayer Vascular Grafts Based on Collagen-Mimetic Proteins. *Acta biomaterialia* **2012,** *8* (3), 1010-1021.
52. Kumar, V. A.; Caves, J. M.; Haller, C. A.; Dai, E.; Liu, L.; Grainger, S.; Chaikof, E. L. Acellular Vascular Grafts Generated from Collagen and Elastin Analogs. *Acta biomaterialia* **2013,** *9* (9), 8067-8074.
53. Santana, D. B.; Armentano, R. L.; Zocalo, Y.; Perez Campos, H.; Cabrera, F. E.; Graf, S.; Saldias, M.; Silva, W.; Alvarez, I. Functional Properties of Fresh and Cryopreserved Carotid and Femoral Arteries, and of Venous and Synthetic Grafts: Comparison with Arteries from Normotensive and Hypertensive Patients. *Cell Tissue Bank* **2007,** *8* (1), 43-57.
54. Lovett, M. L.; Cannizzaro, C. M.; Vunjak-Novakovic, G.; Kaplan, D. L. Gel Spinning of Silk Tubes for Tissue Engineering. *Biomaterials* **2008,** *29* (35), 4650-4657.
55. Karimi, A.; Navidbakhsh, M.; Shojaei, A.; Faghihi, S. Measurement of the Uniaxial Mechanical Properties of Healthy and Atherosclerotic Human Coronary Arteries. *Materials Science and Engineering: C* **2013,** *33* (5), 2550-2554.

Chapter 5: Synthesis and Characterization of the Novel Nitric Oxide (NO) Donating Compound, S-nitroso-N-acetyl-D-penicillamine Derivatized Cyclam (SNAP-Cyclam)[2]

5.1. Abstract

Nitric oxide (NO) has been heavily studied over the past two decades due to its multiple physiological functions and its potential therapeutic promise. Of major interest is the desire to fabricate or coat implanted devices with an NO releasing material that will impart the appropriate dose and duration of NO release to positively mediate the biological response to the medical device, thereby improving its safety and efficacy. To date, this goal has not yet been achieved, despite very promising early research.

Herein, we describe the synthesis and NO release properties of a novel NO donor which covalently links the S-nitrosothiol, S-nitroso-N-acetyl-D-penicillamine (SNAP), to the macrocycle, cyclam (SNAP-cyclam). This compound can then be blended into a wide variety of polymer matrices, thereby imparting NO release to the polymer system. This release can be initiated and controlled by transition metal catalysis, thermal degradation or photolytic release of NO from the composite NO-releasing material. SNAP-cyclam is capable of releasing physiologically relevant levels of NO for up to 3 months *in vitro* when blended into poly(L-lactic acid) thin films.

5.2. Introduction

Nitric oxide (NO) is a short-lived free radical gas with important roles in intracellular signaling pathways of diverse physiological systems, ranging from neuronal signaling to the regulation of vascular tone and thrombosis[1-2]. In particular, NO has widespread roles in the vascular system, having been shown to inhibit smooth muscle cell migration and proliferation[3-5], promote endothelial cell growth and proliferation[5-7], and inhibit platelet activation and inflammation[8-9]. Although found in many systems, the extremely short half-life of NO (less than one second in an oxygenated environment) sharply restricts its activity to the vicinity of its production source[10-12]. These beneficial properties make compounds with the ability to sustainably deliver specific levels of NO highly desirable for biomedical applications[13]. Consequently, NO has been heavily investigated in recent years as a therapeutic drug for biomedical applications.

Endogenous NO is produced through several classes of nitric oxide synthases (NOS), enzymes that convert L-arginine into L-citrulline and NO[14]. The major donors reliant on the passive release of NO are a class of zwitterions known as diazeniumdiolates[9]. NO donor molecules known as S-nitrosothiols (RSNOs) are also present physiologically in several forms, the most common of which is S-nitrosoglutathione[10, 15]. In addition to endogenous forms, RSNOs of varied chemical structures can be synthesized and have

[2]The material contained in this chapter has been submitted to *ACS Applied Materials & Interfaces*.

been used for passive or controlled NO release, both *in vitro* and *in vivo*[8, 10]. S-nitrosothiols donate NO in a controlled manner in response to several external factors, including transition metal ion catalysis, thermal degradation and photolytic cleavage[15-16]. Photolytic cleavage is the preferred mode of release for *in vitro* experimentation as the dose and duration of NO delivered can be precisely controlled, whereas transition metal ion and thermal mediated release are utilized for *in vivo* applications which do not require precise control over the NO release profiles[10, 15-16].

In the present study, a novel NO donor, S-nitroso-N-acetyl-D-penicillamine (SNAP), covalently linked to the macrocycle, cyclam (SNAP-cyclam), was synthesized, characterized and then used as the NO donor in poly(L-lactic acid) films which showed physiologically relevant NO release for 3 months. The self-protected NAP-thiolactone can be attached to the secondary amine groups of the macrocyclic base, 1,4,8,11-tetraazacyclotetradecane (cyclam). This compound is simple to synthesize and shows uniquely stable, controllable, long term NO release through mechanisms common to S-nitrosothiols[15-16]. The new donor demonstrates promise for long term, stable release of NO, and has a wide range of potential applications in polymeric biomaterials and device coatings due to its ease of synthesis and the ability to blend the compound into a variety of polymeric materials.

5.3. Materials & Methods

5.3.1. Synthesis of NAP-Cyclam

N-acetyl-D-penicillamine, acetic anhydride, chloroform, hexanes, and sodium nitrite (99.999% trace metals basis) were obtained from Sigma-Aldrich (St. Louis, MO). Pyridine, hydrochloric acid, and sulfuric acid were obtained from EMD Chemicals (Gibbstown, NJ). Magnesium sulfate was purchased from Alfa Aesar (Ward Hill, MA). 1,4,8,11-tetraazacyclotetradecane (99%+) (cyclam) was obtained from Acros Organics (Geel, Belgium).

N-acetyl-D-penicillamine thiolactone (NAP-thiolactone) was prepared according to a previously reported method[17]. Briefly, 5 grams of N-acetyl-D-penicillamine were dissolved in 10 mL of pyridine and cooled over ice for one hour. Concurrently, 10 mL of pyridine and 10 mL of acetic anhydride were mixed and cooled over ice. After one hour, the solutions were mixed and stirred for 24 hours or until the solution turned light red. The solvents were then evaporated until only an orange liquid remained. This product was then dissolved in chloroform and washed with 1M hydrochloric acid. The organic layer was dried with magnesium sulfate, after which the solid was removed by vacuum filtration and the liquid collected. The liquid was evaporated to remove the chloroform and the remaining solid was suspended in hexanes and the crystalline product collected by vacuum filtration. The resultant product was a white, crystalline powder.

To prepare NAP-cyclam, equimolar quantities of cyclam and NAP-thiolactone were added to a sufficient volume of chloroform to ensure full dissolution. These components were allowed to react on a shaker table for 30 minutes. After reacting, the solvent is evaporated on a rotary evaporator (Heidolph Laborota 4000; Elk Grove Village, IL). The resultant viscous liquid is then vacuum dried for 24 hours, ground and homogenized, and vacuum dried for a further 24 hours. The typical recovery is approximately 85% (wt/wt).

5.3.2. Synthesis of SNAP-Cyclam

Two nitrosation mechanisms were employed to form SNAP-cyclam. The first method utilized tert-butyl nitrite (90%; Acros Organics; Geel, Belgium) as the nitrosating agent, while the second method employed sodium nitrite (Sigma-Aldrich; St. Louis, MO). Dodecylbenzenesulfonic acid (DBSA) was purchased from Sigma-Aldrich (St. Louis, MO). To nitrosate the compound with tert-butyl nitrite, NAP-cyclam was dissolved in chloroform. Tert-butyl nitrite was cleaned using 30 mM aqueous cyclam to remove copper (II) stabilizing ions. A slight molar excess of cleaned tert-butyl nitrite was added to NAP-cyclam in solution. Immediately upon addition, a mint green precipitate formed at the surface of the solution. When the vial was shaken, the solution would turn a characteristic emerald green. 20 µL of DBSA was added to nitrosate the solution fully. Rotary evaporation was used to isolate the resultant green solid, SNAP-cyclam.

Solid sodium nitrite was also used to nitrosate NAP-cyclam. In a typical nitrosation process, NAP-cyclam and a molar excess of sodium nitrite are added to 1 mL of deionized water (18MΩ·cm) and shaken to dissolve both solids. 20 µl of concentrated (17.8M) sulfuric acid (EMD Chemicals; Gibbstown, NJ) was then injected into the solution. The vial was shaken several times to ensure a complete reaction has occurred. An emerald green precipitate formed immediately, which was isolated by vacuum filtration followed by several rinses in deionized water. The green powder, SNAP-cyclam, is then vacuum dried. The typical recovery was approximately 64% (wt/wt).

5.3.3. Copper Chelation Analysis

Reaction times and product stability of NAP-cyclam were determined using a copper chelation assay[18]. When copper (II) chloride (Alfa Aesar; Ward Hill, MA) is added to a solution containing cyclam in chloroform, the solution becomes purple, indicating copper chelation by the cyclam has occurred. NAP-cyclam dissolved in chloroform is unable to chelate copper. By exploiting this phenomenon, the reaction's progress can be evaluated, and the stability and reaction time of NAP-cyclam was determined. Analysis was performed with ultraviolet visible light (UV/Vis) spectroscopy.

5.3.4. Free Thiol Analysis of NAP-Cyclam

Free thiol analysis was used to determine the molar ratio of NAP-thiolactone to cyclam in NAP-cyclam. The reaction of 5,5'-dithiobis-(2-nitrobenzoic acid) (Ellman's reagent,

DTNB; Sigma Aldrich; St. Louis, MO) with free thiols was exploited to evaluate this ratio. The absorbance of a dilute solution at 412 nm was recorded with a Perkin Elmer Lambda 35 UV/Vis spectrometer, and the results are directly proportional to the sulfur content in NAP-cyclam. L-cysteine (Sigma-Aldrich; St. Louis, MO) was used to generate a standard curve.

5.3.5. HPLC Analysis of NAP-Cyclam

High performance liquid chromatography (HPLC) was used to verify the molar ratio of NAP to cyclam in the final compound. Methanol (Chromasolv; 99.9%) and trifluoroacetic acid (TFA) were purchased from Sigma-Aldrich (St. Louis, MO). A Sonoma C18(2) 5 µ, 100 Å column manufactured by ES Industries (West Berlin, NJ) that measured 10 cm in length with a 3.2 mm inside diameter was used for all experiments. The HPLC system consisted of a Perkin Elmer Flexar PDA Plus detector, Series 200 pump with a 20 µL injection loop, and Series 200 vacuum degasser (Waltham, MA). The mobile phase for all experiments was 30% water and 70% methanol with 0.1% TFA added to both components as a buffer. The flow rate in all experiments was 1 mL/minute.

HPLC experiments were performed by first reacting the colorimetric thiol tag, Measure-iT (Life Technologies; Grand Island, NY), with NAP-cyclam. Samples were prepared according to the manufacturer's instructions and allowed to react for 20 minutes prior to each injection. The PDA detector was set to measure both 270 nm and 497 nm with a bandwidth of 10 nm.

5.3.6. UV/Vis Analysis of SNAP-Cyclam

NAP-cyclam and SNAP-cyclam were analyzed by UV/Vis spectroscopy in phosphate buffered saline (PBS) (Sigma-Aldrich; St. Louis, MO) (pH 7.4) at concentrations of 250 µM on a Perkin Elmer Lambda 35 spectrometer (Waltham, MA).

5.3.7. FTIR Analysis of (S)NAP-Cyclam

Transmittance Fourier transform infrared spectroscopy (FTIR) was performed on an Analect Diamond 20 (Applied Instrument Technologies; Upland, CA). Samples were made by pressing 7 mm diameter potassium bromide pellets (Sigma Aldrich; St. Louis, MO) and running a transmittance scan on the sample (64 scans, 2 cm^{-1} resolution) under inert nitrogen.

5.3.8. Quantitative Nitric Oxide Analysis

Total NO release from SNAP-cyclam was directly measured via chemiluminescence detection with a Siever's 280i Nitric Oxide Analyzer (Boulder CO). Phosphate buffered saline (PBS; pH 7.4), dichloromethane, and sodium ascorbate were obtained from Sigma-Aldrich (St. Louis, MO). Chelex 100 Resin (sodium form) was purchased from Bio-Rad Laboratories (Hercules, CA). Copper (II) chloride was obtained from Alfa Aesar (Ward

Hill, MA). Tert-butyl nitrite was obtained from Acros Organics (Geel, Belgium). All measurements were made at room temperature. Approximately 50 mg of NAP-cyclam was nitrosated for each trial with clean tert-butyl nitrite for 6 hours in dichloromethane. This sample was diluted 1:10 in dichloromethane immediately prior to analysis. 1 mL of PBS and 100 µL of SNAP-cyclam were injected into a quartz reaction cell. 100 µL of 10 mM $CuCl_2$ and 300 µL of 100 mM sodium ascorbate were added to initiate release of NO from SNAP-cyclam. Once NO evolution returned to baseline levels, an additional 100 µL of 10 mM $CuCl_2$ and 300 µL of 100 mM sodium ascorbate were added to ensure full decomposition of the RSNO. Theoretical calculations of the total NO present in the sample were compared to the total measured NO obtained through chemiluminescent detection. The total NO evolved was normalized to sample mass.

5.3.9. Nitric Oxide Release from poly(L-lactic acid) Film Samples

Poly(L-lactic acid) (PLLA) film samples were prepared by making a 4% (wt/wt) solution of PLLA (Natureworks, LLC; Minnetonka, MN) in chloroform (Sigma-Aldrich; St. Louis, MO). NAP-cyclam was added to the dissolved PLLA to produce solutions with final SNAP-cyclam concentrations of 30 mM and 68 mM. 100 µl of clean tert-butyl nitrite (Acros Organics; Geel, Belgium) was added to each solution followed by 20 µl of DBSA (Sigma-Aldrich; St. Louis, MO). The resulting solutions were solvent cast on 12 mm diameter glass coverslips (VWR; Radnor, PA) using 100 µl of solution per sample. The films were allowed to dry under ambient conditions protected from light.

Film samples were incubated at 37°C submerged in PBS (pH 7.4) (Sigma Aldrich; St. Louis, MO) for 91 days. NO released from the samples was measured with a Sievers 280i NOA at 37°C for 15 minutes on days 0, 15, 40, 62, and 91. Films were removed from the PBS solution during NO release measurements, and promptly returned after 15 minutes. A 385 nm (± 5 nm) light emitting diode (LED) (SSL-LXTO461UV1C; Lumex; Carol Stream, IL) was attached to the sample vial to promote NO release. The LED was powered with 73 mW at 27 mA and placed 5.2 cm above the sample. Four samples were evaluated per group.

5.4. Results

Cyclam has a total of 4 secondary amines that could be potential binding sites for the reaction of the self-protected NAP-thiolactone to covalently link to the ring[19]. It was confirmed through several analytical techniques that NAP-thiolactone reacts with the secondary amines present in the cyclam ring in a 1:1 molar ratio.

5.4.1. Copper Chelation Analysis of NAP-Cyclam

Cyclam will form a deep purple color when in solution upon chelation of Cu^{2+}. The reaction of NAP-thiolactone with cyclam prevents the chelation of copper by NAP-cyclam. Therefore, an absorbance based analysis technique was developed to confirm

that the reaction is occurring on the secondary amine sites present in the cyclam ring, thereby disrupting the ability of cyclam to chelate copper (II). Figure 5.1 shows the UV/Vis spectra over a range of 545–553 nm demonstrating the completion of the reaction required to form NAP-cyclam. In this approach, the magnitude of the absorbance corresponds to the degree of copper chelation. A reduction in absorbance at 545 nm between the 5 minute and 15 minute NAP-cyclam samples to background levels demonstrates a complete reaction between NAP-thiolactone and cyclam after 15 minutes.

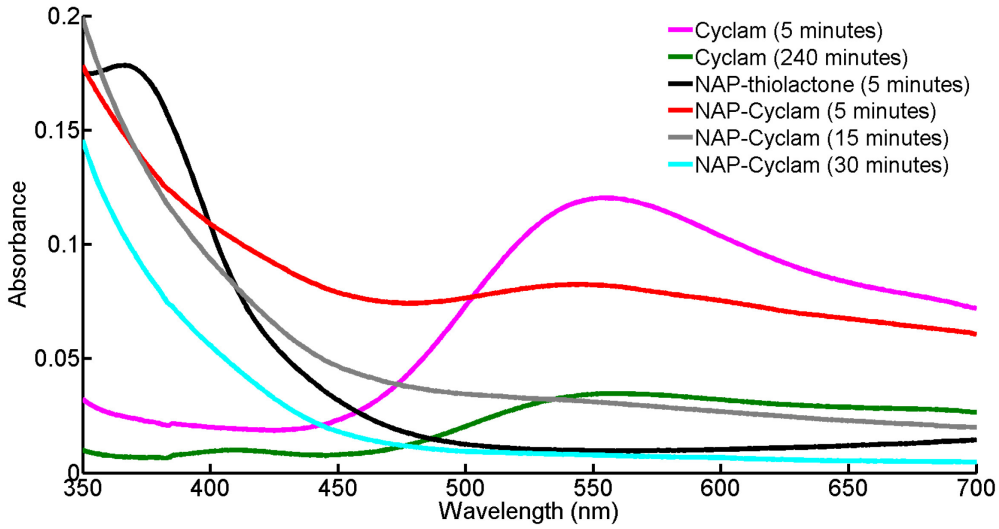

Figure 5.1. Reaction time determination of NAP-Cyclam. This figure shows the copper chelation analysis of NAP-cyclam. Cyclam (5 minutes; pink) and cyclam (240 minutes; green) demonstrate the characteristic absorbance change of copper loaded cyclam. NAP-thiolactone (5 minutes; black) does not demonstrate this phenomenon. NAP-cyclam (5 minutes; red) shows an increase in absorbance, while NAP-cyclam (15 minutes; gray) does not, indicating the completion of the reaction.

5.4.2. Free Thiol Analysis of NAP-Cyclam

The four secondary amine sites on the cyclam macrocycle make up to four molar additions of NAP-thiolactone possible. To determine the reaction stoichiometry of NAP-cyclam, an Ellman's test for free thiols present in NAP-cyclam was performed using UV/Vis spectroscopy. Figure 5.2 shows the calibration curve created using L-cysteine as the thiol standard. Three averaged samples of three independent NAP-cyclam samples (red, green, and blue) were plotted with standard deviations. The average molar ratio of thiol present was 0.80 ± 0.02:1.

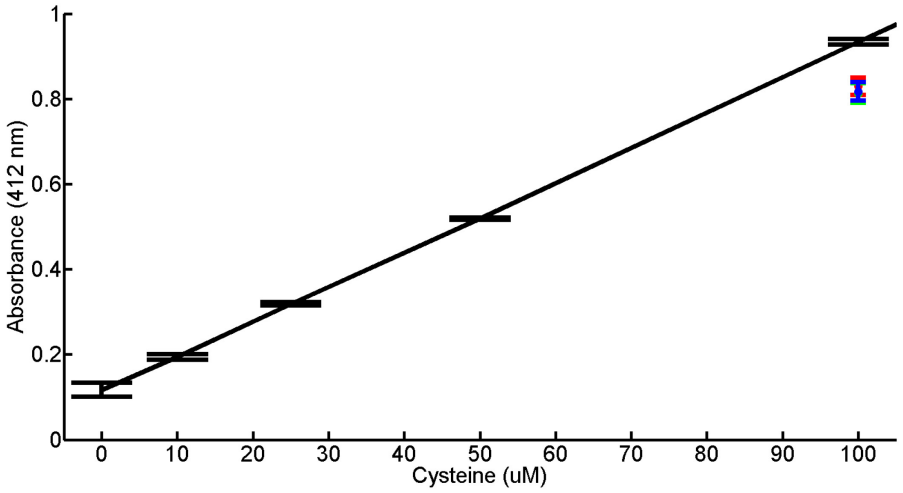

Figure 5.2. Free thiol analysis of NAP-Cyclam. Free thiol analysis using Ellman's reagent demonstrates a linear L-Cysteine standard curve. Three averaged samples of three independent NAP-cyclam samples (red, green, blue) show the experimental results. This data proves that the compound is composed of equimolar ratios of cyclam and NAP-thiolactone.

5.4.3. HPLC Analysis of NAP-Cyclam

Figure 5.3 shows the results of the HPLC elution of Measure-iT tagged NAP-cyclam. These results demonstrate a single elution peak (1.94 minutes) of the tagged compound, indicating a single molar ratio of NAP-cyclam exists. UV/Vis spectroscopy of the components used in the HPLC elutions are presented in Figure 5.4. The chromatograms of the respective eluents are provided in Figure 5.5 for positive identification.

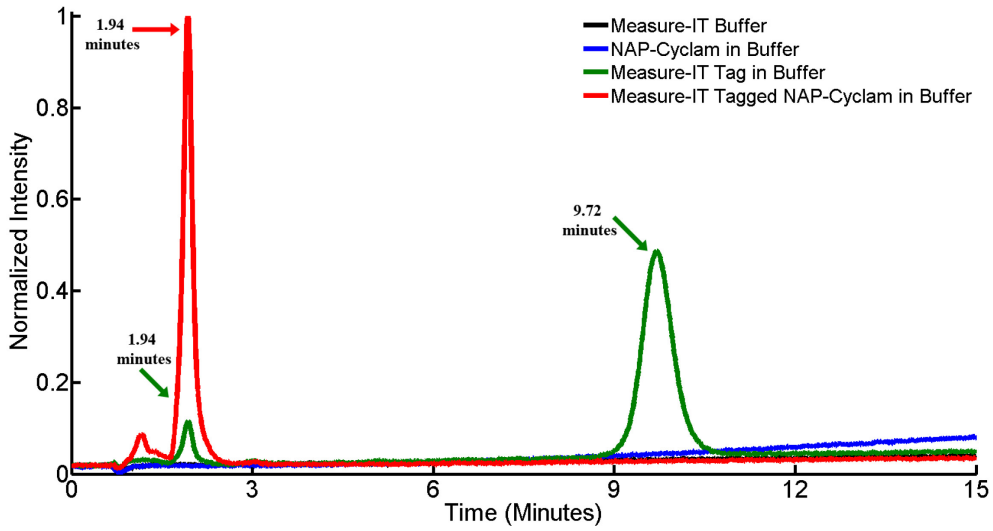

Figure 5.3. Chromatography of NAP-Cyclam. Figure 5.3 shows the chromatograms of the Measure-IT tagged NAP-cyclam and the respective components. As demonstrated in red (t = 1.94 minutes) NAP-cyclam exits the column as one entity, rather than multiple peaks, thus proving that an equimolar compound exists. The Measure-iT tag, when unreacted, exits the column after 9.72 minutes. This peak is not presented in the Measure-iT tagged NAP-cyclam. Measure-IT buffer – Black; NAP-cyclam in buffer – Blue; Measure-IT tag in buffer – Green; Measure-IT tag reacted with NAP-cyclam in buffer – Red. Peaks - Red; 1.94 minutes: Green; 1.94 minutes, 9.72 minutes.

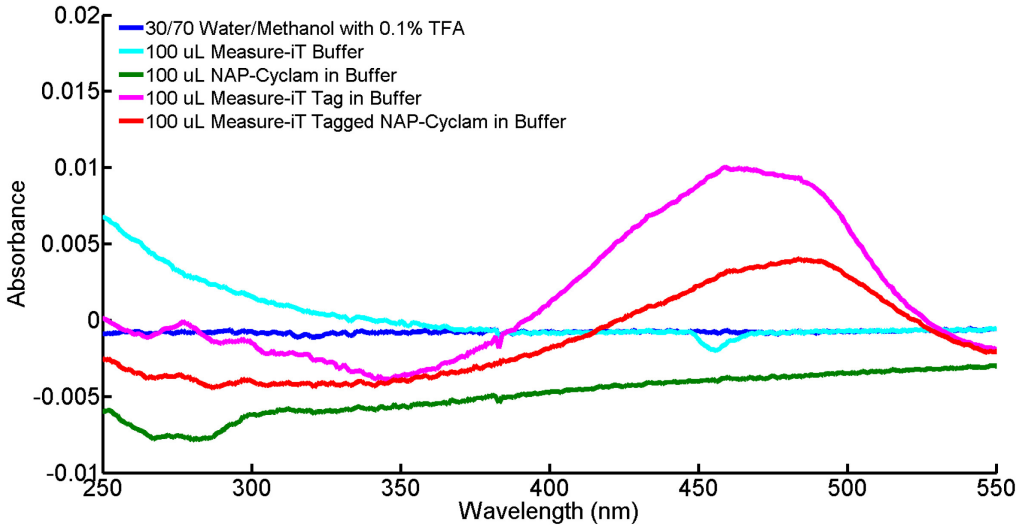

Figure 5.4. UV/Vis analysis of chromatography components. Figure 5.4 shows the UV/Vis spectra of the components used in the HPLC evaluation of NAP-cyclam. Both the Measure-iT tag (pink; 460 nm) and the Measure-iT tagged NAP-cyclam (red; 490 nm) show an absorption peak. This peak is also seen in the chromatogram of the components (Figure 7).

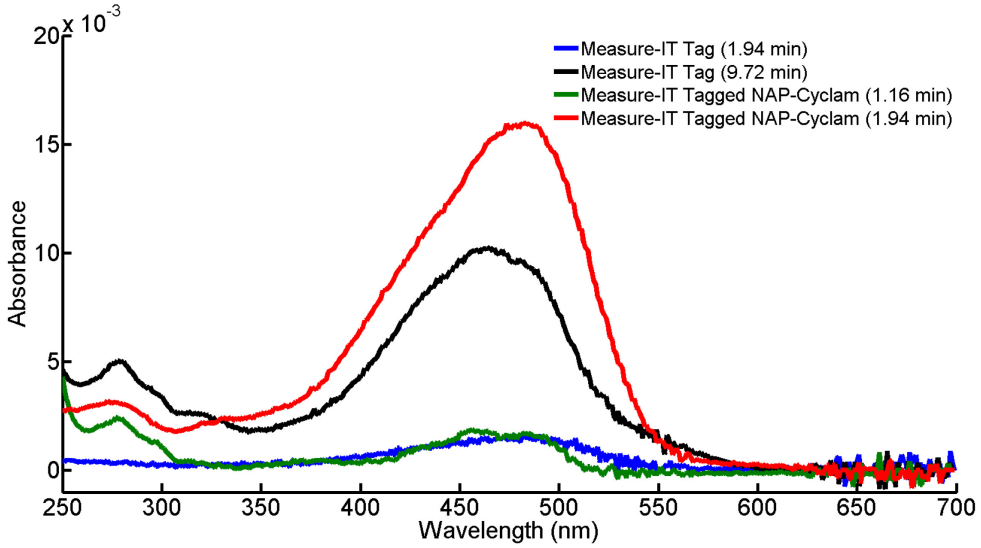

Figure 5.5. UV/Vis chromatograms of chromatography elution peaks. Figure 5.5 shows the chromatograms associated with the peaks in the HPLC elution of Measure-IT tagged NAP-cyclam. The peak profiles of the eluted peaks are similar to those in Figure 6, proving the identity of the components. Blue – Measure-IT tag (1.94 minutes); Black – Measure-iT tag (9.72 minutes); Green – Measure-iT tagged NAP-cyclam (1.16 minutes); Red – Measure-iT tagged NAP-cyclam (1.94 minutes).

5.4.4. UV/Vis Analysis of SNAP-Cyclam

Solution phase samples were evaluated for spectral changes after nitrosation of NAP-cyclam with tert-butyl nitrite in chloroform (Figure 5.6) to form the corresponding S-nitrosothiol, SNAP-cyclam. The characteristic S-nitrosothiol peaks formed are seen in the UV/Vis spectrum of SNAP-cyclam at 349 nm ($\varepsilon = \sim 340\ M^{-1}\cdot cm^{-1}$) and 597 nm ($\varepsilon = \sim 10\ M^{-1}\cdot cm^{-1}$). These peaks correspond to known absorption maxima of nitrosothiols reported as 330–350 nm ($\varepsilon = \sim 10^3\ M^{-1}\cdot cm^{-1}$) and 550–600 nm ($\varepsilon = \sim 20\ M^{-1}\cdot cm^{-1}$)[16]. This confirms that the thiolactone ring opens upon reaction with the secondary amines present in cyclam, exposing the thiol group. The free thiol can then be nitrosated to form the RSNO, S-nitroso-N-acetyl-D-penicillamine. Without a ring opening reaction exposing the primary thiol, the S-nitrosothiol could not form.

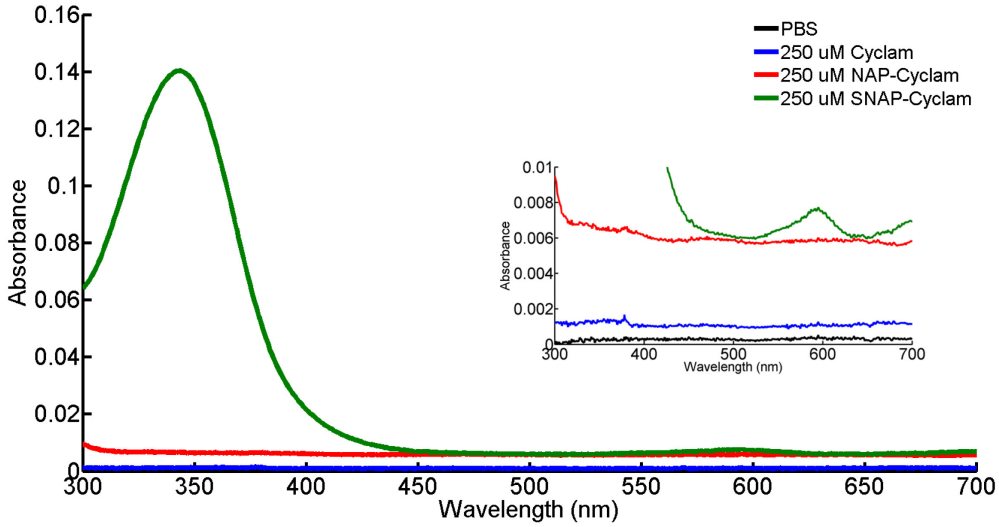

Figure 5.6. SNAP-Cyclam demonstrates characteristic UV/Vis absorption spectra. This figure shows the characteristic S-nitrosothiol peaks at 349 and 597 nm. These peaks have been previously reported to exist between 330–350 nm (ε = ~10^3 $M^{-1}cm^{-1}$) and 550–600nm (ε = ~20 $M^{-1}cm^{-1}$). PBS – Black; 250 μM cyclam – Blue; 250 μM NAP-cyclam – Red; 250 μM SNAP-cyclam – Green.

5.4.5. FTIR Analysis of (S)NAP-Cyclam

In order to confirm the formation of SNAP-cyclam, FTIR was performed on pressed potassium bromide pellets of cyclam, NAP-thiolactone, NAP-cyclam, and SNAP-cyclam (Figure 5.7). Included for reference in the figure is the parent material to NAP-thiolactone, N-acetyl-D-penicillamine. It can be seen that the secondary amine sites on the cyclam macrocycle (3180 cm^{-1} and 3272 cm^{-1}) are significantly diminished (~8%) after the reaction with NAP-thiolactone. This evidence shows that the secondary amine sites on cyclam are the site of addition for NAP-thiolactone. The band at 2532 cm^{-1}, corresponding to free thiols, indicates the successful ring opening reaction of NAP-thiolactone.

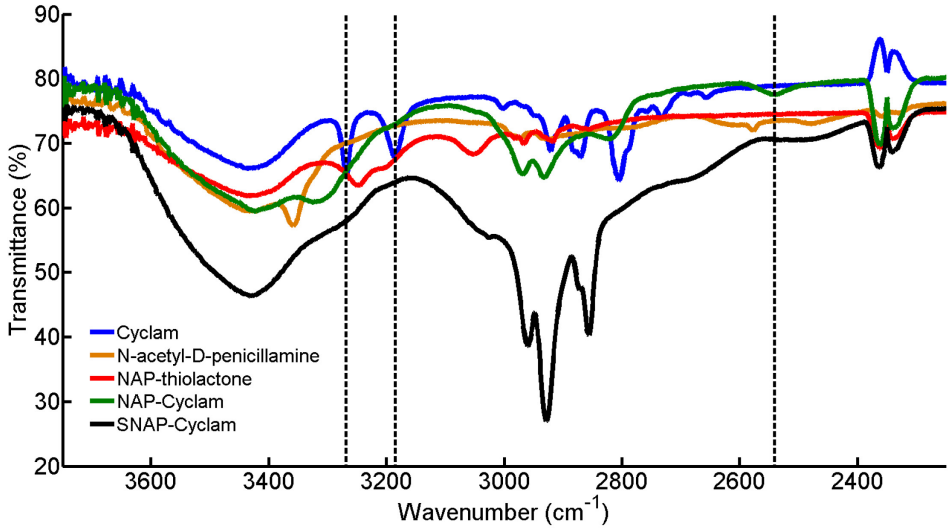

Figure 5.7. FTIR analysis of (S)NAP-Cyclam. FTIR results illustrate the progression of the synthesis of (S)NAP-cyclam. Bands at 3180 cm^{-1} and 3272 cm^{-1} indicate the secondary amine sites in cyclam (blue line). These are significantly diminished in NAP-cyclam (green), identifying the secondary amines as the site of reaction for NAP-thiolactone. A single band in appearing in NAP-cyclam (green) at 2532 cm^{-1} indicates the presence of a free thiol, demonstrating the successful ring opening reaction of NAP-thiolactone.

5.4.6. Quantitative Nitric Oxide Release

The total NO released from SNAP-cyclam was determined to be 94. ± 0.023 % (n = 4) of the total theoretical NO available. The nitrosation resulted in 2.3 ± 0.056 µmols NO/mg of compound.

5.4.7. Proposed Structure of SNAP-Cyclam

Figure 5.8 shows the proposed chemical structure of SNAP-cyclam. The data suggests that the compound exists as a majority 1:1 molar ratio of NAP-thiolactone to cyclam.

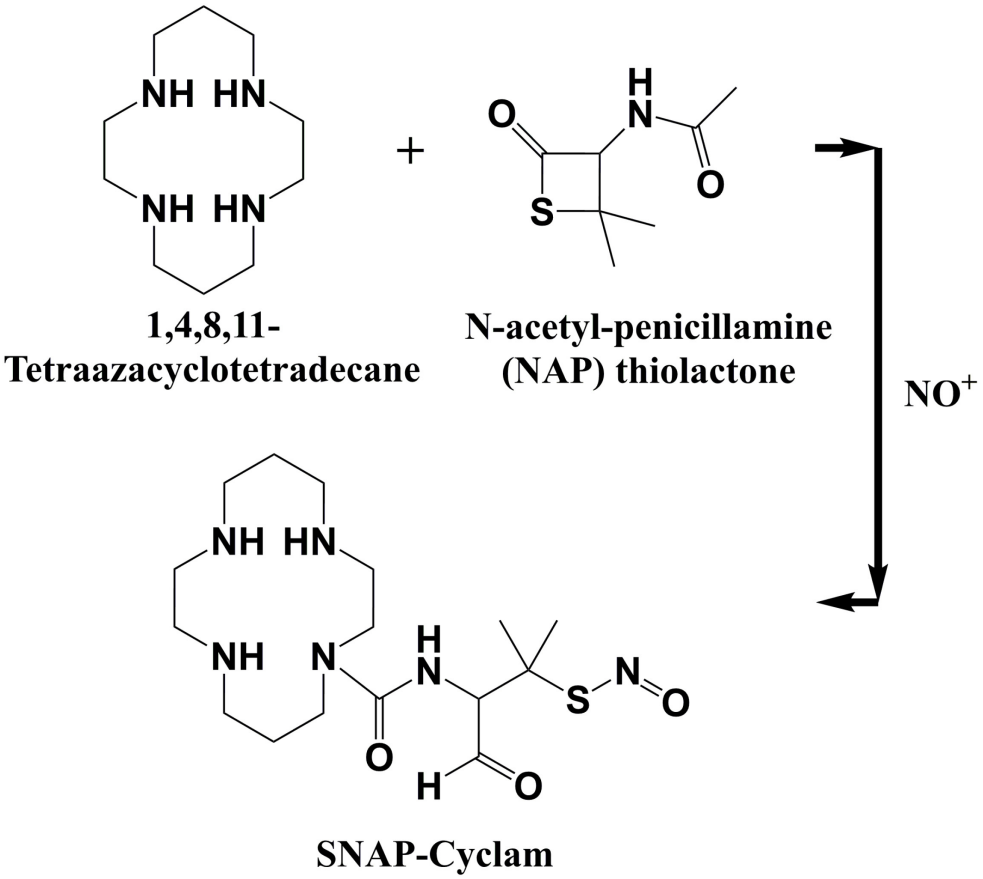

Figure 5.8. Proposed structure of SNAP-Cyclam. Figure 5.8 shows the proposed structure of SNAP-cyclam, representing the equimolar ratio of components. The structure is approximated.

5.4.8. Nitric Oxide Release from poly(L-lactic acid) Films Containing SNAP-Cyclam

In order to create a NO releasing polymeric material, SNAP-cyclam was blended into PLLA and cast into a thin film with final concentrations of 30 mM and 68 mM. Figure 5.9 shows photolytic NO release averages for these film samples over 91 days at 37°C immersed in PBS (pH 7.4) (n = 4 per group). The characteristic green coloration of the RSNO was no longer perceptible after day 2. However, the sample released physiologically relevant amounts of NO upon stimulation with light.

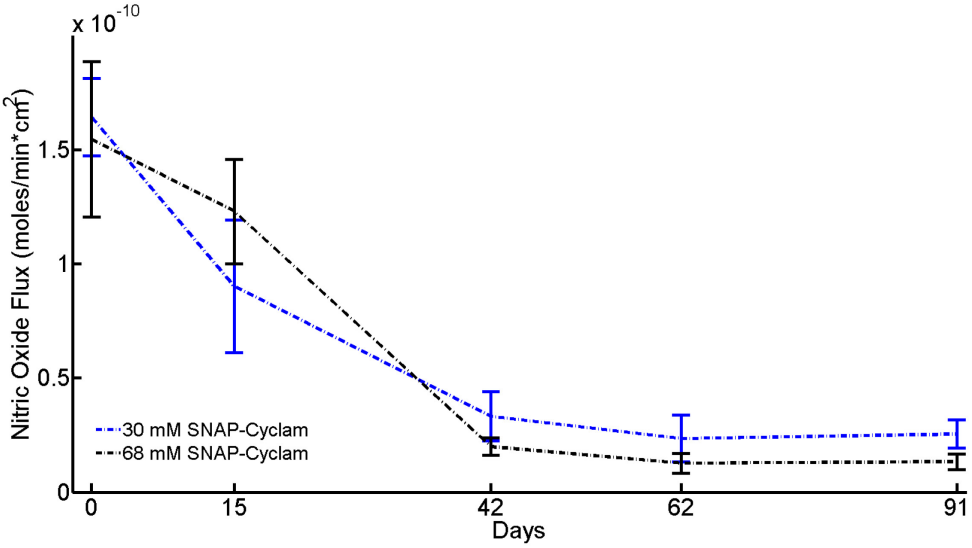

Figure 5.9. Average nitric oxide release from SNAP-Cyclam loaded PLLA films. This figure shows the average NO released over 91 days from 30 mM and 68 mM SNAP-cyclam loaded PLLA films soaked in PBS (pH 7.4) at 37°C. Films were removed from solution and irradiated by a 385 nm LED to promote NO release from the films.

5.5. Discussion

Two primary types of NO donors undergoing extensive research and development for therapeutic applications are diazeniumdiolates and S-nitrosothiols. Although diazeniumdiolates have been investigated for many decades and hold promise for NO based therapies, they require a high pressure system pathway for nitrosation. To directly attach diazeniumdiolates to polymer backbones requires covalent attachment of a parent compound to the base polymer, which necessitates additional reaction steps to develop a functional material and will often fundamentally alter the mechanical properties of the polymer itself. Additionally, modifications to the NO release profile (which are often application specific and require extensive processing revisions) require relatively sophisticated and nuanced manipulations of the chemical pathway. These intrinsic limitations have accelerated the development of blended NO donors applicable to a wide variety of polymeric materials, where NO flux profiles can be altered by changing the quantity of compound.

Here, we have developed a novel, stable NO donor, SNAP-cyclam, through a rapid, simple, and thermodynamically favorable reaction between NAP-thiolactone and cyclam. The compound exhibits high solubility in a wide range of solvents, including water. This property allows the new NO donor to be readily blended (and for NO release levels to be quickly modified) within a wide range of conventional polymeric materials for biomedical applications, surmounting the major recognized limitations of previous NO

donors. The release profile can be easily adjusted to optimize the flux of NO delivered by increasing the amount of SNAP-cyclam.

As demonstrated in Figure 5.9, SNAP-cyclam incorporated into PLLA films and submerged in PBS exhibits consistent long-term, ion-mediated NO release at therapeutic levels. The estimated endogenous NO flux from intact, healthy endothelium is reported to be $0.5–4x10^{-10}$ mols·cm^{-2}·sec^{-1} [20]. When the material is hydrated in PBS, metal ion mediated release (attributed to ion permeation from the PBS through the PLLA) as well as thermal mediated release contribute to the overall surface flux of NO obtained. The larger NO flux generated by the 30 mM sample after day 42 can be attributed to the lack of UV light penetration into the more opaque 68 mM sample. In clinical applications, light mediated mechanisms would be replaced by metal ion mediated or thermal mediated NO release methods. The stability of the NO donor and sustained release shown *in vitro* suggests that it may serve as a long-term NO donor, *in vivo*.

To fully characterize NAP-cyclam, the compound's molar ratio after formation were essential to determine the NO reservoir and predict the stability of the compound. FTIR results demonstrate direct involvement of the secondary amine sites on the cyclam macrocycle in the reaction, as evidenced by the disappearance of the characteristic secondary amine peaks at 3180 cm^{-1} and 3272 cm^{-1}. FTIR also indicated a complete ring opening reaction of NAP-thiolactone by the presence of the free thiol band at 2532 cm^{-1}. The proposed reaction mechanism for this product is has been previously alluded to in literature[21-22]. Reports of this reaction mechanism suggested that S_N2 type nucleophilic substitution may be responsible for the formation of compounds between secondary amines and β-thiolactones[21-22]. Although the stoichiometry of NAP-cyclam was determined to be equimolar between NAP-thiolactone and cyclam, further work will be required to confirm the reaction mechanism.

Due to the relative ease of synthesis of SNAP-cyclam and demonstrated stability under ambient conditions, this NO donor has potential applications in many medical device applications. The donor can be readily synthesized with few compounds: an appropriate solvent for the application, NAP-thiolactone, cyclam, an acid, and an appropriate nitrosating agent. This lends itself well to batch synthesis and mass production. Due to the donor's solubility in many organic solvents and water, it is capable of being incorporated into a wide variety of medical polymers. To date, the donor has been successfully processed utilizing solvent casting, spin coating, electrospinning, and liquid atomization techniques (data not shown). In addition, the donor has been successfully sterilized by ethylene oxide treatment while encapsulated in polycaprolactone without loss of NO (data not shown). Ultimately, this donor is well suited to applications in conjunction with polymers (tubing, films, and constructs) and medical device coatings.

In applications for medical devices, the ideal storage and transportation conditions for a drug delivering material should include a wide margin of temperatures, and few, if any, special handling considerations. To this end, the material developed here has demonstrated stability at room temperature for over 12 months, with the only special handling precaution being protection from ambient light. This should not be taken as a deficiency of the material, as the requirement to keep it protected from light is easily provided for by the material's packaging in a clinical setting.

Future development of this class of compounds should investigate the use of other macrocycles and secondary amine containing compounds. Elucidation of the mechanism of reaction may be possible by studying a secondary amine containing cyclic molecule (piperidine) or a porphyrin (porphine). 1,4,7,10-tetraazacyclododecane (cyclen), may exhibit similar properties as those of cyclam. To increase the molar ratio of NO available on a single macrocycle, and thus increase the amount of NO that can be stored within a polymer, bicyclam molecules could be evaluated[23].

5.6. Conclusion

NO has many potential therapeutic applications due to its ubiquitous physiological prevalence. We have demonstrated that SNAP-cyclam, a novel NO donor formed in an equimolar reaction between the self-protected NAP-thiolactone and cyclam, can be formed in a straight forward manner. SNAP-cyclam demonstrated excellent stability after formation, and when blended with PLLA, also demonstrated sustained, long term delivery of NO under physiological conditions, *in vitro*. In addition to describing a promising NO donor, this work has demonstrated a novel reaction involving a commonly employed NO donor in research and clinical applications. This new approach has the potential to produce novel compounds with large NO reservoirs available for release over clinically relevant time periods.

Long term *in vivo* evaluation of SNAP-cyclam will be required to determine its clinical relevancy. SNAP-cyclam holds promise as a valuable tool in the clarification of the biological effects of NO on physiological systems due to its ease of synthesis, incorporation into a wide range of polymers, and potential use as a clinical therapeutic.

5.7. Acknowledgements

This work was funded by the National Institutes of Health grant R15HL113954 and the National Science Foundation - Division of Materials Research Grant number 1410192. C.W.M. was supported by the National Institutes of Health grant R15HL113954.

5.8. References

1. Lahdenranta, J.; Hagendoorn, J.; Padera, T. P.; Hoshida, T.; Nelson, G.; Kashiwagi, S.; Jain, R. K.; Fukumura, D. Endothelial Nitric Oxide Synthase Mediates Lymphangiogenesis and Lymphatic Metastasis. *Cancer Res* **2009,** *69* (7), 2801-2808.
2. Moncada, S.; Higgs, E. A. Molecular Mechanisms and Therapeutic Strategies Related to Nitric Oxide. *FASEB J* **1995,** *9* (13), 1319-1330.
3. Sarkar, R. Mechanisms of Inhibition of Vascular Smooth Muscle Cell Function by Nitric Oxide. University of Michigan, **1995**.
4. Bohl, K. S.; West, J. L. Nitric Oxide-Generating Polymers Reduce Platelet Adhesion and Smooth Muscle Cell Proliferation. *Biomaterials* **2000,** *21* (22), 2273-2278.
5. Chen, C.; Hanson, S. R.; Keefer, L. K.; Saavedra, J. E.; Davies, K. M.; Hutsell, T. C.; Hughes, J. D.; Ku, D. N.; Lumsden, A. B. Boundary Layer Infusion of Nitric Oxide Reduces Early Smooth Muscle Cell Proliferation in the Endarterectomized Canine Artery. *J Surg Res* **1997,** *67* (1), 26-32.
6. Bohlen, H. G.; Wang, W.; Gashev, A.; Gasheva, O.; Zawieja, D. Phasic Contractions of Rat Mesenteric Lymphatics Increase Basal and Phasic Nitric Oxide Generation in Vivo. *Am J Physiol Heart Circ Physiol* **2009,** *297* (4), H1319-1328.
7. Hagendoorn, J.; Padera, T. P.; Kashiwagi, S.; Isaka, N.; Noda, F.; Lin, M. I.; Huang, P. L.; Sessa, W. C.; Fukumura, D.; Jain, R. K. Endothelial Nitric Oxide Synthase Regulates Microlymphatic Flow Via Collecting Lymphatics. *Circ Res* **2004,** *95* (2), 204-209.
8. Gkaliagkousi, E.; Ferro, A. Nitric Oxide Signalling in the Regulation of Cardiovascular and Platelet Function. *Front Biosci (Landmark Ed)* **2011,** *16*, 1873-1897.
9. Carpenter, A. W.; Schoenfisch, M. H. Nitric Oxide Release: Part Ii. Therapeutic Applications. *Chem Soc Rev* **2012,** *41* (10), 3742-3752.
10. Al-Sa'doni, H.; Ferro, A. S-Nitrosothiols: A Class of Nitric Oxide-Donor Drugs. *Clin Sci (Lond)* **2000,** *98* (5), 507-520.
11. Vaughn, M. W.; Kuo, L.; Liao, J. C. Effective Diffusion Distance of Nitric Oxide in the Microcirculation. *Am J Physiol* **1998,** *274* (5 Pt 2), H1705-1714.
12. Goldstein, S.; Czapski, G. Kinetics of Nitric Oxide Autoxidation in Aqueous Solution in the Absence and Presence of Various Reductants. The Nature of the Oxidizing Intermediates. *Journal of the American Chemical Society* **1995,** *117* (49), 12078-12084.
13. Reynolds, M. M.; Frost, M. C.; Meyerhoff, M. E. Nitric Oxide-Releasing Hydrophobic Polymers: Preparation, Characterization, and Potential Biomedical Applications. *Free Radic Biol Med* **2004,** *37* (7), 926-936.
14. Bonavida, B.; Khineche, S.; Huerta-Yepez, S.; Garban, H. Therapeutic Potential of Nitric Oxide in Cancer. *Drug Resist Updat* **2006,** *9* (3), 157-173.
15. Williams, D. L. H. A Chemist's View of the Nitric Oxide Story. *Organic & biomolecular chemistry* **2003,** *1* (3), 441-449.
16. Williams, D. L. H. The Chemistry of S-Nitrosothiols. *Accounts of Chemical Research* **1999,** *32* (10), 869-876.

17. Frost, M. C.; Meyerhoff, M. E. Synthesis, Characterization, and Controlled Nitric Oxide Release from S-Nitrosothiol-Derivatized Fumed Silica Polymer Filler Particles. *Journal of Biomedical Materials Research Part A* **2005,** *72* (4), 409-419.
18. Meallet-Renault, R.; Herault, A.; Vachon, J. J.; Pansu, R. B.; Amigoni-Gerbier, S.; Larpent, C. Fluorescent Nanoparticles as Selective Cu(Ii) Sensors. *Photochem Photobiol Sci* **2006,** *5* (3), 300-310.
19. Moynihan, H. A.; Roberts, S. M. Preparation of Some Novel S-Nitroso Compounds as Potential Slow-Release Agents of Nitric Oxide in Vivo. *J. Chem. Soc., Perkin Trans. 1* **1994,** (7), 797-805.
20. Vaughn, M. W.; Kuo, L.; Liao, J. C. Estimation of Nitric Oxide Production and Reaction Rates in Tissue by Use of a Mathematical Model. *Am J Physiol-Heart C* **1998,** *274* (6), H2163-H2176.
21. Crich, D.; Sana, K. Sn2-Type Nucleophilic Opening of B-Thiolactones (Thietan-2-Ones) as a Source of Thioacids for Coupling Reactions. *The Journal of organic chemistry* **2009,** *74* (9), 3389-3393.
22. Yang, X.; Gooding, J. J.; Hibbert, D. B.; Kumar, N. Synthesis of N-(3-Mercaptopropanoyl)-Aza-18-Crown-6, N-(4-Mercaptobutanoyl)-Aza-18-Crown-6 and Their Dimers. *Organic preparations and procedures international* **1999,** *31* (4), 425-429.
23. De Clercq, E. The Bicyclam Amd3100 Story. *Nature Reviews Drug Discovery* **2003,** *2* (7), 581-587.

Chapter 6: Transition Metal Mediated Release of Nitric Oxide (NO) from S-nitroso-N-acetyl-D-penicillamine (SNAP): Potential Applications for Endogenous Release of NO on the Surface of Stents via Corrosion Products[3]

6.1. Abstract

Nitric oxide (NO), identified over the last several decades in many physiological processes and pathways as both a beneficial and detrimental signaling molecule, has been the subject of extensive research. Physiologically, NO is transported by a class of donors known as S-nitrosothiols. Both endogenous and synthetic S-nitrosothiols have been reported to release NO during interactions with certain transition metals, namely Cu^{2+} and Fe^{2+}. Based on the electronic structure of the reported metals, alternative transition metals could be potential catalysts for the evolution of NO from RSNOs.

Current coronary stents utilize biostable metals to provide mechanical support during coronary artery disease. However, these stents often fail due to in-stent thrombosis and restenosis. Alternatively, biodegradable stents have shown significant promise to reduce or eliminate both thrombosis and restenosis. One potential pathway to achieve this is by exploiting NO generation from endogenous RSNOs, caused by biodegradable stents releasing metal ions capable of decomposing RSNOs at the stent-blood interface.

Here, we evaluate Pt^{2+}, Fe^{2+}, Fe^{3+}, Mg^{2+}, Zn^{2+}, Mn^{2+}, Co^{2+}, Ni^{2+}, and Cu^{2+} for their ability to generate NO from S-nitroso-N-acetyl-D-penicillamine (SNAP) under physiological pH conditions. Specifically, we report NO generation from RSNOs by three transition metal ions; Co^{2+}, Ni^{2+}, and Zn^{2+}, which have not been previously reported to generate NO. Additionally, preliminary *in vivo* evidence of wires implanted in the rat arterial wall and circulating blood is presented which demonstrated inhibited thrombus formation after 6 months.

6.2. Introduction

Nitric oxide (NO), a physiologically ubiquitous free radical gas, has been the center of extensive research over the past several decades after it was proven to be endothelial derived relaxing factor[1]. Though its functions in the physiological environment are extensive, NO's most notable roles are within the realms of intracellular signaling[2-3], vascular regulation[4-5], and wound repair[6]. Due to NO's state as a free radical gas, its half-life in the physiological environment is short[7-8]. To allow physiological transport of this reactive molecule, NO is shuttled to specific targets in the form of endogenous S-nitrosothiols (RSNOs). These compounds degrade to products of NO and a disulfide after transferring NO[9].

[3]The material contained in this chapter has been submitted to *ACS Applied Materials & Interfaces*.

Endogenous RSNOs, such as S-nitrosoalbumin, S-nitrosoglutathione, and S-nitrosocysteine, are present throughout the body and in high concentrations in circulating blood[10-11]. Synthetic NO donors, such as S-nitroso-N-acetyl-D-penicillamine (SNAP) have been extensively studied as *in vivo* donors and are often used to replicate the physiological environment, *in vitro*[12]. RSNOs are also mediators of NO's cytoprotective and cytotoxic effects[6]. This class of NO donors has been previously shown to degrade through several mechanisms including; photolytic cleavage of the S-N bond, transition metal mediated decomposition, and decomposition through interactions with ascorbate[13].

Of particular interest to us is the transition metal catalyzed release of NO[14-15]. Prior research has linked both Cu^{2+} and Fe^{2+}, as well as Hg^{2+} and Ag^{+}, as initiating NO release from both endogenous and synthetic RSNOs[15-17]. In the case of the copper mediated release of NO from RSNOs, Cu^{+}, not Cu^{2+}, is responsible for the decomposition and ultimate release of NO due to a thiolate reduction[16]. Interestingly, Co^{2+}, Ni^{2+}, and Zn^{2+} were reported as being incapable of promoting NO release through RSNO decomposition[16, 18].

NO possess significant potential for therapeutic applications within the vasculature due to the presence of constantly regenerating, free RSNOs in circulation[19-21]. Endogenously circulating ions essential for normal physiological function, such as Cu^{2+}, Fe^{2+}, Mg^{2+}, and Zn^{2+}, are also present in the blood. The physiological presence of both NO donor and catalyst could result in the discovery of clinical therapeutics, interventions, and devices which make use of these naturally occurring components and further the understanding of NO's physiological roles.

The potential applications of transition metal ion based NO production from endogenous RSNOs in the treatment and resolution of clinical pathologies are vast. One such application is the fabrication of bare metal, biodegradable stents. Annually, there are over 445,000 deaths associated with coronary artery disease (CAD)[22]. CAD occurs after the formation of atherosclerotic lesions on the endothelium of coronary arteries, limiting the nutrient and oxygen supply to the heart. Coronary bare metal stent (BMS) failure rates vary between 20%–30%[22]. The common failure mechanisms for BMSs, typically made of stainless steel and nitinol[23], are attributed to in-stent thrombosis and restenosis[22, 24-25]. There is evidence to suggest that NO generation at the stent-blood interface may be effective in the prevention and resolution of thrombosis and restenosis[4, 26-27].

Many transition metals and their alloys, including magnesium and zinc, have been shown to be bioabsorbable and have undergone development as materials for BMSs[28-29]. These

metals may evolve interfacial ions and degradation products with the potential to generate a NO flux at the luminal interface of the stent from circulating endogenous donors, thereby reducing or preventing stent failure by in-stent thrombosis and restenosis.

To evaluate these ions for NO generation from RSNOs, SNAP was utilized to simulate endogenously present RSNOs in the circulating blood[30]. In addition to evaluating metal ions, wires, typical of the materials which might be implanted as BMSs, were dissolved and the resultant solutions were used to evaluate their ability to generate NO. *In vivo* images showing the biological response toward 4N zinc wires implanted into the aortic wall and lumen of rats after 6 months is presented.

6.3. Materials & Methods

6.3.1. ICP-OES Analysis

70% nitric acid (≥ 99.999% trace metals basis) and metal standards ($PtCl_2$, $ZnCl_2$, $FeCl_2$, $FeCl_3$, $MgCl_2$, $CoCl_2$, $MnCl_2$, $NiCl_2$, and $CuCl_2$) were obtained from Sigma Aldrich (St. Louis, MO) in 99.99%+ trace metals basis and/or anhydrous grades. Certificates of analysis were collected and inspected for each standard to ensure purity. Standards were made by dissolving each sample in 2% nitric acid to make 1 mM analytical standards of each metal ion.

Wire samples of platinum (99.998% pure), zinc (99.99% pure), magnesium (99.9%+ pure), 4N iron (99.99%+ pure), and American Iron and Steel Institute (AISI) 316L stainless steel (Fe/Cr18/Ni10/Mo3) were obtained from Goodfellow Corporation (Coraopolis, PA). All samples had a diameter of 250 μm. Wire samples were cut to equal lengths (approx. 5 mm) and their masses were recorded before being placed into 10 mL of 2% nitric acid for 5 days to dissolve. Wires that did not fully dissolve after 5 days (platinum and 316L stainless steel) were removed from the solution, dried, and weighed to determine the mass lost while in solution. 5 mL of each sample was sent for analysis by inductively coupled plasma-optical emission spectrometry (ICP-OES) to Origin Analytical Inc. (Houston, TX). Origin Analytical processed all samples prior to analysis by diluting each by 10% in 5% aqua regia.

6.3.2. Preparation of S-nitroso-N-acetyl-D-penicillamine (SNAP)

SNAP was synthesized according to the procedure of Field, et. al[31]. N-acetyl-D-penicillamine (NAP), methanol, and fuming hydrochloric acid (37%) were obtained from Sigma-Aldrich (St. Louis, MO). Sulfuric acid (95.0–98.0%) was obtained from EMD Chemicals (Gibbstown, NJ). Sodium nitrite (99.999% trace metals basis) was acquired from Alfa Aesar (Ward Hill, MA).

To prepare SNAP crystals, 1000 mg of N-acetyl-D-penicillamine were dissolved in 25 mL of methanol and sonicated. Once dissolved, 15 mL of 1M HCl and 500 µL concentrated H_2SO_4 were added. Then, 724.5 mg of sodium nitrite was added to this solution and the solution was mixed until all solids had dissolved. The solution was allowed to react for one hour, developing a darkened, green color. The solution was then cooled in an ice bath for 45 minutes. All solvents were then removed by rotary evaporation, yielding a dark green, crystalline product. The crystals were ice cooled for 30 minutes and isolated by vacuum filtration in deionized water, followed by 30 minutes under vacuum to ensure all solvents had been eliminated.

6.3.3. Sample Preparation for Nitric Oxide Release Experiments

Phosphate buffered saline (PBS), dibasic sodium phosphate (Na_2HPO_4), LC-MS Ultra Chromasolv water, and hydrochloric acid (99.999% trace metals basis) were obtained from Sigma Aldrich (St. Louis, MO). Sodium chloride (NaCl) was obtained from Macron Chemicals (Center Valley, PA). Potassium chloride (KCl) was sourced from EMD Chemicals (Gibbstown, NJ). Chelex 100 resin (sodium form) was obtained from Bio-Rad Laboratories (Hercules, CA).

1 mM metal standards were made from the same stock salts as those sent for ICP-OES analysis using 10 mM PBS (138 mM NaCl; 2.7 mM KCl) made with LC-MS Ultra Chromasolv water and treated with Chelex 100 resin to remove metal impurities. The pH of the resulting solution was adjusted to 7.4 through the dropwise addition of 1M HCl as measured by an electrochemical pH probe (Symphony SB80PI; VWR; Radnor, PA). Similarly, a 1 mM SNAP solution was prepared using the 10 mM PBS for the ensuing NO release experiments. SNAP solutions were freshly made every 2 hours during the experiments.

Wire samples were used as prepared from the ICP-OES analysis to facilitate dissolution of the solid wire samples. A 100 mM PBS solution (138 mM NaCl; 2.7 mM KCl) made in LC-MS Ultra Chromasolv water was prepared and treated with Chelex 100 resin. The pH of the resultant buffer was adjusted to 7.4 through a dropwise addition of 1M HCl as measured by an electrochemical pH probe (Symphony SB80PI; VWR; Radnor, PA). A 1 mM SNAP solution was prepared using this 100 mM phosphate buffer for use in the wire sample NO release experiments. SNAP solutions were freshly made every 2 hours during the experiments.

6.3.4. Nitric Oxide Release

The potential of the metal standards and dissolved wire samples to release NO were evaluated by measuring the NO generated from 2 mL of 1 mM SNAP solution when 100

μL of either the standards or samples were injected. The final concentration of SNAP used in the experiments was 2.73 mM, and the concentration of the metal standards was 90.9 μM. The final pH of the metal standards was 7.4, while the wire samples had a final pH ranging between 6.2–6.9. To measure NO release by chemiluminescence, a Siever's 280i Nitric Oxide Analyzer (NOA) (Boulder, CO) was used to collect the NO release data. Quartz sample cells were connected to the NOA, while ambient air was swept through the sample cell to carry generated NO to the reaction chamber. A stir bar was added to the sample cell to agitate the solution. All experiments were conducted with the sample cell protected from ambient light. During experiments, SNAP was allowed to equilibrate for 2 minutes to obtain a representative baseline prior to addition of the metal ion standard/sample. 100 μL of the standard or sample was injected at 2 minutes using a Hamilton glass syringe (Reno, NV) through a septum, and sample data was collected for a further 8 minutes. After 8 minutes, 100 μL of 1 mM $CuCl_2$ was injected as a positive control. Metal ion standards were tested in triplicate (n = 3), while metal wire samples had four replicates (n = 4) evaluated.

6.3.5. Preliminary Platinum & Zinc Wire In Vivo Studies

Pure platinum (99.998%) and 4N zinc (99.99%+) wire with diameters of 250 μm were obtained from Goodfellow Corporation (Coraopolis, PA). Absolute ethanol was obtained from Pharmco Aaper (Brookfield, CT). Adult Sprague-Dawley rats were used for all *in vivo* experiments (Harlan Laboratories; Indianapolis, IN).

All animal work was approved by Michigan Technological University's Internal Animal Care and Use Committee (IACUC; #L0182). The surgical procedure has been previously published[32]. 4 mm (2 hours) and 10 mm (6 months) lengths of zinc wire were cut prior to implantation and stored in 70% ethanol for 30 minutes until use. Rats were anesthetized with 2.1% inhaled isoflurane in oxygen gas. One subset of samples was implanted into the abdominal aorta wall, while another was implanted into the blood contacting lumen. The wires were carefully pushed through the adventitial layer of the abdominal aortic tissue and advanced within the arterial wall along the full length of the specimen. Platinum and zinc wires were implanted for 2 hours to assess early stage thrombus formation. Zinc wires were implanted for 6 months in both the arterial wall and lumen to assess long term performance, *in vivo*.

Animals were sacrificed at 2 hour and 6 month end points by increasing the inhaled isoflurane concentration from 2.1% to 5% after the animals were fully anesthetized. The diaphragms were punctured, and the hearts were removed to ensure death.

Platinum and zinc samples collected at the 2 hour time point were carefully excised with

a transverse arterial incision to ensure that the neotissue formed on the wires was undisturbed. Samples were dehydrated in a graded ethanol series and mounted on conductive carbon tape. Samples were coated with 5 nm of Pt/Pd with a Hummer 6.2 sputter coater (Anatech, Ltd.; Denver, NC). Samples were stored in a desiccator prior to imaging. Imaging was performed on a Hitachi S4700 field emission scanning electron microscope (5kV accelerating voltage, 10 μA beam current; Tokyo, Japan).

The implant sites of the 6 month zinc samples were isolated and the abdominal aortas containing the entire specimen were excised. Samples were placed into Polyfreeze freezing medium (Sigma-Aldrich; St. Louis, MO), snap frozen in liquid nitrogen, and stored at −80 °C until cryosectioning. 8 μm sections were collected on Histobond slides (VWR; Radnor, PA) with a Microm HM 550 (Microm International GmbH; Walldorf, Germany).

Hematoxylin & Eosin staining was performed on the 6 month zinc wire samples to assess the performance of the implanted specimens. All components were purchased from Sigma Aldrich (St. Louis, MO) with the exception of the Gill's no. 3, purchased from Leica Biosystems (Buffalo Grove, IL). Sections were fixed immediately prior to cryosectioning by immersing them in -20°C chilled ethanol for 60 seconds. Samples were washed in three changes of PBS (pH 7.4) for 5 minutes each, followed by a wash in deionized water for 5 minutes. Sections were then placed in Gill's no. 3 for 5 minutes. The slides were then differentiated by dipping into dilute hydrochloric acid (pH 2). Once differentiated, the slides were placed into deionized water for 1 minute. The blued samples were placed into two changes of 95% ethanol for 5 minutes each. Eosin Y (0.25%) counterstained the sections for 30 seconds, prior to being dehydrated in absolute ethanol and cleared in xylene substitute. The samples were then mounted and imaged on an Olympus BX-51 microscope (Waltham, MA).

6.4. Results

6.4.1. ICP-OES Analysis of Metal Standards and Wire Samples

ICP-OES results coincide with the reported data from the certificates of analysis for all standards. As shown in Table 6.1, all 1 mM wire standards contained only their parent ion in significant quantities. The metal ion composition of the wire samples are shown in Table 6.2. Analysis showed zinc, iron, and magnesium solutions contained only their parent ion present in solution. Platinum did not show any significantly detectable platinum ion in solution. 316L stainless steel, though composed of iron, cobalt, nickel, and manganese, showed only trace quantities of iron in solution.

Table 6.1. ICP-OES analysis of metal ion standards. Table 6.1 summarizes the ICP-OES results for the metal ion standards. Analytical standards were made as 1 mM solutions in 2% nitric acid. Values are reported in ppm (mg/kg). A blank cell indicates that no data was reported for the method.

	$PtCl_2$	$ZnCl_2$	$MgCl_2$	$FeCl_3$	$CoCl_2$	$NiCl_2$	$MnCl_2$	$CuCl_2$
Pt	153							
Zn	< 0.100	52.6	< 0.100	< 0.100	< 0.100	0.209	< 0.100	< 0.100
Mg	< 0.100	< 0.100	20.4	< 0.100	< 0.100	< 0.100	< 0.100	< 0.100
Fe				50.6				
Co					4.47			
Ni						45.3		
Mn							4.56	
Cu								47.9

Table 6.2. ICP-OES analysis of metal wire samples. Table 6.2 summarizes the ICP-OES results for the metal wire samples. Values are reported in ppm (mg/kg). A blank cell indicates that no data was reported for the method.

	Platinum	Zinc	Magnesium	Iron	316L Stainless Steel
Pt					
Zn		222.5	< 0.100	< 0.100	
Mg			55.15		
Fe	< 0.100			243.3	< 0.100
Co					
Ni					
Mn					
Cu					

6.4.2. Nitric Oxide Release in Metal Standards

Figure 6.1 shows the NO generated from the SNAP solution under physiological pH and ionic strength from Pt^{2+}, Fe^{2+}, Fe^{3+}, Mg^{2+}, Zn^{2+}, Mn^{2+}, Co^{2+}, Ni^{2+}, and Cu^{2+} via chemiluminescence. Figure 6.2 shows a magnified view with the copper standard omitted. Figure 6.3 shows Figure 6.2 plotted with standard deviations. In this work, a level of NO release 150% of the baseline value will be established as significant. The two ions reported in literature to generate NO from RSNOs, Cu^{2+} and Fe^{2+}, both initiated NO release upon injection into the SNAP solution. Co^{2+}, Ni^{2+}, and Zn^{2+} also initiated release of NO from RSNOs. Pt^{2+}, Fe^{3+}, Mg^{2+}, and Mn^{2+} did not demonstrate any significant release of NO.

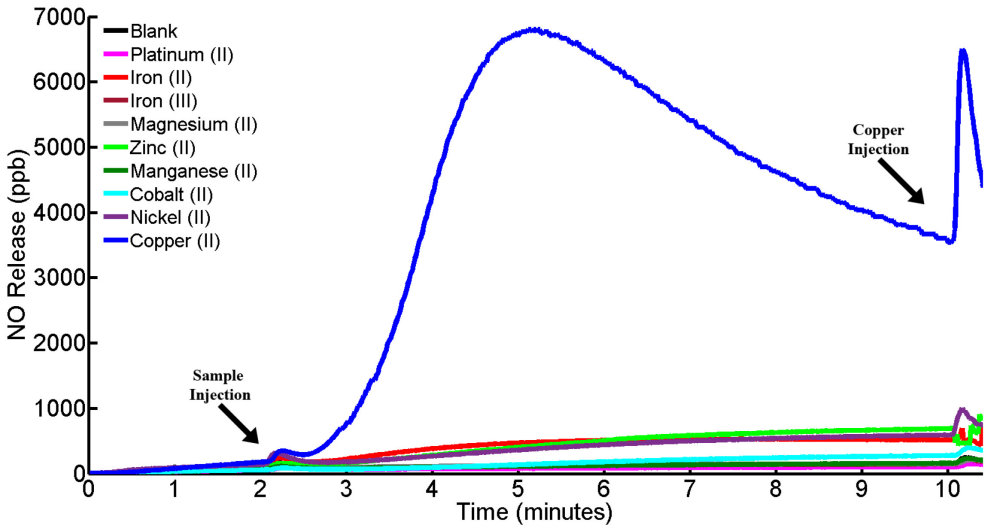

Figure 6.1. S-nitrosothiol decomposition by metal ion standards. Metal ion standards were evaluated for their ability to evolve NO from RSNOs. Copper(II), (blue), is known to cause RSNO decomposition and is shown here as a positive control. Iron(II) (red) has been previously reported to cause NO generation from RSNOs. Nickel(II) (purple) and zinc(II) (light green) demonstrated NO release at levels similar to those of Iron(II). Cobalt(II) (cyan) is also observed to be elevated above the baseline. Notably, iron(III) (burgundy) and magnesium(II) (gray) did generate NO release over the baseline. As expected, platinum(II) (pink) was also inactive. All samples were injected at 2 minutes. Copper(II) was injected after 10 minutes to demonstrate the presence of RSNO in the sample. The pH of the solution was 7.4. The plots represent n = 3 averaged values per sample. This data is available in the supporting information related to this article with standard deviations plotted for each sample. Legend: Blank-black; Platinum(II)-pink; Iron(II)-red; Iron(III)-burgundy; Magnesium(II)-gray; Zinc(II)-light green; Manganese(II)-dark green; Cobalt(II)-cyan; Nickel(II)-purple; Copper(II)-blue.

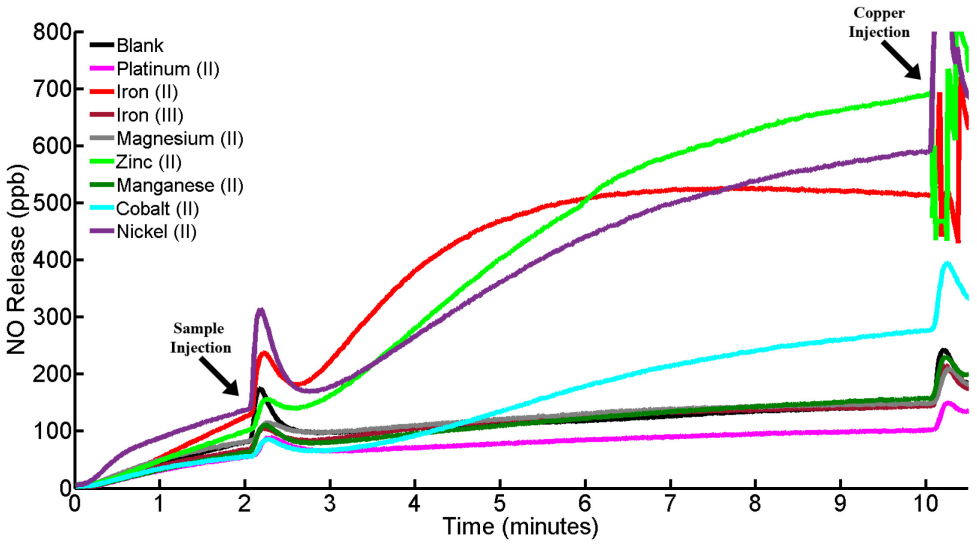

Figure 6.2. Decomposition of S-nitrosothiols by metal ion standards. Figure 6.2 shows an enlarged view of figure 6.1 to enhance the detail of the ions of interest. Copper(II) has been omitted from this figure for simplicity. In this figure, iron(II), nickel(II), and zinc(II) are seen to be more clearly separated than in the previous figure. All samples were injected at 2 minutes. Copper(II) was injected after 10 minutes to demonstrate the presence of RSNO in the samples. The plots represent n = 3 averaged values for each sample. This data is available in the supporting information related to this article with standard deviations plotted per sample. Legend: Blank-black; Platinum(II)-pink; Iron(II)-red; Iron(III)-burgundy; Magnesium(II)-gray; Zinc(II)-light green; Manganese(II)-dark green; Cobalt(II)-cyan; Nickel(II)-purple.

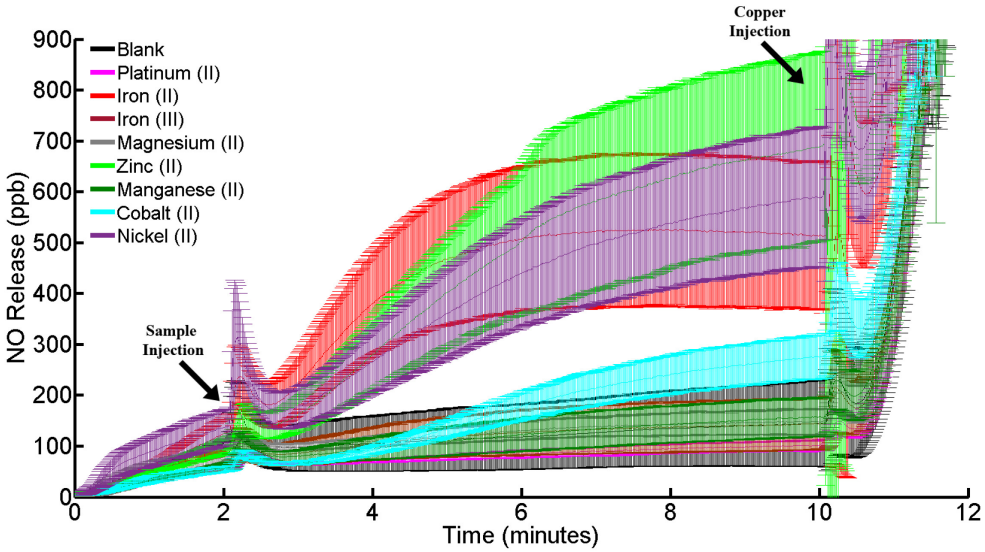

Figure 6.3. Decomposition of S-nitrosothiols by metal ion standards - statistics. Figure 6.3 shows figure 6.2 with standard deviations plotted for each sample. n = 3 per sample. Copper(II) has been omitted from this figure. All samples were injected at 2 minutes. Copper(II) was injected after 10 minutes to demonstrate the presence of RSNO in the sample. The plots represent n = 3 averaged values per sample. Legend: Blank-black; Platinum(II)-pink; Iron(II)-red; Iron(III)-burgundy;

Magnesium(II)-gray; Zinc(II)-light green; Manganese(II)-dark green; Cobalt(II)-cyan; Nickel(II)-purple.

6.4.3. Nitric Oxide Release in Metal Wire Samples

The NO generation from solutions of the metal wire samples can be seen in Figure 6.4. The same figure with plotted standard deviations is represented in Figure 6.5. Again, NO release exceeding 150% of the baseline value was deemed to be significant. Zinc and 316L stainless steel wires demonstrated elevated release of NO over the 150% threshold. Magnesium, iron and platinum generated NO from SNAP at levels higher than the baseline, but not above the 150% threshold.

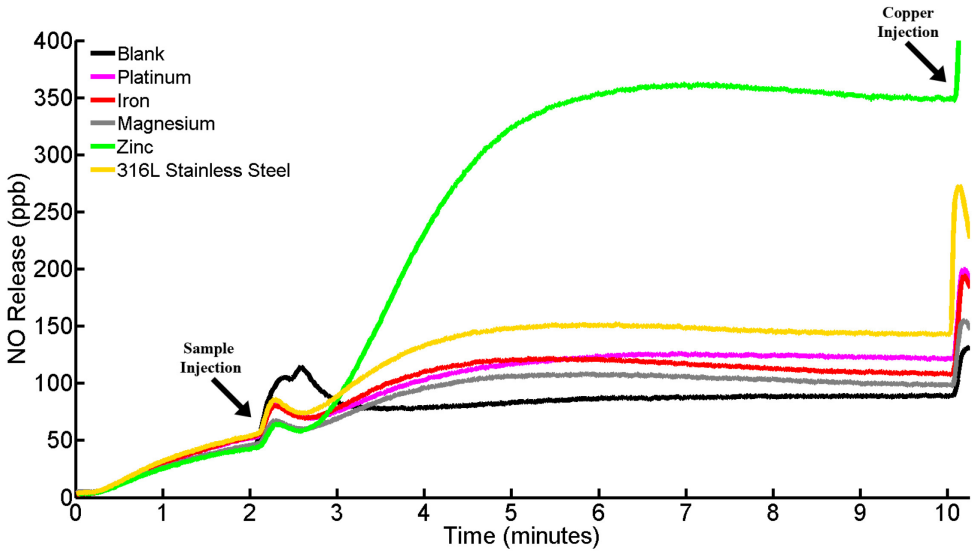

Figure 6.4. Decomposition of S-nitrosothiols by metal wire samples. Metal wires were evaluated in a similar manner as their respective metal standards. As observed in the standards, the zinc wire (light green) used here shows elevated release over the 2% nitric acid blank. 316L stainless steel (yellow) is also elevated. Due to the acid used to dissolve the wires, the pH of the samples varied between 6.20 and 6.90. All samples were injected at 2 minutes. Copper(II) was injected after 10 minutes to demonstrate the presence of RSNO in the sample. The plots represent n = 4 averaged values per sample. This data is available in the supporting information related to this article with standard deviations plotted for each sample. Legend: Blank-black; Platinum-pink; Iron-red; Magnesium-gray; Zinc-light green; 316L stainless steel-yellow.

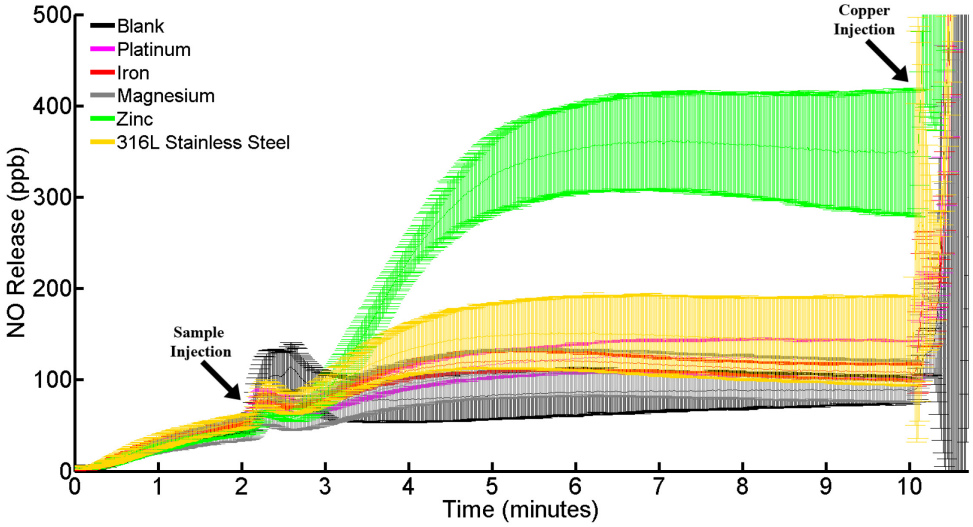

Figure 6.5. Decomposition of S-nitrosothiols by metal wire samples - statistics. Figure 6.5 shows figure 6.4 plotted with standard deviations for each sample. n = 4 per sample. All samples were injected at 2 minutes. Copper(II) was injected after 10 minutes to demonstrate the presence of RSNO in the sample. The plots represent n = 4 averaged values per sample. Legend: Blank-black; Platinum-pink; Iron-red; Magnesium-gray; Zinc-light green; 316L stainless steel-yellow.

6.4.4. In Vivo Zinc & Platinum Wire Implants

In vivo implantations of zinc and platinum wires into the bloodstream are represented in Figure 6.6. As can be seen in Figure 6.6A, implanted platinum wires showed a significant thrombotic response with full occlusion of the implant surface. Platinum wires demonstrated extensive cellular and fibrin coverage. In contrast, the implanted zinc wires (Figure 6.6B) showed minimal cellular deposition leaving the majority of the implant surface free of material. In addition, individual cells can be identified on the zinc wire samples whereas no individual cells were discernable on the platinum wire samples.

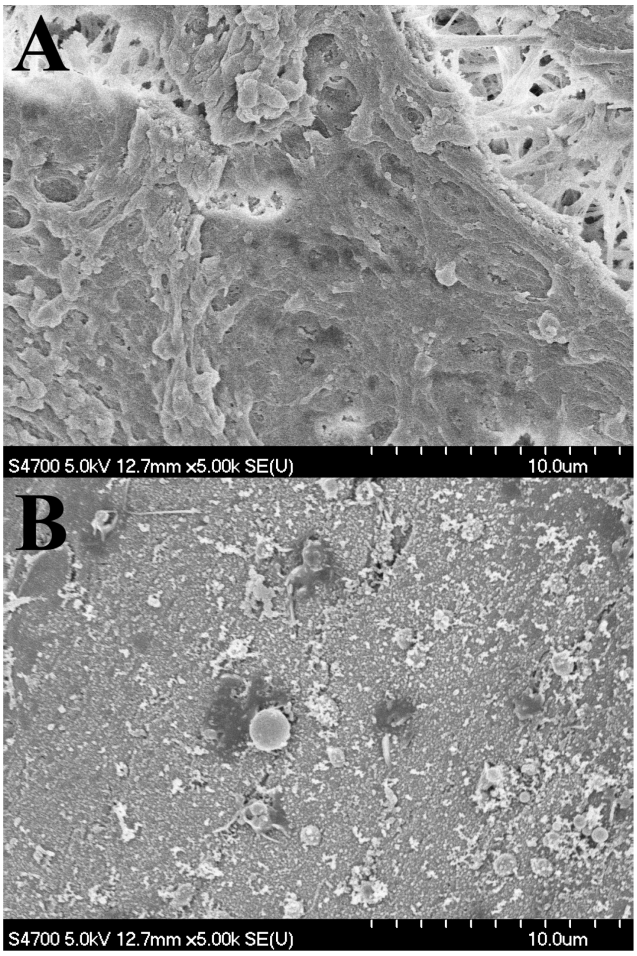

Figure 6.6. Images of intraluminal platinum and zinc wire implants. Figure 6.6 shows representative images of the relative differences in thrombotic response between platinum (A) and zinc (B) wires implanted into the bloodstream of a rat.

Figure 6.7 shows a typical result of the 6 month zinc wire luminal implant study. The green asterisks denote the corrosion layer in Figure 6.7A and the displaced wire in Figure 6.7B. The wire implanted into the adventitia of the artery (Figure 6.7A) shows signs of substantial encapsulation and increased cellular density. Necrotizing, apoptotic cells and nucleic disparity is evident. Minimal cell penetration into the dense corrosion layer characterizes the sample shown in Figure 6.7A.

The intra-luminal implant (Figure 6.7B), exposed to flowing blood throughout the trial, shows little thrombus with an intact neo-endothelium (red arrows). The corrosion layer[32], denoted by yellow arrows in Figure 6.7B, demonstrates a loose, low density structure with signs of cellular infiltration and significant extracellular matrix remodeling. The corrosion layer consists of a thin, external calcium/phosphate layer while internally a

mixture of zinc oxide and zinc carbonate dominate the environment[32]. The yellow asterisk highlights the intact media of the artery.

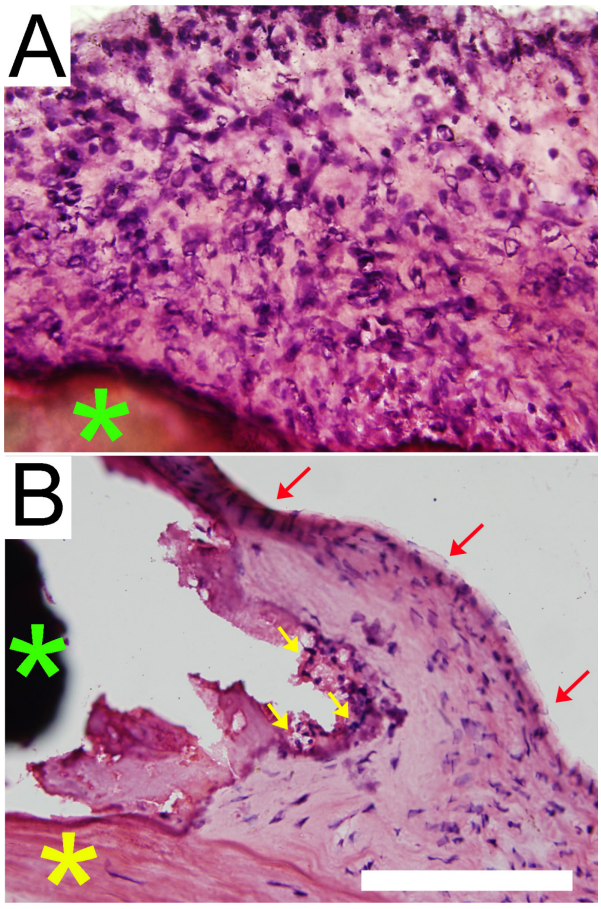

Figure 6.7. Histology of intraluminal zinc wire implants. This figure shows a representative result for 4N zinc wires implanted into the wall (A) and the luminal space (B) of a rat abdominal aorta. The green stars identify the corrosion layer (A) and wire (B). The yellow star identifies the medial layer of the native artery. The yellow arrows in B identify mononuclear cells within the corrosion layer. Red arrows denote neo-endothelium. The open space beyond the red arrows is the arterial lumen. The open space between the wire and corrosion layer in B is an artifact of sectioning whereby the wire was displaced from the corrosion layer. The scale bar represents 100 μm.

6.5. Discussion

The combination of manufacturer certificates of analysis and ICP-OES analysis of prepared solutions indicates that all standards, with the exception of $NiCl_2$, used in these experiments were free of any other interfering ions. $NiCl_2$ showed trace amounts of Zn, though the level was more than two orders of magnitude lower than the corresponding $ZnCl_2$ sample. Importantly, Cu^{2+} and Fe^{2+}, known to be strong catalysts of NO generation from RSNOs, were not present except in their respective ion/wire samples. Wire samples

were also free from undesirable transition metal ions. The solutions of the platinum and stainless steel wires showed that none of the dissolved ions tested (Pt^{2+}, Fe^{2+}, Fe^{3+}, Mg^{2+}, Zn^{2+}, Mn^{2+}, Co^{2+}, Ni^{2+}, and Cu^{2+}) were present. Chelex 100 resin treatment of the phosphate buffers removed potential transition metal ion contaminates, such as extraneous Cu^{2+} and Fe^{2+}. Care was taken to avoid contamination at all points in the experimental work to eliminate NO generation from ions other than the primary transition metal present in the specific test solution.

Current theories speculate that NO is carried by endogenous RSNOs and is delivered through trans-nitrosation reactions[13]. However, the mechanism of this process and the role transition metals play is not currently well understood[9, 33].

Identification of Co^{2+}, Ni^{2+}, and Zn^{2+} as reactive ions capable of generating NO from RSNOs is an important step in harnessing NO for investigations into its biological relevance, but also for clinical applications and therapies. Elucidating a mechanism of action for the transition metal catalyzed release of NO from RSNOs would represent a significant advancement in the overall understanding of the physiological transport, behavior, and mechanisms responsible for NO's inherent biological activity.

Not previously reported to induce NO release, Zn^{2+} has the potential to alter strategies in the fabrication of metal implants due to its proclivity to generate NO from RSNOs, demonstrated in both zinc ion standards and zinc wire samples. NO demonstrates great potential in the treatment and resolution of many clinical outcomes associated with thrombosis, intimal hyperplasia, and restenosis through control of platelet aggregation and inhibition of smooth muscle cell proliferation[4, 26-27].

Though some of the ions evaluated here demonstrated release of NO from RSNOs, it is important to note that on average, they were one order of magnitude lower than those of Cu^{2+}. Though significantly lower, this reduced level of NO release from RSNOs by alternative transition metals could be advantageous *in vivo* when applied to clinical devices. Estimated values for endogenous NO flux from intact, healthy endothelium is reported to be $0.5–4x10^{-10}$ $mols \cdot cm^{-2} \cdot sec^{-1}$ as being the requisite therapeutic flux for endothelial cells[34]. In the potential application presented here, the endothelial lining of the vascular lumen is in direct contact with the stent following deployment. This represents an ideal circumstance in which the degrading surface releases metal ions directly into a replenishing supply of endogenous RSNOs.

We have demonstrated that zinc, a material currently undergoing development for use in biodegradable bare metal stents[32], is capable of eliciting NO from RSNOs. Coupled with

its favorable degradation characteristics[32], zinc has significant potential in this application. Though the available physiological concentration of RSNOs in the body is likely significantly reduced from the levels used above, the release of physiologically relevant NO from the interaction between Zn^{2+} and endogenous RSNOs is possible.

The platinum and zinc wire samples shown in Figure 6.6 exhibit vastly different thrombotic responses after only 2 hours of *in vivo* implantation into the flowing blood of rats. In the case of the platinum wires, extensive thrombus deposition was prevalent, completely occluding the surface of the wire. In general, the platinum wire samples exhibited this active coagulation response resulting in complete coverage including an observable fibrin mesh, cellular adhesion, and complete coating of the surface. Alternatively, the zinc samples presented a less extensively covered surface and a response exhibiting fewer signs of highly activated intrinsic coagulation. Based on the results of this work, a later term study was conducted on 4N zinc wires to assess their long term performance when exposed to flowing blood and implanted in the vascular wall of rats for 6 months.

The 6 month implanted zinc wires shown in Figure 6.7 demonstrate remarkable differences between the biological response observed in the vascular wall and in flowing blood. Figure 6.7A presents a picture of chronic inflammation, apoptosis, and necrosis, with little if any resolution of the initial insult. Figure 6.7B appears to consist of mainly healthy tissue, with active removal of the degradation products and a reformed endothelium with significant progress towards resolution. As a potential candidate material for bare metal stent struts, endogenous production of NO from zinc would be a beneficial attribute for the control over the immune response.

The differences in the biological response observed during the *in vivo* studies are potentially attributable to low level NO generation from endogenous RSNOs present in the blood, with supporting data for this theory available from the *in vitro* results. It is important to note that the kinetics of diffusion for the circulating endogenous RSNOs attributed to these results are location dependent. Rates of RSNO replenishment within circulating blood will be more rapid than in the vessel wall, resulting in a higher level of NO generation within the flowing blood[16, 35-36]. Further studies will be required to ascertain whether NO is solely responsible for the observed results.

6.6. Conclusion

This work demonstrates the potential for alternative transition metal ions; Co^{2+}, Ni^{2+}, and Zn^{2+}, to generate NO from endogenous RSNOs under physiological conditions. Fe^{3+}, Mg^{2+}, Mn^{2+}, and Pt^{2+} did not demonstrate significant release. The wire samples represent

a clinically relevant application of this novel information for applications including bioabsorbable metal stents, device coatings, and targeted NO therapies. While this study investigated some of the more common transition metals, many more remain to be evaluated.

While the *in vivo* data presented highlights one possible application and potential explanation for the observed results, a multitude of applications exist for biocompatible metal ions capable of generating NO from endogenous sources. In these capacities, NO generation at or near an implant surface can potentially maintain control over device failure through common rejection pathways such as thrombosis, chronic inflammation, intimal hyperplasia, and restenosis.

6.7. Acknowledgements

This work was funded by the National Science Foundation - Division of Materials Research Grant number 1410192 and the National Institutes of Health grant R15HL113954. C.W.M. was supported by the National Institutes of Health grant R15HL113954.

6.8. References

1. Marsh, N.; Marsh, A. A Short History of Nitroglycerine and Nitric Oxide in Pharmacology and Physiology. *Clinical and Experimental Pharmacology and Physiology* **2000,** *27* (4), 313-319.
2. Lahdenranta, J.; Hagendoorn, J.; Padera, T. P.; Hoshida, T.; Nelson, G.; Kashiwagi, S.; Jain, R. K.; Fukumura, D. Endothelial Nitric Oxide Synthase Mediates Lymphangiogenesis and Lymphatic Metastasis. *Cancer research* **2009,** *69* (7), 2801-2808.
3. Moncada, S.; Higgs, E. Molecular Mechanisms and Therapeutic Strategies Related to Nitric Oxide. *The FASEB Journal* **1995,** *9* (13), 1319-1330.
4. Carpenter, A. W.; Schoenfisch, M. H. Nitric Oxide Release: Part Ii. Therapeutic Applications. *Chem Soc Rev* **2012,** *41* (10), 3742-3752.
5. Gkaliagkousi, E.; Ferro, A. Nitric Oxide Signalling in the Regulation of Cardiovascular and Platelet Function. *Frontiers in bioscience (Landmark edition)* **2010,** *16*, 1873-1897.
6. Burke, A. J.; Sullivan, F. J.; Giles, F. J.; Glynn, S. A. The Yin and Yang of Nitric Oxide in Cancer Progression. *Carcinogenesis* **2013,** *34* (3), 503-512.
7. Ignarro, L. J., *Nitric Oxide: Biology and Pathobiology*. Academic press: **2000**.
8. Al-Sa'doni, H.; Ferro, A. S-Nitrosothiols: A Class of Nitric Oxide-Donor Drugs. *Clinical science* **2000,** *98* (5), 507-520.
9. Singh, R. J.; Hogg, N.; Joseph, J.; Kalyanaraman, B. Mechanism of Nitric Oxide Release from S-Nitrosothiols. *Journal of Biological Chemistry* **1996,** *271* (31), 18596-18603.
10. Nagababu, E.; Rifkind, J. M. Routes for Formation of S-Nitrosothiols in Blood. *Cell biochemistry and biophysics* **2013,** *67* (2), 385-398.
11. Guzik, T.; Korbut, R.; Adamek-Guzik, T. Nitric Oxide and Superoxide in Inflammation. *Journal of physiology and pharmacology* **2003,** *54*, 469-487.
12. Nisoli, E.; Clementi, E.; Paolucci, C.; Cozzi, V.; Tonello, C.; Sciorati, C.; Bracale, R.; Valerio, A.; Francolini, M.; Moncada, S. Mitochondrial Biogenesis in Mammals: The Role of Endogenous Nitric Oxide. *Science* **2003,** *299* (5608), 896-899.
13. Broniowska, K. A.; Diers, A. R.; Hogg, N. S-Nitrosoglutathione. *Biochim Biophys Acta* **2013,** *1830* (5), 3173-3181.
14. Feelisch, M.; Stamler, J. S., *Methods in Nitric Oxide Research*. John Wiley & Sons Ltd.: **1996**; p 712.
15. Lyn H áWilliams, D. Direct No Group Transfer from S-Nitrosothiols to Iron Centres. *Chemical Communications* **2001,** (18), 1732-1733.
16. Williams, D. L. H. The Chemistry of S-Nitrosothiols. *Accounts of Chemical Research* **1999,** *32* (10), 869-876.
17. Lyn H áWilliams, D. Identification of Cu+ as the Effective Reagent in Nitric Oxide Formation from S-Nitrosothiols (Rsno). *Journal of the Chemical Society, Perkin Transactions 2* **1996,** (4), 481-487.
18. Naghavi, N.; de Mel, A.; Alavijeh, O. S.; Cousins, B. G.; Seifalian, A. M. Nitric Oxide Donors for Cardiovascular Implant Applications. *Small* **2013,** *9* (1), 22-35.
19. Foster, M. W.; Pawloski, J. R.; Singel, D. J.; Stamler, J. S. Role of Circulating S-Nitrosothiols in Control of Blood Pressure. *Hypertension* **2005,** *45* (1), 15-17.

20. Giustarini, D.; Milzani, A.; Colombo, R.; Dalle-Donne, I.; Rossi, R. Nitric Oxide and S-Nitrosothiols in Human Blood. *Clinica Chimica Acta* **2003,** *330* (1-2), 85-98.
21. Hess, D. T.; Matsumoto, A.; Kim, S.-O.; Marshall, H. E.; Stamler, J. S. Protein S-Nitrosylation: Purview and Parameters. *Nature Reviews Molecular Cell Biology* **2005,** *6* (2), 150-166.
22. Martin, D. M.; Boyle, F. J. Drug-Eluting Stents for Coronary Artery Disease: A Review. *Medical engineering & physics* **2011,** *33* (2), 148-163.
23. Moravej, M.; Mantovani, D. Biodegradable Metals for Cardiovascular Stent Application: Interests and New Opportunities. *International journal of molecular sciences* **2011,** *12* (7), 4250-4270.
24. Brilakis, E. S.; Patel, V. G.; Banerjee, S. Medical Management after Coronary Stent Implantation: A Review. *JAMA* **2013,** *310* (2), 189-198.
25. Palmerini, T.; Biondi-Zoccai, G.; Della Riva, D.; Stettler, C.; Sangiorgi, D.; D'Ascenzo, F.; Kimura, T.; Briguori, C.; Sabatè, M.; Kim, H.-S. Stent Thrombosis with Drug-Eluting and Bare-Metal Stents: Evidence from a Comprehensive Network Meta-Analysis. *The Lancet* **2012,** *379* (9824), 1393-1402.
26. Fleser, P. S.; Nuthakki, V. K.; Malinzak, L. E.; Callahan, R. E.; Seymour, M. L.; Reynolds, M. M.; Merz, S. I.; Meyerhoff, M. E.; Bendick, P. J.; Zelenock, G. B.; Shanley, C. J. Nitric Oxide-Releasing Biopolymers Inhibit Thrombus Formation in a Sheep Model of Arteriovenous Bridge Grafts. *J Vasc Surg* **2004,** *40* (4), 803-811.
27. Moncada, S.; Higgs, E. A. The Discovery of Nitric Oxide and Its Role in Vascular Biology. *Br J Pharmacol* **2006,** *147 Suppl 1*, S193-201.
28. Hermawan, H.; Dubé, D.; Mantovani, D. Developments in Metallic Biodegradable Stents. *Acta Biomaterialia* **2010,** *6* (5), 1693-1697.
29. Gu, X.-N.; Zheng, Y.-F. A Review on Magnesium Alloys as Biodegradable Materials. *Frontiers of Materials Science in China* **2010,** *4* (2), 111-115.
30. Frost, M. C.; Meyerhoff, M. E. Synthesis, Characterization, and Controlled Nitric Oxide Release from S-Nitrosothiol-Derivatized Fumed Silica Polymer Filler Particles. *Journal of Biomedical Materials Research Part A* **2005,** *72* (4), 409-419.
31. Field, L.; Dilts, R. V.; Ravichandran, R.; Lenhert, P. G.; Carnahan, G. E. An Unusually Stable Thionitrite from N-Acetyl-D,L-Penicillamine; X-Ray Crystal and Molecular Structure of 2-(Acetylamino)-2-Carboxy-1,1-Dimethylethyl Thionitrite. *Journal of the Chemical Society, Chemical Communications* **1978,** (6), 249.
32. Bowen, P. K.; Drelich, J.; Goldman, J. Zinc Exhibits Ideal Physiological Corrosion Behavior for Bioabsorbable Stents. *Advanced Materials* **2013,** *25* (18), 2577-2582.
33. McAninly, J.; Williams, D. L. H.; Askew, S. C.; Butler, A. R.; Russell, C. Metal Ion Catalysis in Nitrosothiol (Rsno) Decomposition. *Journal of the Chemical Society, Chemical Communications* **1993,** (23), 1758.
34. Vaughn, M. W.; Kuo, L.; Liao, J. C. Estimation of Nitric Oxide Production and Reaction Rates in Tissue by Use of a Mathematical Model. *Am J Physiol-Heart C* **1998,** *274* (6), H2163-H2176.

35. Rassaf, T.; Feelisch, M.; Kelm, M. Circulating No Pool: Assessment of Nitrite and Nitroso Species in Blood and Tissues. *Free Radic Biol Med* **2004,** *36* (4), 413-422.
36. Rassaf, T.; Preik, M.; Kleinbongard, P.; Lauer, T.; Heiß, C.; Strauer, B.-E.; Feelisch, M.; Kelm, M. Evidence for in Vivo Transport of Bioactive Nitric Oxide in Human Plasma. *Journal of Clinical Investigation* **2002,** *109* (9), 1241-1248.

Chapter 7: Summary and Future Directions

7.1. Conclusions and Summary of Findings

The work presented within this document is intended to approach the problems associated with current small diameter vascular grafts through engineering approaches by fabricating hybrid constructs with targeted components. This methodology provides flexibility in tailoring aspects of the mechanical properties to better match the native architecture. Additionally, a hybrid engineered construct gleans benefits of both the native elastin, with the ability to easily incorporate drug releasing mechanisms in close proximity.

The development and production of thrombotic and neointimal hyperplasia resistant small diameter vascular grafts has been outlined in chapter 4. These constructs were fabricated by exploiting the non-thrombogenic properties of native elastin matrices as blood contacting surfaces. The results indicated promising performance of the blood contacting layer, with minimal thrombosis evident. Additionally, mechanical testing of the graft revealed an elastic moduli which closely matched that of a native coronary artery. Burst pressure testing of the construct also provided ample evidence for the graft's suitability, exceeding the physiological requirements. The grafts demonstrated stability under ambient conditions for over 6 months when stored at room temperature, furthering their potential for clinical success.

Chapter 5 delved into the synthesis and performance of a novel macrocyclic NO donor, SNAP-cyclam, which demonstrated excellent stability and controlled release of NO through several mechanisms. The compound maintains a straight forward synthesis route using a macrocyclic base, which is in current use as a cancer therapeutic and drug delivery agent. During development, SNAP-cyclam revealed a novel reaction mechanism which could result in the discovery of a multitude of novel NO donors, all with potential research and clinical relevancy. Coupled with a novel release mechanism, SNAP-cyclam is poised for a significant impact on the NO community.

While the photolytically catalyzed release of NO from potential donors is an invaluable tool in diagnostics and research, its application in clinical practice is severely hindered in all but the most superficial applications. Chapter 6 presents data demonstrating metal catalyzed release of NO from a common NO donor, S-nitroso-N-acetyl-D-penicillamine. Previous research had indicated the efficacy of two transition metal ions, copper and iron, as being capable of metal catalyzed NO release. The data presented here indicates that additional transition metals; cobalt, nickel, and zinc, are also capable of causing RSNO decomposition and resultant NO release. Zinc is a bioabsorbable material already known

to be physiologically present and biocompatible, and its incorporation into NO releasing scaffolds may provide a route to precisely alter the NO flux generated by an implant.

7.2. Future Directions

The body of work presented thus far has led to a culmination of research which attempts to address the current shortcomings in small diameter vascular grafts; namely, thrombosis and late stage neointimal hyperplasia. In addition, this research has shown a practical route to utilize native elastin scaffolds to produce shelf stable, small diameter vascular grafts. The chapters of this document describe the three elements of a hybrid, engineered vascular construct. As the development of the individual components has been completed, the fabrication of a multi-component, hybrid engineered construct is now feasible.

This engineered graft will be constructed in a manner similar to the native artery, with an elastin derived layer comprising the intima of the vessel, providing a non-thrombogenic blood contacting surface. The media will be comprised of several alternating polymeric layers, containing either zinc or SNAP-cyclam, which provide active protection against thrombosis and neointimal hyperplasia. The adventitia of the vascular construct will provide mechanical support and be composed of an elastic polyether urethane, electrospun fiber mat.

The native elastin derived from rat thoracic aortas performed admirably, however their size and elastin content is not optimal for translation to clinical use. The use of an alternative vessel from a larger donor is necessary to more optimally match the size and properties of the intended human recipients. Ideally, this vessel would be readily available and easily isolated. Improvements on the performance of the current graft can be made through the retention of collagens in the adventitial zone, permitting better handling and mechanical characteristics. Additionally, the use of alternative donor material high in elastin, such as the porcine internal mammary artery, may significantly improve graft performance by reducing the quantity of immunogenic collagen near the luminal surface.

SNAP-cyclam, presented within chapter 5, has significant potential for use in NO based therapies and research applications, as it is highly soluble in many common organic solvents and can be readily incorporated into polymer constructs as a blended material. Preliminary work with SNAP-cyclam embedded in electrospun polycaprolactone has demonstrated promising results, *in vivo*. Further studies will be required to assess its performance. Following the same reaction scheme as SNAP-cyclam, alternative secondary amine based S-nitrosothiol donors have been produced and are awaiting evaluation.

Information gleaned from the work presented in chapter 6 presents new possibilities for the release of NO from both endogenous and synthetic RSNOs. The three identified ions are applicable to a wide range of applications: as a NO release mechanism in vascular grafts, as bare metal stents capable of generating NO from endogenous S-nitrosothiols, or as research tools to better understand the roles and relationships of NO in the physiological environment. Importantly, zinc is undergoing development as a biodegradable vascular bare metal stent material[1-6]. The newly discovered ability of zinc to elicit S-nitrosothiol decomposition provides new pathways to the prevention of thrombosis, neointimal hyperplasia, and restenosis in medical implants.

7.3. References

1. Bowen, P. K.; Drelich, J.; Goldman, J. Zinc Exhibits Ideal Physiological Corrosion Behavior for Bioabsorbable Stents. *Advanced Materials* **2013,** *25* (18), 2577-2582.
2. Bennington-Castro, J. Bio Focus: Is Zinc the Perfect Material for Bioabsorbable Stents? *MRS Bulletin* **2013,** *38* (06), 438-440.
3. Liu, X.; Sun, J.; Yang, Y.; Pu, Z.; Zheng, Y. In Vitro Investigation of Ultra-Pure Zn and Its Mini-Tube as Potential Bioabsorbable Stent Material. *Materials Letters* **2015**.
4. Debusschere, N.; De Beule, M.; Segers, P.; Verhegghe, B.; Dubruel, P. In *Modeling of Coated Biodegradable Stents*, ASME 2012 Summer Bioengineering Conference, American Society of Mechanical Engineers: **2012**; pp 65-66.
5. Durisin, M.; Weber, C.; Seitz, J.; Bach, F.; Kietzmann, M.; Schumacher, S.; Lenarz, T. The Biodegradable Magnesium Stent as an Alternative Treatment in Cases of Chronic Ventilation Disorders of the Paranasal Sinuses. *Biomedical Engineering/Biomedizinische Technik* **2013**.
6. Maeng, M.; Holm, N. R.; Thuesen, L. Deliver the Drug and Disappear: Is the Bioabsorbable Magnesium Stent Growing up or Still Shrinking? *Journal of Endovascular Therapy* **2011,** *18* (3), 416-417.

Appendix 1: Copyright Material for Chapter 2

Figure 2.1

JOHN WILEY AND SONS LICENSE TERMS AND CONDITIONS

Sep 28, 2015

This Agreement between Connor McCarthy ("You") and John Wiley and Sons ("John Wiley and Sons") consists of your license details and the terms and conditions provided by John Wiley and Sons and Copyright Clearance Center.

License Number	3717691381682
License date	Sep 28, 2015
Licensed Content Publisher	John Wiley and Sons
Licensed Content Publication	Journal of Biomedical Materials Research
Licensed Content Title	Addressing thrombogenicity in vascular graft construction
Licensed Content Author	Sandip Sarkar,Kevin M. Sales,George Hamilton,Alexander M. Seifalian
Licensed Content Date	Oct 31, 2006
Pages	9
Type of use	Dissertation/Thesis
Requestor type	University/Academic
Format	Print and electronic
Portion	Figure/table
Number of figures/tables	1
Original Wiley figure/table number(s)	Figure 2
Will you be translating?	No
Title of your thesis / dissertation	Fabrication and Design of a Three Element Hybrid Small Diameter Vascular Graft
Expected completion date	Oct 2015
Expected size (number of pages)	120
Requestor Location	Connor McCarthy 1400 Townsend Dr 309 M&M Building

	HOUGHTON, MI 49931 United States Attn: Connor McCarthy
Billing Type	Invoice
Billing Address	Connor McCarthy 1400 Townsend Dr 309 M&M Building HOUGHTON, MI 49931 United States Attn: Connor McCarthy
Total	0.00 USD

Figure 2.2

ONLINE SERVICES USAGE AGREEMENT ("TERMS OF USE")
For All Britannica Sites, Services and Applications
Advertising-Supported and Subscription, Consumer and Institutional

SECTION 1
Terms of Use for Everyone

Ownership. The content on the Services is the property of Britannica, its affiliated companies or licensors, and is protected by international copyright, patent, and trademark laws.

Advertising. Advertisements, promotions, and marketing messages may appear on the Services from time to time, unless you or your institution has a subscription-based Service. Please see our Privacy Policy for more information.

Use of Content. You may display, reproduce, print or download content on the Services only for your personal, non-commercial use. If you are a teacher, scholar or student, you may copy reasonable portions of the content for lesson plans, interactive whiteboards, reports, dissertations, presentations, school newspapers and for similar nonprofit educational purposes to the extent permitted by applicable law. In each case, however, you may not remove or alter any copyright, trademark, service mark or other proprietary notices or legends. You may not publish, distribute, retransmit, sell or provide access to the content on the Services, except as permitted under applicable law or as described in these Terms of Use. Britannica works to ensure that all the content on its Services is in compliance with applicable U.S. copyright laws. However, in the case of works on the Services authored by parties other than Britannica, you may wish to check on their copyright status before downloading them if you are in another country. You may not use data mining, robots, screen scraping, or similar data gathering and extraction tools on the Services, except with our express written permission. You may not decompile, reverse engineer or disassemble any software or other products or processes accessible through the Services, insert any code or product, or manipulate the content of the Services in any way that affects the user's experience.

Figure 2.4

Order Completed

Thank you very much for your order.

This is a License Agreement between Connor McCarthy ("You") and Oxford University Press ("Oxford University Press"). The license consists of your order details, the terms and conditions provided by Oxford University Press, and the payment terms and conditions.

License Number	3744911224128
License date	Nov 09, 2015
Licensed content publisher	Oxford University Press
Licensed content publication	Cardiovascular Research
Licensed content title	Elastin biosynthesis: The missing link in tissue-engineered blood vessels
Licensed content author	Alpesh Patel,Benjamin Fine,Martin Sandig,Kibret Mequanint
Licensed content date	2006-07-01
Volume number	71
Issue number	1
Type of Use	Thesis/Dissertation
Requestor type	Academic/Educational institute
Format	Print and electronic
Portion	Figure/table
Number of figures/tables	1
Will you be translating?	No
Author of this OUP article	No
Order reference number	None
Title of your thesis / dissertation	Fabrication and Design of a Three Element Hybrid Small Diameter Vascular Graft
Expected completion date	Oct 2015
Estimated size(pages)	120
Publisher VAT ID	GB 125 5067 30
Total	0.00 USD

Appendix 2: Copyright Material for Chapter 4

Dear Mr. McCarthy,

Please know that Prof. Schanze is happy to grant permission for you to use parts of this work in your thesis.

Kindly keep in mind and note the following information from the JPA:

The Author should secure written confirmation (via letter or email) from the respective ACS journal editor(s) to avoid potential conflicts with journal prior publication/embargo policies. Appropriate citation of the Published Work must be made. If the thesis or dissertation to be published is in electronic format, a direct link to the Published Work must also be included using the ACS Articles on Request author-directed link (see http://pubs.acs.org/page/policy/articlesonrequest/index.html).

Best wishes as you complete this important requirement.

Sincerely,

Barbara M. Schanze

Coordinating Editor, ACS Applied Materials & Interfaces